Long-Term Performance Predictions of the North Halawa Valley Viaduct

Xianping Li

Ian N. Robertson

Research Report UHM/CEE/03-04
June 2003

ABSTRACT

This report compares long-term field measurements recorded by instrumentation on the North Halawa Valley Viaduct (NHVV) with long-term predictions from SFRAME, a time dependent finite element analysis program. The long-term structural responses considered in this study are the concrete longitudinal strain, span shortening, prestress losses, and vertical deflection. Field measurements are compared to SFRAME predictions using as-built input files developed by T.Y. Lin International during design and construction of the viaduct. Updated material properties and improved creep and shrinkage prediction models were used by prior researchers to develop an improved SFRAME prediction model for the instrumented Unit 2IB of the NHVV. This improved prediction model is applied to all six units of the NHVV and compared with optical surveys performed by the State of Hawaii during regular maintenance of the structure. In order to provide a tool for use in estimating future long-term bridge performance, a prediction envelope is proposed. This envelope is based on short-term material property tests and estimated parametric variability to provide upper and lower bounds for the long-term structural response. The envelope is applied to all six units of the NHVV for vertical deflection, span shortening, and tendon prestress losses and is shown to provide a reliable estimate of the measured response.

ACKNOWLEDGEMENTS

This report is based on a Masters Research Report prepared by Xianping Li under the direction of Dr. Ian N Robertson. The authors wishes to express their gratitude to Dr. Ronald Riggs and Dr. Si-Hwan Park for their assistance in reviewing this report, and for their valuable comments and suggestions.

This project was supported by funds from the Hawaii State Department of Transportation and the U.S. Department of Transportation, Federal Highway Administration. This support is gratefully acknowledged. The content of this report reflects the views of the authors, who are responsible for the facts and the accuracy of the data presented herein. The contents do not necessarily reflect the official views or policies of the State of Hawaii, Department of Transportation, or the Federal Highway Administration. This report does not constitute a standard, specification or regulation.

TABLE OF CONTENTS

LIST OF FIGURES

LIST OF TABLES

CHAPTER 1

INTRODUCTION

Segmentally constructed prestressed concrete box girder bridges have become very popular for medium and long span bridge structures around the world in situations where continuously supported formwork is impractical or uneconomical. These bridges have been widely used in North American highway construction, since they meet the demand for economy and aesthetically pleasing appearance. Since their introduction in 1964, more than 360,000 linear feet of segmental bridge have been built, with a trend toward increasing popularity (Shushkewich and Vo, 1998). They are the best choices in many cases. These bridges are generally long span post-tensioned structures, which are subject to the same prestress losses as all other prestressed structures. The long-term performance of these long span structures is very complicate and has not been fully understood; hence it is almost impossible to appropriately predict their long-term behavior.

The North Halawa Valley Viaduct (NHVV), portion of the H-3 Freeway on Oahu, a segmentally erected prestressed concrete box girder bridge, was constructed in 1994 using the cast-in-place cantilever construction method. The H-3 Freeway is the newest portion of the Hawaii highway system, connecting the windward and leeward sides of the Island of Oahu. The NHVV was opened to the traffic along with the rest of the H-3 Freeway in Nov, 1997. Chapter 2 provides an overview of the NHVV project. An extensive instrumentation program was initiated by the University of Hawaii (UH) and T. Y. Lin International personnel during construction of Unit 2 inbound (IB) of the NHVV in 1994. Four of the spans in this unit were instrumented for long-term monitoring as described in Chapter 4. The focus of this study is the long-term performance

predictions of the NHVV after nine years of monitoring, including vertical deflection, span shortening, prestress tendon force losses, and concrete strain.

T.Y. Lin International used a state-of-the-art SFRAME computer program during the original analysis and design of the NHVV. SFRAME is a finite element structural analysis program specifically developed for the time-dependent analysis of segmentally erected prestressed concrete plane frame bridge structures (Ketchum, 1986). The SFRAME input file for Unit 2IB was updated by T. Y. Lin to be consistent with the actual construction history, producing an as-built input file. In this report, two different versions of SFRAME are considered due to changes in computer operating systems. Chapter 3 compares results from these two versions, and concludes that there is no significant difference between them.

In order to monitor the actually deflection behavior of the NHVV, the Department of Transportation (DOT) of the State of Hawaii took optical surveys during construction of the viaduct, and every two to three years after the completion of the bridge. Both the UH instrumentation measurements and optical surveys indicated a significant difference between the original SFRAME model prediction for Unit 2IB and the actual bridge behavior. Comparison of SFRAME predictions with the optical surveys are discussed in Chapter 5.

The T. Y. Lin as-built model was unable to predict the long-term structural response for all six spans of Unit 2IB of the NHVV. In order to determine the concrete material properties in the NHVV, including creep and shrinkage, extensive testing was performed by Construction Technology Laboratory (CTL) in Skokie, Illinois. The test results were included in the SFRAME

input files as material parameters used to predict the long-term concrete behavior**.** Inclusion of creep and shrinkage predictions based on short-term laboratory tests improved the SFRAME predictions, but the results are still inadequate as predictions of the structural response. The initial laboratory model was detailed by Dong and Robertson (1999). Based on the optical survey results and the instrumentation measurements, as well as the laboratory test results, the concrete parameters were modified to approach the actual results. Those parameters include relative humidity, creep coefficient, shrinkage coefficient, and the initial tendon prestress. However, those modifications were suitable for Unit 2IB only; and may not work for the other five units of the NHVV. In order to verify whether the final model material parameters created by both Dong (1999) and Wa Hoi (2003) for Unit 2IB work for the other five units, a comparison of the SFRAME predictions using the final model material parameters with the optical surveys is presented in Chapter 6. An SFRAME model with modified parameters providing envelopes of the NHVV long-term vertical deflection is presented, which provides a reasonable bound of long-term behavior, giving the best and worst scenarios. Long-term deflection envelopes are generated for all six units of the NHVV and discussed in Chapter 6.

Finally, conclusions are presented in Chapter 7.

CHAPTER 2

THE NORTH HALAWA VALLEY VIADUCT

INSTRUMENTATION PROGRAM

2.1 Overview of the North Halawa Valley Viaduct

The H-3 Interstate Highway starts from the Halawa Valley Interchange in Honolulu, Hawaii and ends at the Marine Corps station in Kaneohe, Hawaii (Figure 2.1).

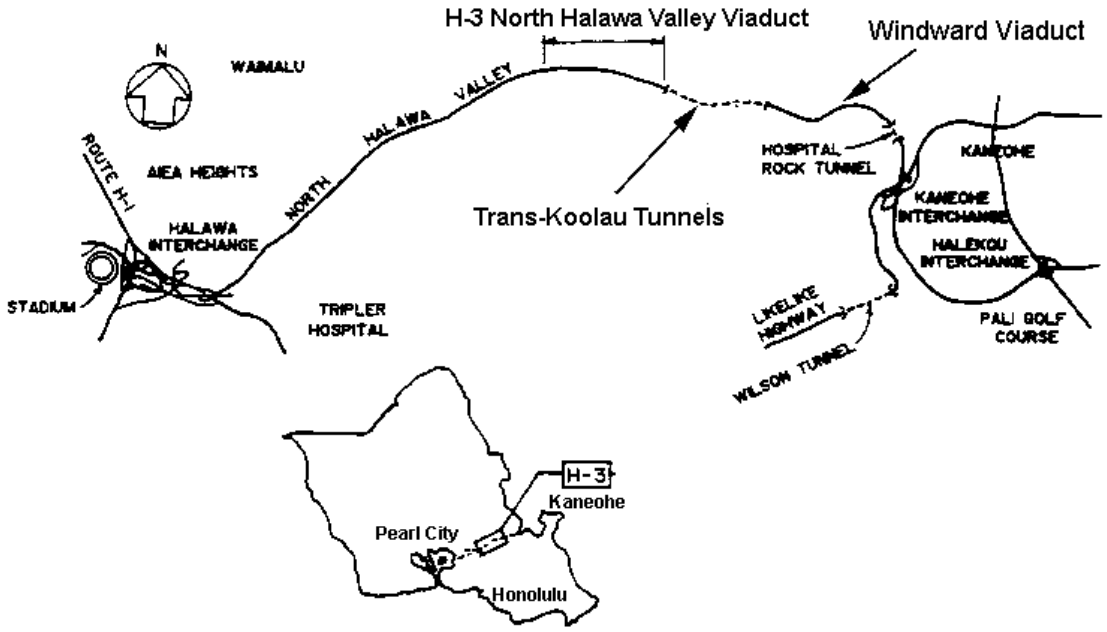

Figure 2.1: H-3 Freeway Location

One of the most important portions of the H-3 freeway is the North Halawa Valley Viaduct. A general plan and elevation of the bridge are shown in Figure 2.2. The project actually consists of two parallel viaducts, one carrying two lanes of traffic inbound to Honolulu and the other one carrying two lanes of outbound traffic. The inbound viaduct is 1897 m (6225 ft) long and the outbound viaduct is 1667 m (5470 ft), each consisting of three independent units named 1IB, 2IB, 3IB, 1OB, 2OB, and 3OB, respectively. Both viaducts are aligned horizontally on a curve

with radii of approximately 1800m (5906 ft) at the lower end of the valley and 2900 m (9514 ft) at the upper end of the valley. The viaducts are on a nearly constant 6 percent grade sloping up toward the mountains.

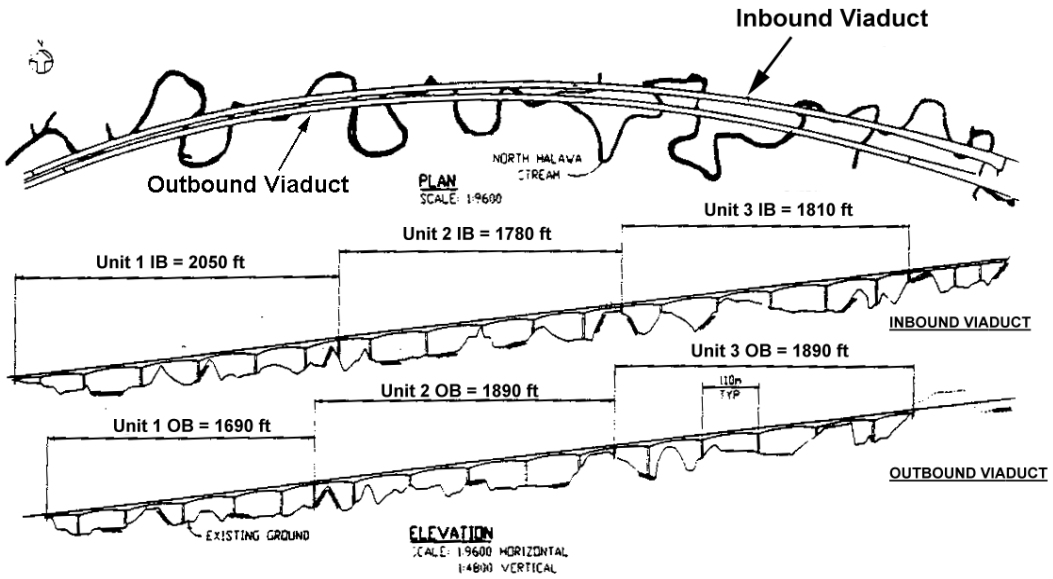

Figure 2.2: North Halawa Valley Viaduct Plan and Profile

The twin viaducts are segmental cast-in-place post-tensioned concrete single-cell box girders designed by T. Y. Lin International of San Francisco. They were constructed by the cantilever overhead gantry method. Each unit has six spans supported by seven piers. Each unit length varied from the shortest Unit 1OB of 515 m (1690 ft) to the longest Unit 1IB of 625 m (2050 ft). The maximum span length is 109.7 m (360 ft), with some span lengths as small as 48 m (155 ft) to accommodate the variations of the terrain and the stream in the valley. The expansion joints between the units are typically located at the top of so-called end piers. This was done to avoid the excessive deflections that sometimes accompany midspan hinges and the construction problems that often accompany cantilever construction past a quarter-point hinge (Shushkewich and Vo, 1998). The out-to-out width of the box girder top slab is 41 feet and the cell box is 23 feet wide throughout the whole length of the viaduct. The depth of each segment varies from 8

feet at midspan to18 feet near the piers. Typical midspan and endspan cross sections are shown in Figure 2.3.

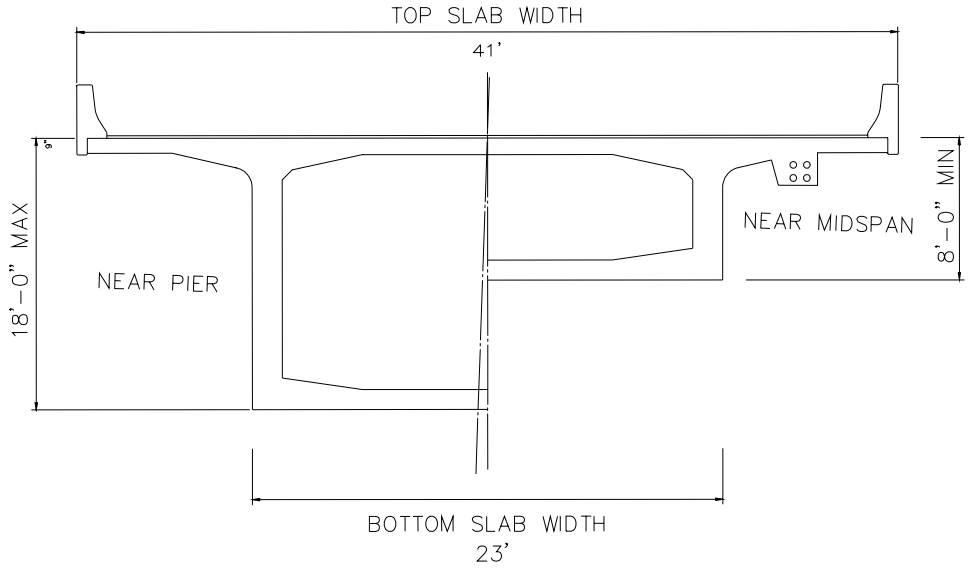

Figure 2.3: Typical Box Girder Cross Sections

2.2 Instrumentation of the NHVV

The second unit of the inbound viaduct (Unit 2IB) was instrumented and monitored by personnel from the University of Hawaii (UH) and Construction Technology Laboratory (CTL). This unit extends from an expansion joint at pier P7 to the next expansion joint at pier P13. Top of piers P9 and P10 are continuous with the box girder and are referred to as fixed piers, while the other five piers have slide bearings between the top of pier and the box girder and are referred to as expansion piers. Seven sections of Unit 2IB were selected for instrumentation to record the viaduct behavior, as shown in Figure 2.3. The instrumented sections are typically located at the midspan and support sections. Lee and Robertson (1995) present the details of the instrumentation system installed in Unit 2IB.

During construction of Unit 2IB, numerous vibrating wire and electrical resistance strain gages were installed at the instrumented sections to monitor concrete strains. Thermocouples were also

embedded in the concrete to monitor temperature variation through the cross sections. Load cells were installed in selected span tendons during stressing to monitor prestress losses. After completion of each span, a base-line deflection system was installed to monitor vertical deflections while tiltmeters were installed above each pier to monitor support rotations. Optical surveys of the roadway were used to verify the base-line measurements. Finally, an LVDT-based extensometer was installed in each instrumented span to monitor overall span shortening. This report will focus on analyzing long-term data gathered from the vibrating wire strain gages, base-line deflection system, prestress load cells, extensometers, and optical surveys. Figure 2.4 shows the instrumented sections of Unit 2IB, referred to as sections A to G. Sections A, D, E, and G are at or close to midspan of the four instrumented spans. Sections B, C, and F are close to the end of the instrumented spans.

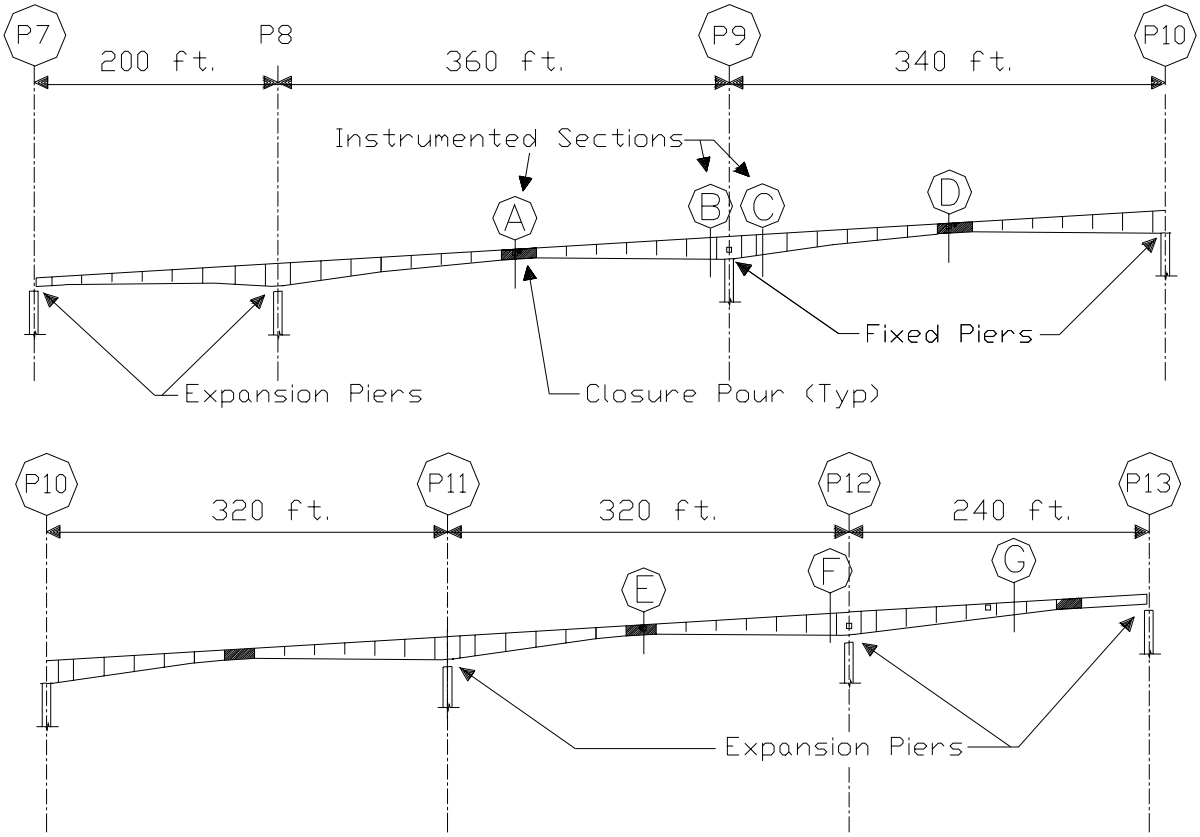

Figure 2.4: Unit 2IB Instrumentation Sections

CHAPTER 3

COMPUTER MODELING—SFRAME

3.1 Introduction

SFRAME is a structural analysis program specifically developed for the time-dependent analysis of segmentally erected prestressed concrete bridge structures (Ketchum, 1986). The analysis is based on step forward integration in the time domain of a plane frame finite element model of the structure. The structural model uses beam elements to model the box girder and piers, tendon elements to model the prestressing, and special traveler elements to model moving formwork. At each solution step, a complete analysis of the finite element system is performed, providing a record of stresses and displacements in the structure.

Segmental construction methods are implemented by providing the capability to change the configuration of the structure at any time step of the solution. Possible configuration changes include restraining and releasing boundary conditions, installing and removing frame elements, stressing and removing prestressing tendons, moving the traveler and applying or removing node and frame element loads. Any structure type and erection sequence, which can be modeled in this context, can be analyzed by the program.

The time dependent effects of creep, shrinkage, aging of the concrete, and relaxation of the prestressing steel are included in the material model for the structural elements. The instantaneous stress-strain relationships for all materials are limited to linear elasticity. The element formulations guarantee static equilibrium of the computed internal element forces with applied external loads.

The program incorporates automated construction and prestressing options, and time dependent material behavior into a command structure allowing the analysis of complex segmental bridge types. The solution includes the effects of creep, shrinkage and aging of the concrete, plus friction, anchorage slip and relaxation of the prestressing steel (Ketchum, 1986).

The application of SFRAME to the NHVV was described by Dong and Robertson (1999). This chapter will focus on the comparison of the SFRAME results produced by different release versions of the program. Since the original version of SFRAME does not run in current computer operating systems, new predictions were produced using the latest version of SFRAME. In order to compare the current version with that used by Dong and Robertson (1999), a number of comparative analyses were performed.

3.2 Comparison of Different SFRAME Versions

The original SFRAME used by T.Y. Lin to analyze the NHVV was version 2.01, which was released in the early 1990's. Since then, this program has been upgraded continuously. The old 2.01 version, which T.Y. Lin authorized to University of Hawaii for research purposes, does not run in newer computer operating systems such as Windows 2000, or XP. T.Y. Lin issued a copy of the latest version SFRAME 2.11 to the University of Hawaii in March 2003. This version runs in Windows 2000 or XP environment.

Because previous SFRAME predictions by Dong and Robertson (1999) were produced using the old version, in order to extend that study to present and future performance, it was necessary to compare the results produced by the different version of SFRAME before using the new version.

The comparisons were performed on Unit 2IB to prediction vertical deflection from March 1995 to June 1997. SFRAME version 2.01 was run using a Windows ME computer, while SFRAME 2.11 was run on a Windows XP computer. The input files used to run the comparisons are Wa Hoi (2003) Unit 2IB Upperbound, Lowerbound, Finalmodel, and Averagemodel. Figures 3.1 to 3.4 show the comparisons of the results from the two SFRAME versions.

3.3 Result of Comparison

From Figure 3.1 to 3.4, it can be concluded that the two versions of SFRAME produce consistent results for all four models. The maximum difference is less than one percent. Therefore, the new SFRAME 2.11 can be used to predict the bridge's long-term behavior in the future. Dong and Robertson's study of the NHVV can be extended without being affected by using the current program version. The prediction can also be extended to other long-term behaviors, such as span shortening and prestress loss.

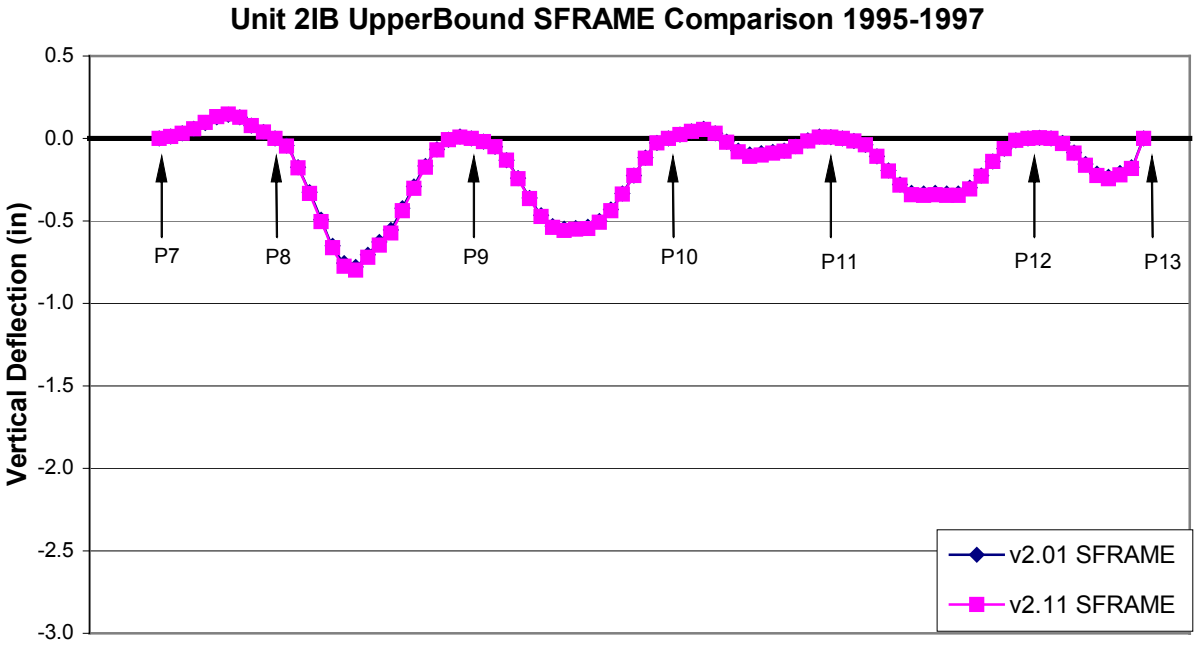

Figure 3.1: SFRAME Version Comparison—Hoi Upperbound 1995-1997

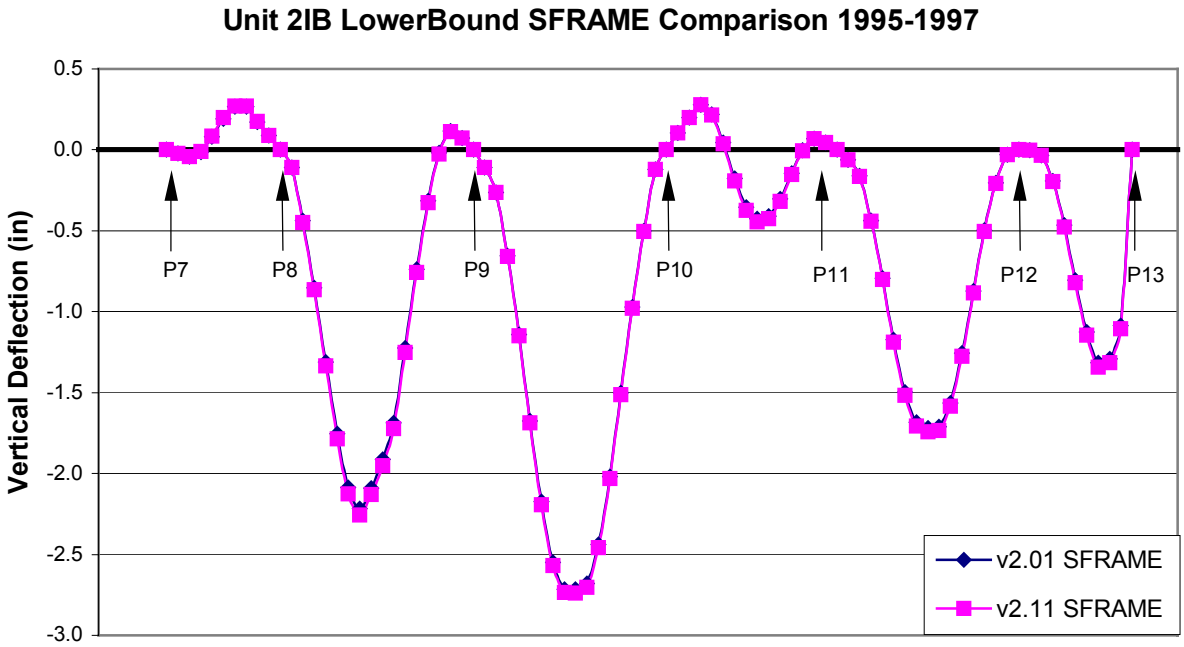

Figure 3.2: SFRAME Version Comparison—Hoi Lowerbound 1995-1997

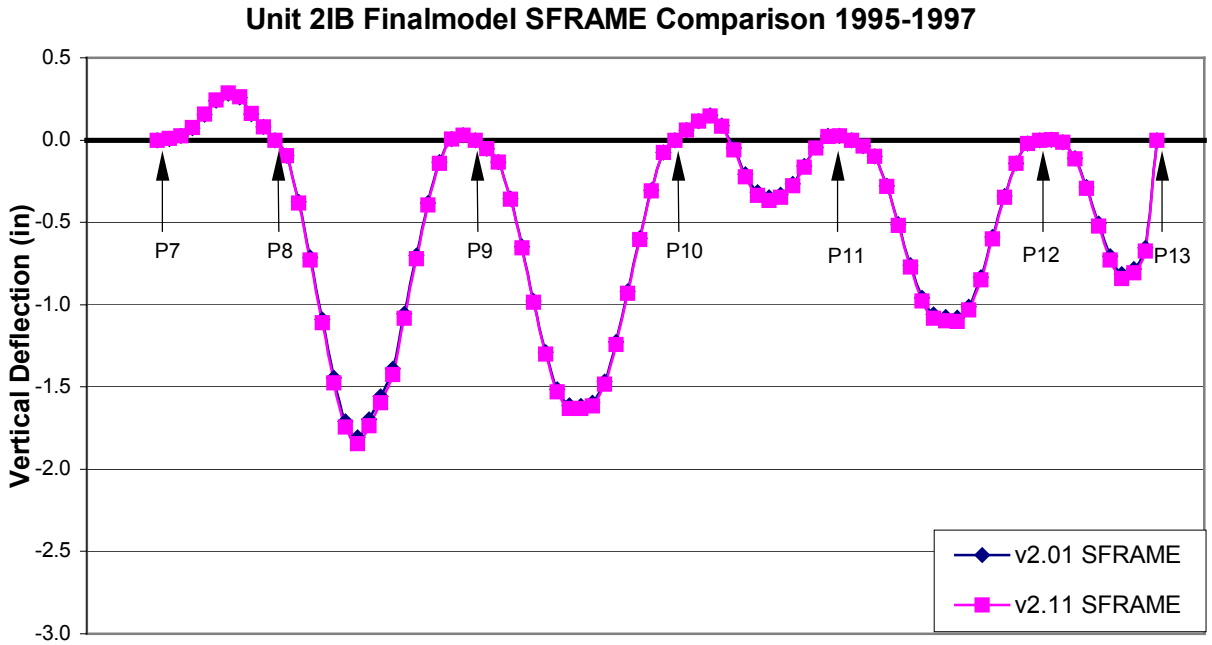

Figure 3.3: SFRAME Version Comparison—Hoi Finalmodel 1995-1997

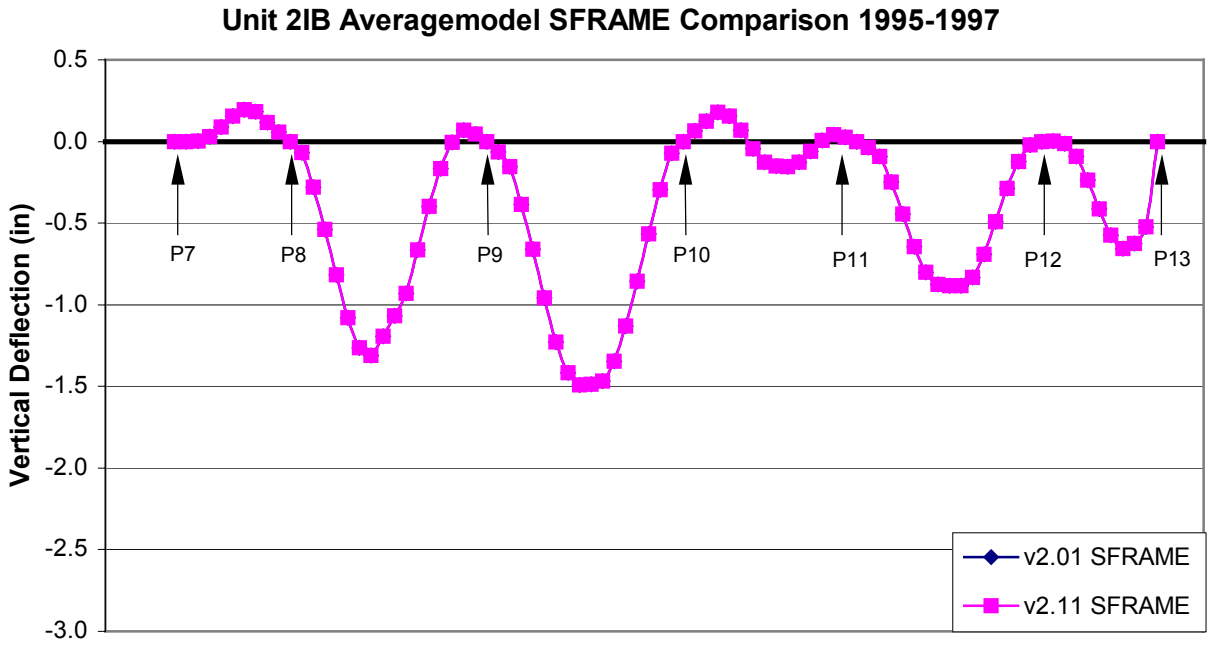

Figure 3.4: SFRAME Version Comparison—Hoi Averagemodel 1995-1997

CHAPTER 4

MEASUREMENT RESULTS

4.1 Introduction

The University of Hawaii and T. Y. Lin personnel initiated an intensive instrumentation system during the construction of Unit 2IB of the NHVV. The instrumentations have continuously gathered data at two-hour intervals since the completion of construction in order to record the viaduct behavior. The instrumentation includes vibration wire strain gages, electrical resistance strain gages, tendon load cells, span extensometers, base-line deflection systems, and tiltmeters. This chapter presents these instrumentation measurement results, and compares some of the measurements with SFRAME predictions.

Section 4.2 presents concrete strain changes measured by the vibrating wire strain gages installed in Unit 2IB during construction. SFRAME does not output predicted strains and so these measured values could not be compared with theoretical predictions. Section 4.3 discusses the bridge span shortening, and compares extensometer measurement results with SFRAME predictions. The average strain readings are also compared with the span shortening, measured by the extensometers. Section 4.4 presents prestress tendon force losses after the completion of the NHVV, and compares the results with those predicted by SFRAME.

4.2 Concrete Strain Measurements

Vibrating wire (VW) strain gages are designed for direct embedment in the concrete at the critical sections. The advantage of the VW gages over more conventional electrical resistance

strain gages lies mainly in the use of frequency measurement as the output signal, which is not affected by changes in the lead. VW strain gages were placed at all seven instrumented sections of Unit 2IB to measure longitudinal strain in the box girder concrete. Typical locations at midspan closure sections and pier support sections are shown in Figures 4.1 and 4.2 respectively. Midspan sections A, D, E, and G each has eight vibrating wire gages around the perimeter of the box girder. Support sections B, C and F each have ten vibrating wire strain gages around the box girder. The as-built locations of the VW strain gages at all sections are recorded by Lee and Robertson (1995). Because some of the VW strain gages at section C were damaged during placement of the concrete, and one gage at section G has failed, sections A, B, C, D, E, F, and G have 8, 10, 6, 8, 8, 10 and 7 gages working properly, respectively. This report will present the data gathered from those gages.

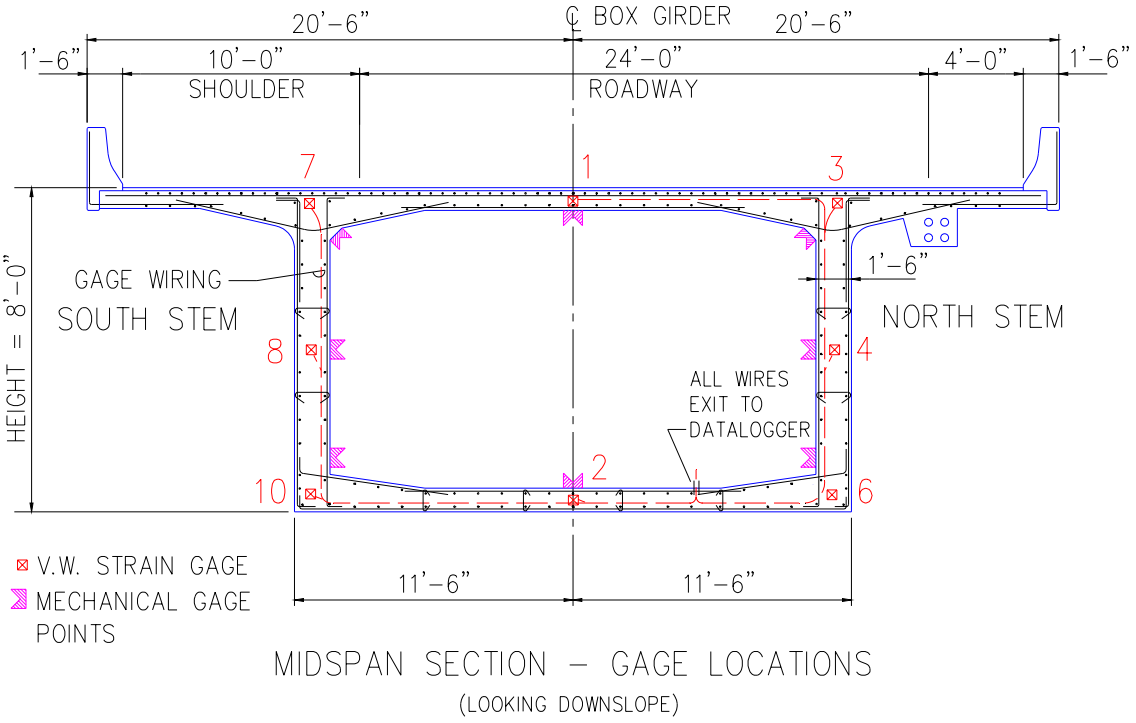

Figure 4.1: Midspan Section Strain Gage Locations

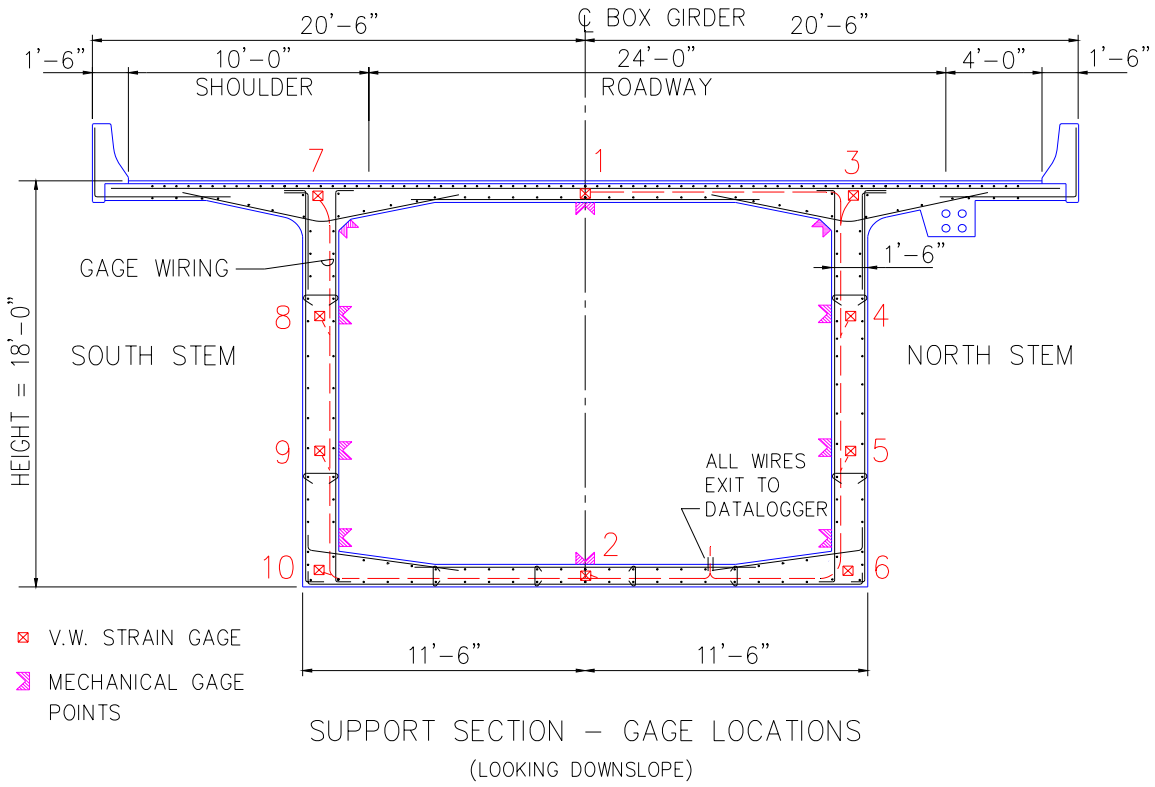

Figure 4.2: Support Section Strain Gage Locations

The data loggers were programmed for two hourly readings, gathering raw data including date and time, ambient temperature, relative humidity, and micro strain. Strain in the concrete is computed from the difference between the initial VW gage readings and subsequent readings. When concrete is subjected to compression, the reading will decrease. In tension, the reading will increase. These readings must be adjusted for changes in the temperature at the gage location, since the wire used in the gage has a different coefficient of thermal expansion than the surrounding concrete. A large amount of data has been collected over the past eight years. In order to save memory space and increase processing speed, the eight-year combination plots only present daily 6:00 am readings. The raw data is processed to account for temperature effects, gage factors, and to include initial reading compensation. The VW strain gage data has been processed according to a procedure previously established by Dong and Robertson (1999).

Figures 4.3 to 4.9 present the concrete strain plots from section construction in 1994 to December 2001 for each of the seven-instrumented sections. From the plots, one can see that the concrete strain increases rapidly during prestressing and during the first year, with smaller strain changes as the concrete age increases. The strains are almost stable after year 2000. However the concrete strain is still continuously increasing at a very slow rate. Ambient temperature has an effect on the concrete strain. The strain plots show that the concrete strain rate increases during the summer seasons and decreases during the winter seasons, although the temperature difference is small between summer and winter season in Hawaii. Figures 4.10 and 4.11 show the typical ambient temperature recorded at Unit 2IB for years 2000 and 2001, respectively.

From the measured concrete strains, an estimate of the overall span length change can be obtained using the average concrete strain at each section times the span length. These average strains are shown in Figures 4.3 to 4.9. Span length changes are presented in section 4.3 along with the extensometer measurements. The average of midspan section and support section measurements are compared with the extensometer measurements.

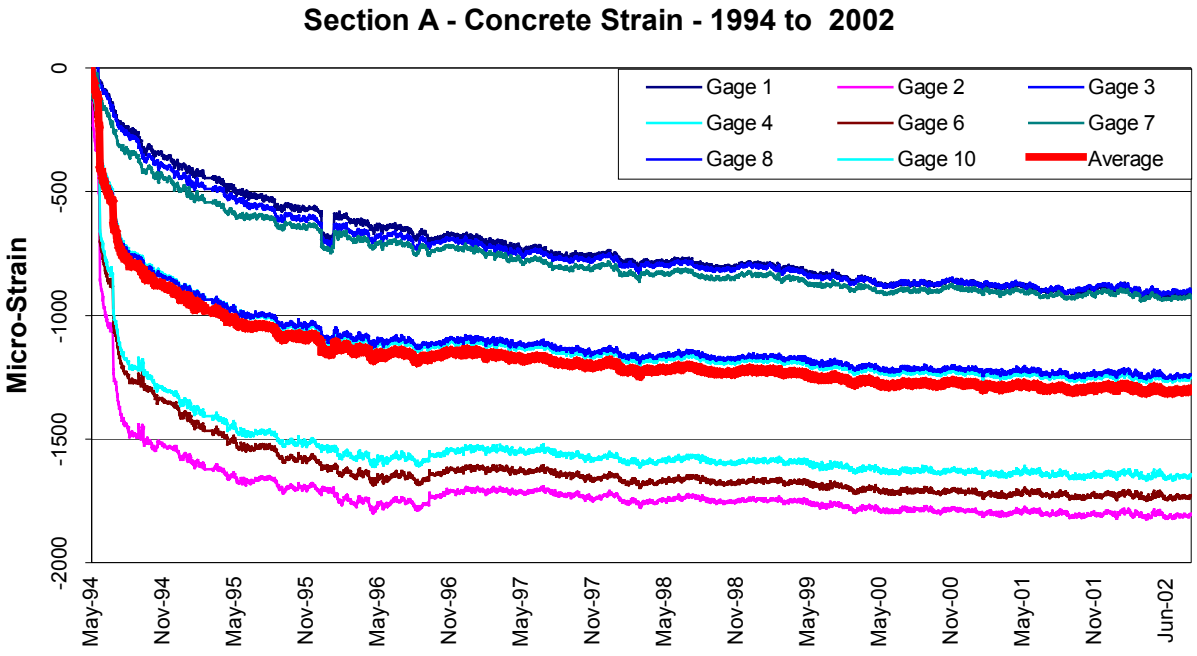

Figure 4.3: Unit 2IB Section A Concrete Strains 1994-2002

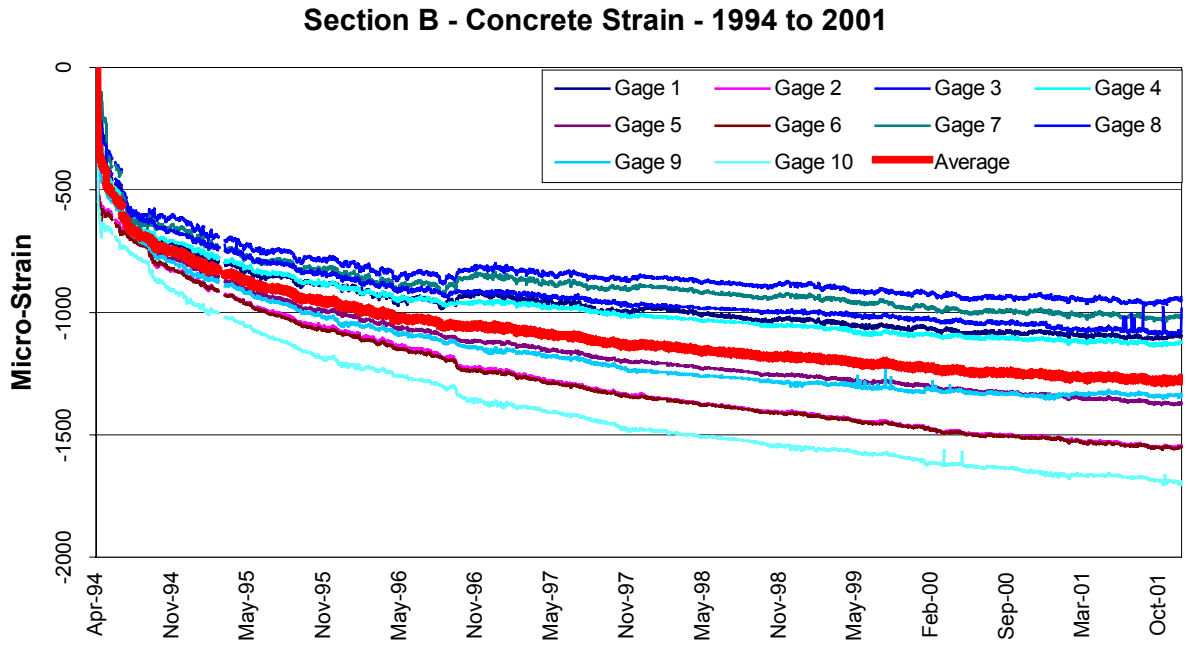

Figure 4.4: Unit 2IB Section B Concrete Strains 1994-2001

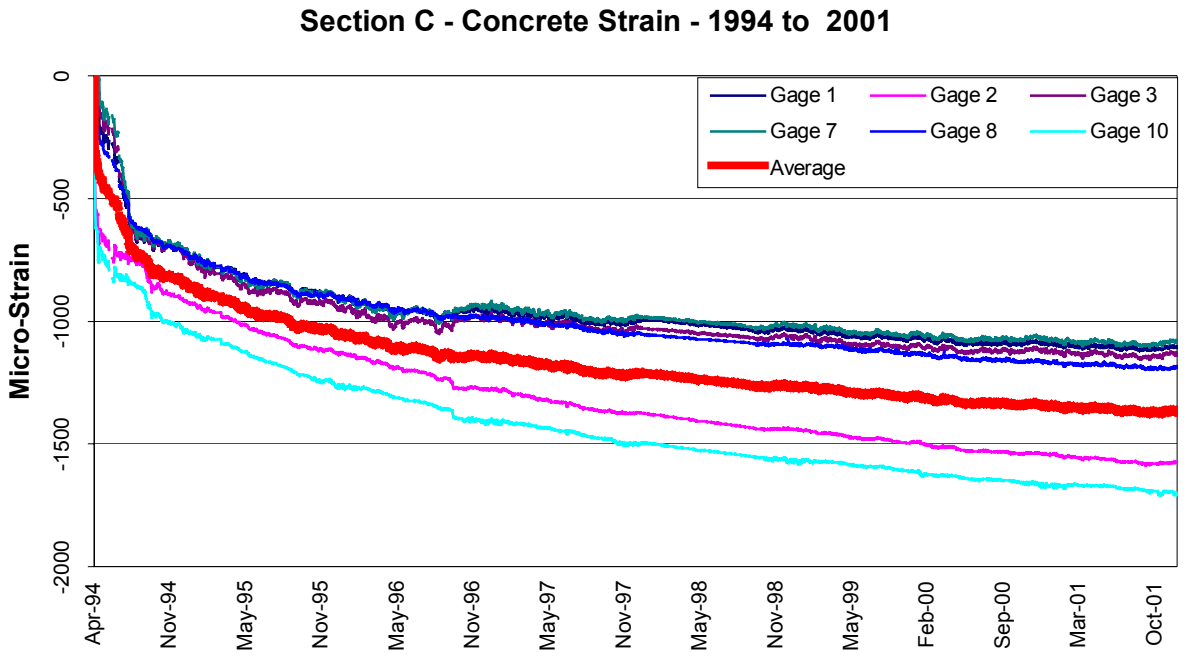

Figure 4.5: Unit 2IB Section C Concrete Strains 1994-2001

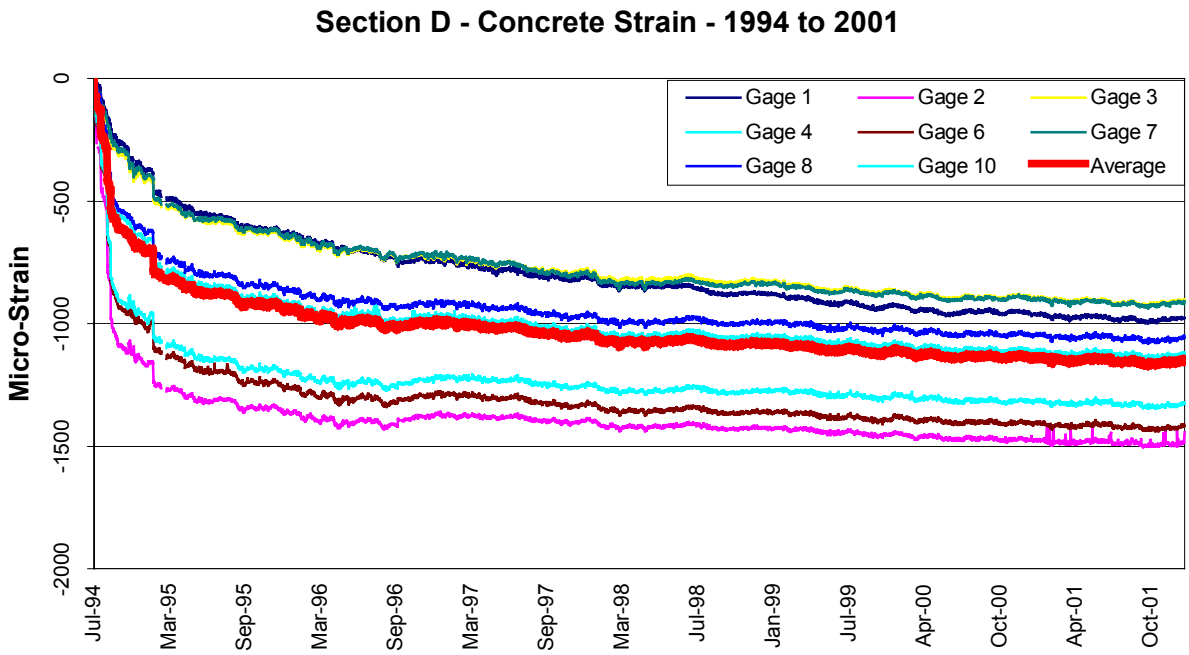

Figure 4.6: Unit 2IB Section D Concrete Strains 1994-2001

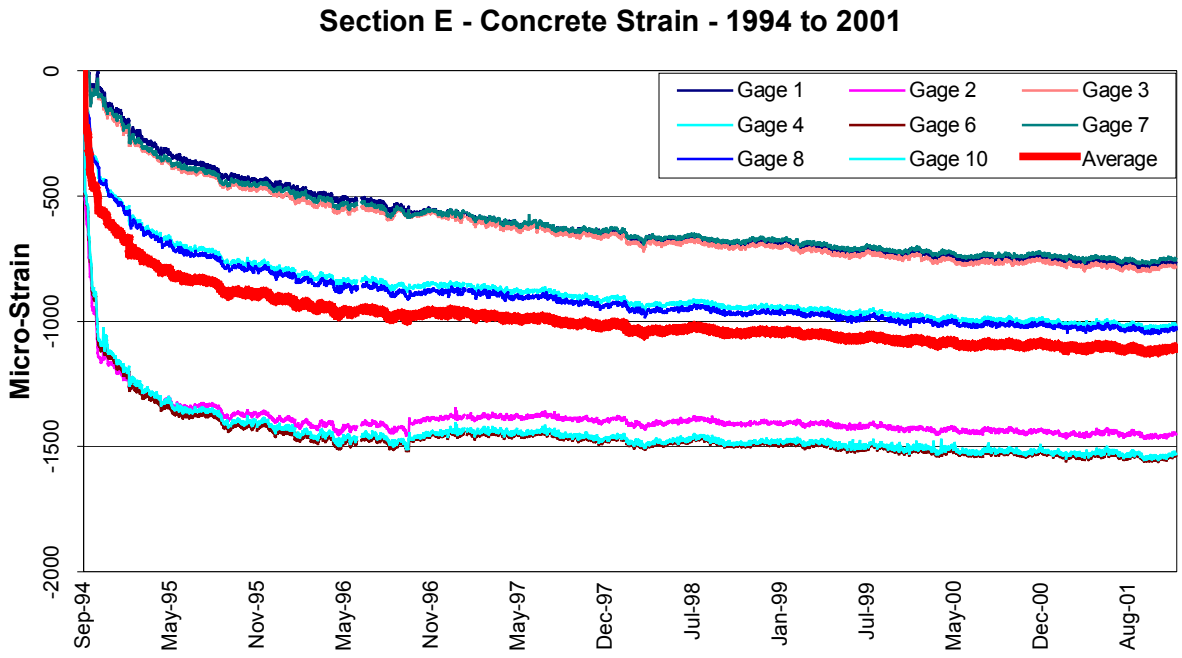

Figure 4.7: Unit 2IB Section E Concrete Strains 1994-2001

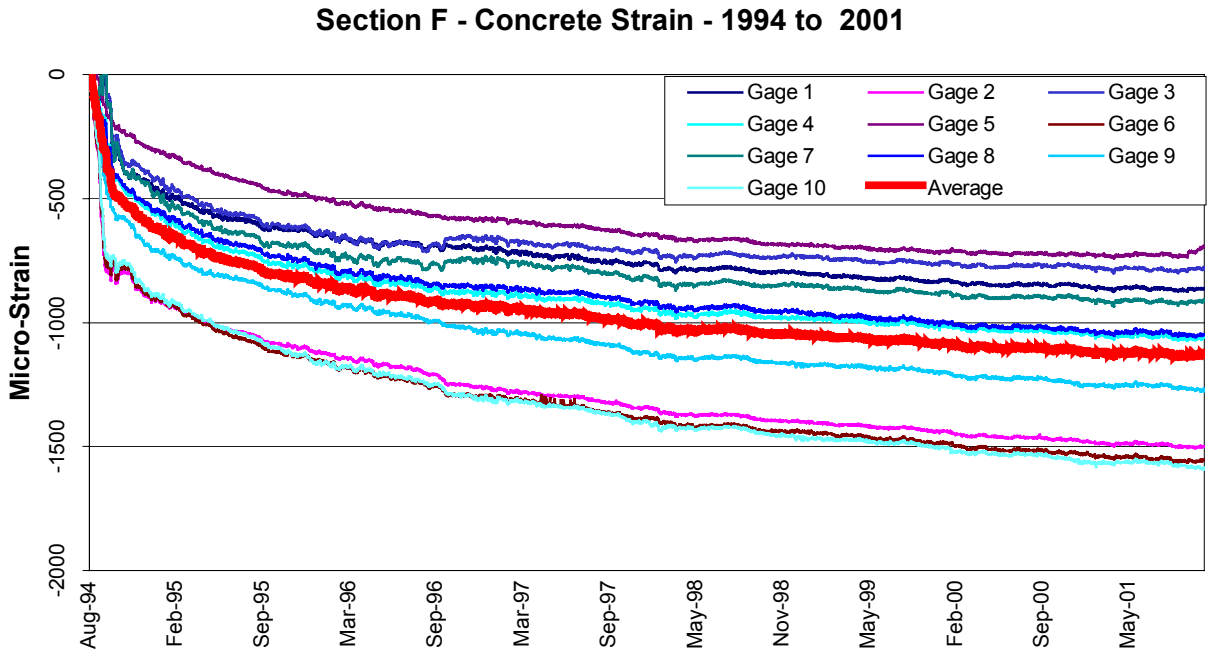

Figure 4.8: Unit 2IB Section F Concrete Strains 1994-2001

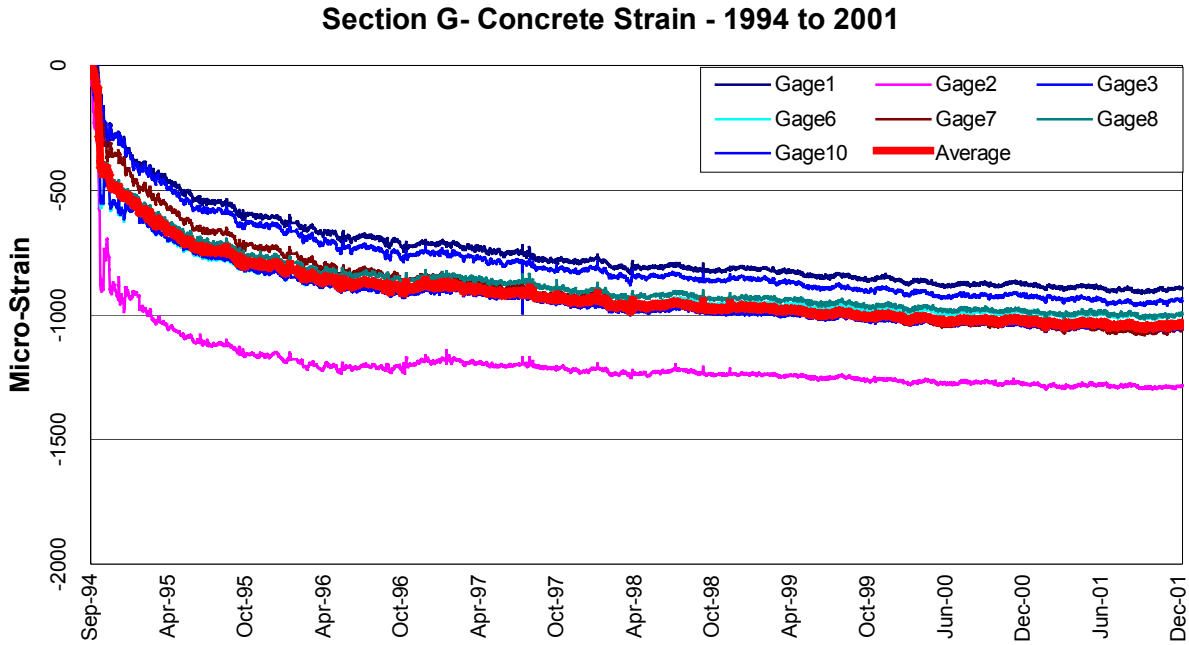

Figure 4.9: Unit 2IB Section G Concrete Strains 1994-2001

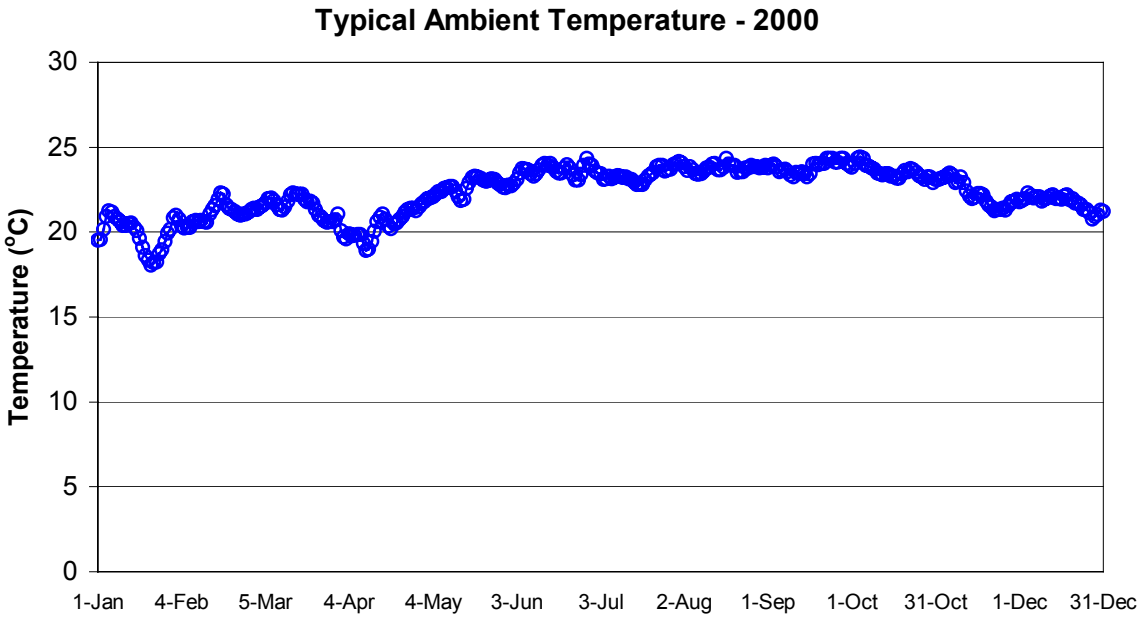

Figure 4.10: Typical Ambient Temperatures in Unit 2IB - 2000

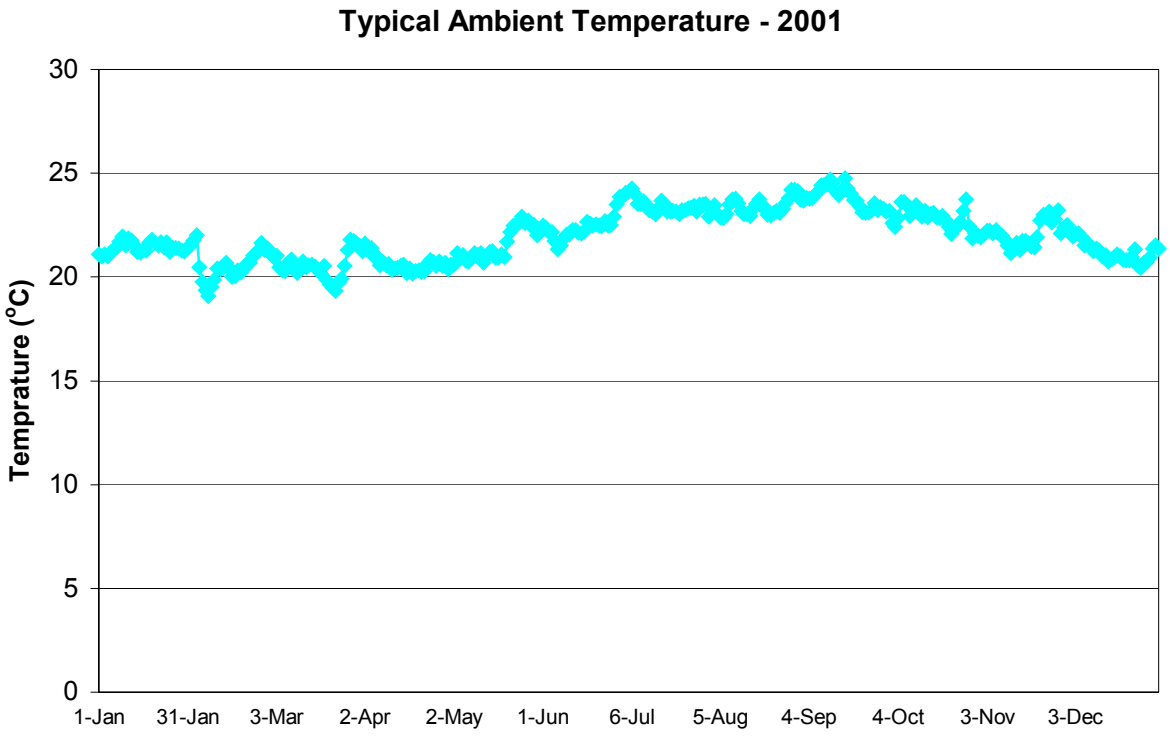

Figure 4.11: Typical Ambient Temperatures in Unit 2IB - 2001

4.3 Span Shortening Measurements

The overall span shortening measurements provide a valuable check of the long-term bridge behavior. The purpose of the extensometers was to measure the axial shortening of the instrumented spans. Extensometers were installed in the four-instrumented spans during the construction of Unit 2IB, that is, between piers P8 and P9, P9 and P10, P11 and P12, P12 and P13. Lee and Robertson (1995) record the as-built locations of the extensometer end brackets in each span.

Each extensometer consists of a series of graphite rods spliced together to span from pier to pier inside the box girder. The graphite rods are connected with rigid couplers and inserted into ¾ inch diameter PVC conduit attached to the underside of the girder top slab. One end of the rod is fixed, while the other end is coupled to a Linear Variable Displacement Transducer (LVDT). The relative displacement of the two ends of the extensometer is measured by the LVDT. The LVDTs operate on the vibrating wire principle. One of the LVDTs has six-inch stroke, while the others have two-inch stroke. Once this limit is reached, they are repositioned so as to continue monitoring the span shortening. Readings are recorded every two hours. The extensometer between pier P8 and P9 was damaged at the end of year 1997, so readings beyond this date were unreliable and are not included in the plots.

An estimate of the span shortening can be obtained from the average strain readings at midspan and endspan sections. Figures 4.12 to 4.15 show comparisons between the axial span shortenings measured by the extensometers and estimated from the average strain readings for spans P8-P9, P9-P10, P11-P12 and P12-P13, respectively. For span P12-P13, only the average midspan strain

is considered. From these figures, it can be concluded that the span shortening estimated using the average VW strain gage readings do not always agree with those measured by the extensometers. There are significant differences in spans P8 to P9 and P9 to P10, while the two measurements are close in spans P11 to P12 and P12 to P13. It is also evident that initially the average strain at midspan sections increased more rapidly than the endspan sections. However, these strains appear to be converging with time.

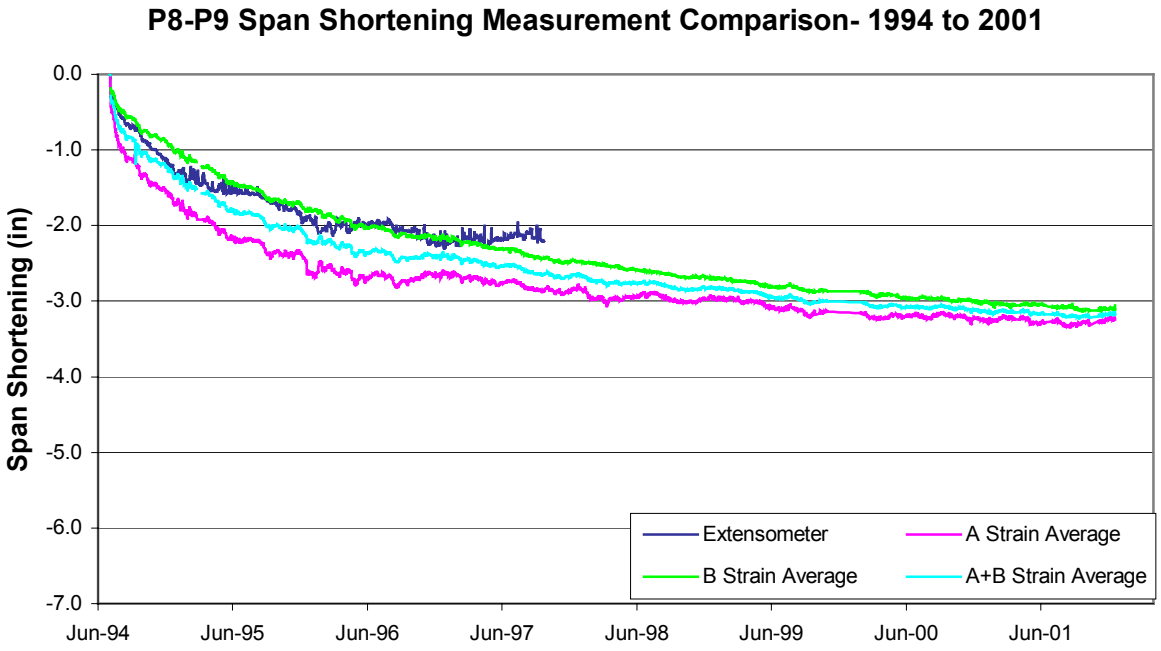

Figure 4.12: P8–P9 Extensometer vs. VW Strain Gage Measurements

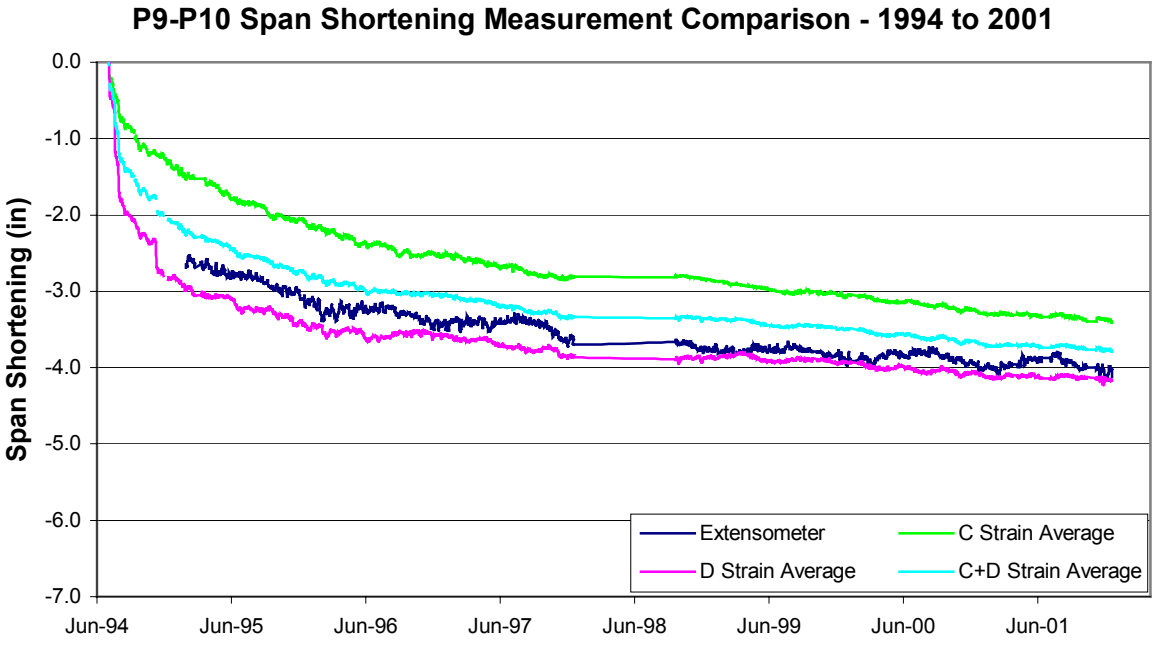

Figure 4.13: P9–P10 Extensometer vs. VW Strain Gage Measurements

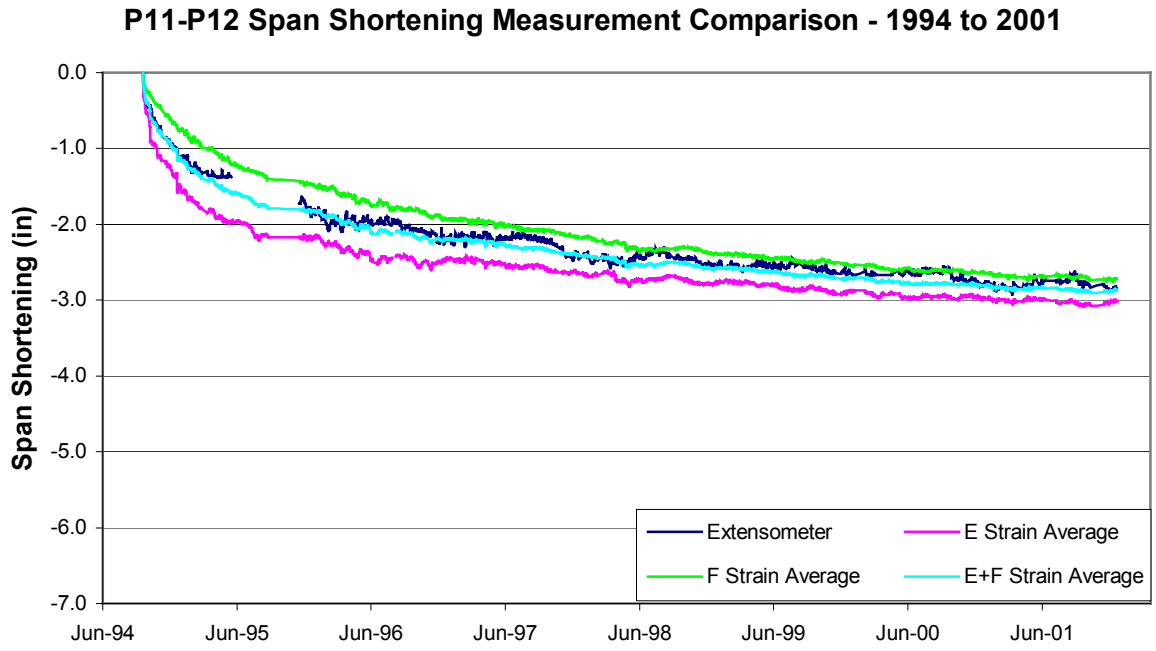

Figure 4.14: P11–P12 Extensometer vs. VW Strain Gage Measurements

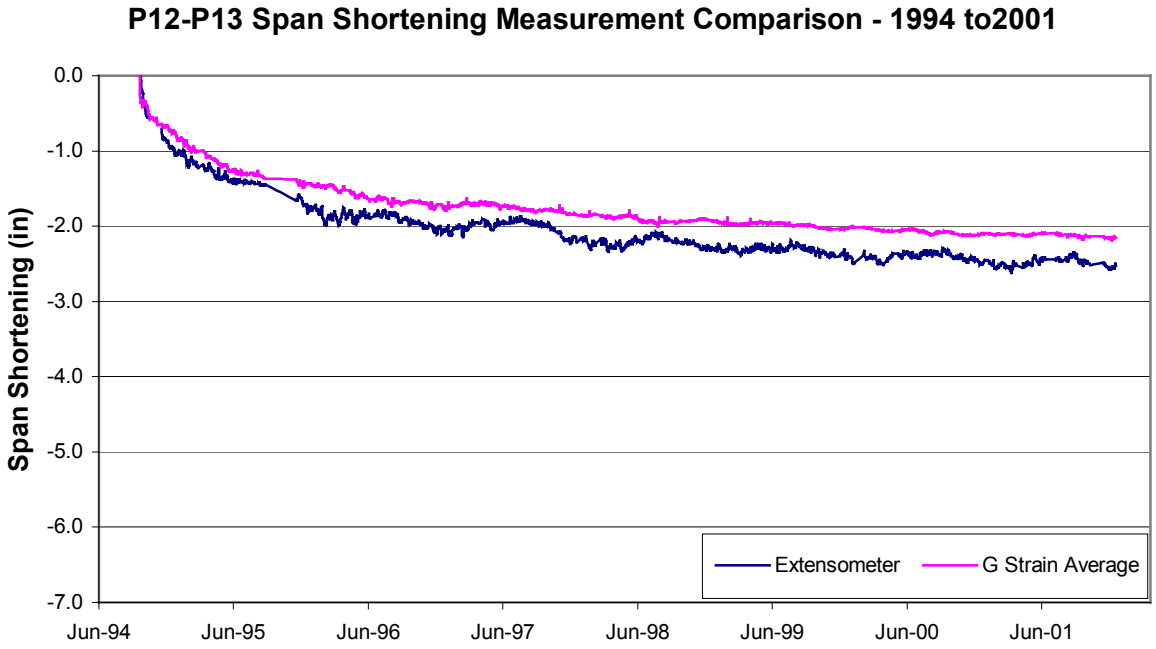

Figure 4.15: P12–P13 Extensometer vs. VW Strain Gage Measurements

Figures 4.16 to 4.19 show the extensometer axial span shortening measurements for spans P8-P9, P9-P10, P11-P12 and P12-P13, respectively, along with Hoi (2003) SFRAME final model predictions. It can be noted that the field measurements fluctuate on a seasonal basis due to ambient temperature variations. As with the longitudinal strain measurements, the spans shorten rapidly during prestressing and the first year after construction. The rate of shortening decreases with time. The span shortening curves are almost stable at the end of year 2000, though the trend indicates slightly more shortening in future years. The current span length changes are mainly attributed to fluctuation in the ambient temperature.

Table 4.1 shows the span shortening of the four instrumented spans at the end of each year as measured by the extensometers. It can be concluded that the span shortening developed rapidly at the early stage, has slowed as the bridge's age increases.

Table 4.1: Span Shortening at the End of Each Year (in)

Span	P8-9		P9-10		P11-12		P12-13	
Span Length (ft)	350.5	Annual Change %	326.8	Annual Change %	314.1	Annual Change %	231.6	Annual Change %
1994	-1.200	-0.029	--	--	-0.975	-0.026	-0.691	-0.025
1995	-1.796	-0.014	-1.677	-0.043	-1.723	-0.020	-1.216	-0.019
1996	-2.210	-0.010	-2.084	-0.010	-2.187	-0.012	-1.505	-0.010
1997	-2.159	0.001	-2.250	-0.004	-2.376	-0.005	-1.352	0.006
1998	--		-2.395	-0.004	-2.523	-0.004	-1.387	-0.001
1999	--		-2.450	-0.001	-2.623	-0.003	-1.520	-0.005
2000	--		-2.452	0.000	-2.662	-0.001	-1.590	-0.003
2001	--		-2.452	0.000	-2.662	0.000	-1.610	-0.001
2002 (August)	--		-2.435	0.0004	-2.662	0	-1.568	-.001

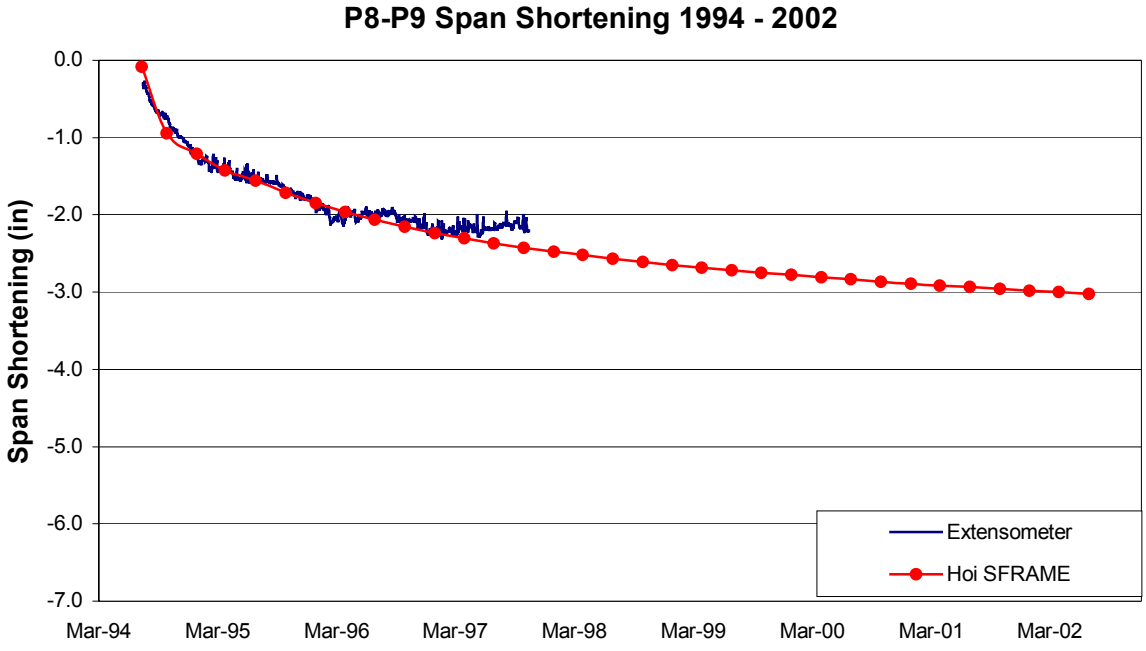

Figure 4.16: P8-P9 Span Shortening 1994-2002

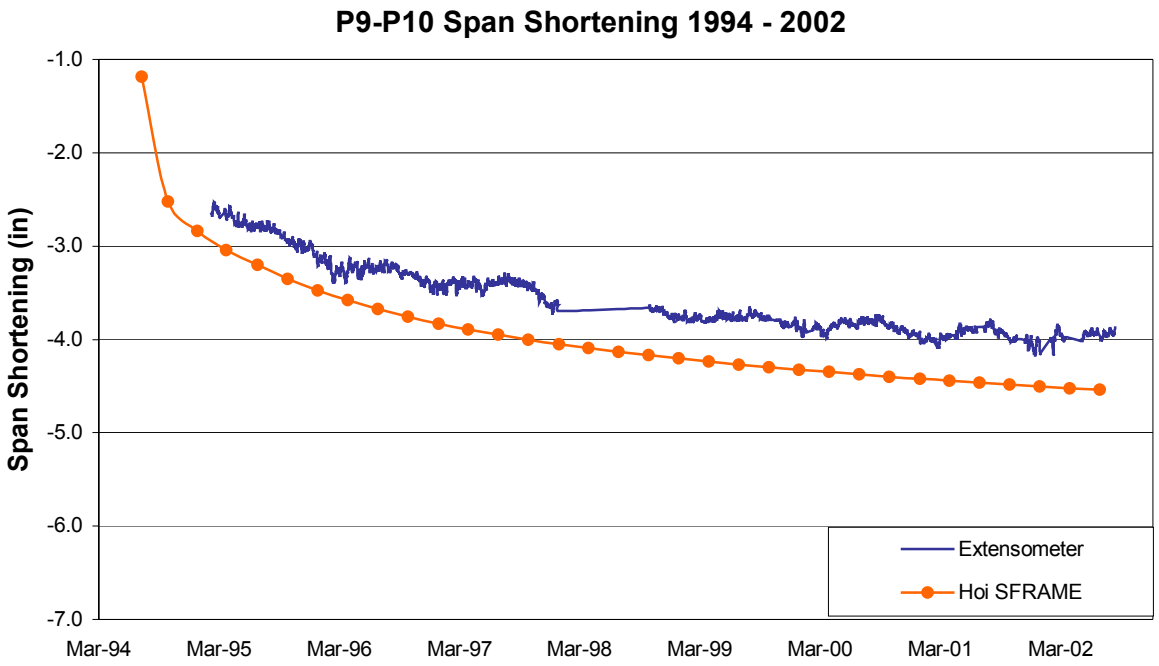

Figure 4.17: P9-P10 Span Shortening 1994-2002

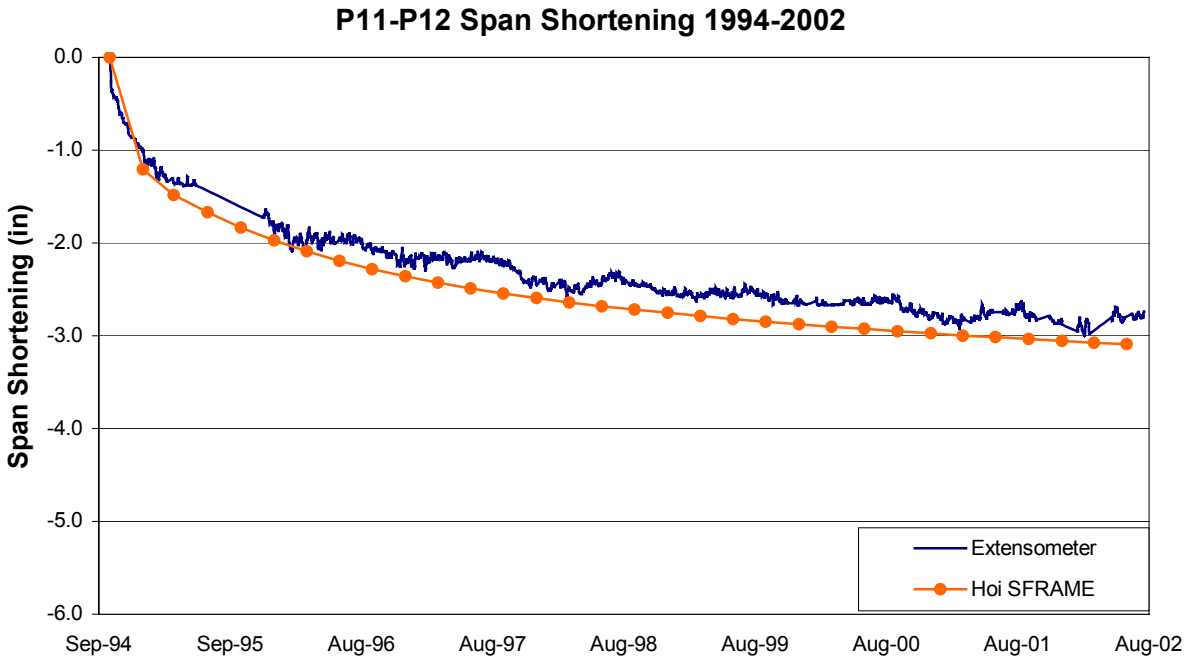

Figure 4.18: P11-P12 Span Shortening 1994-2002

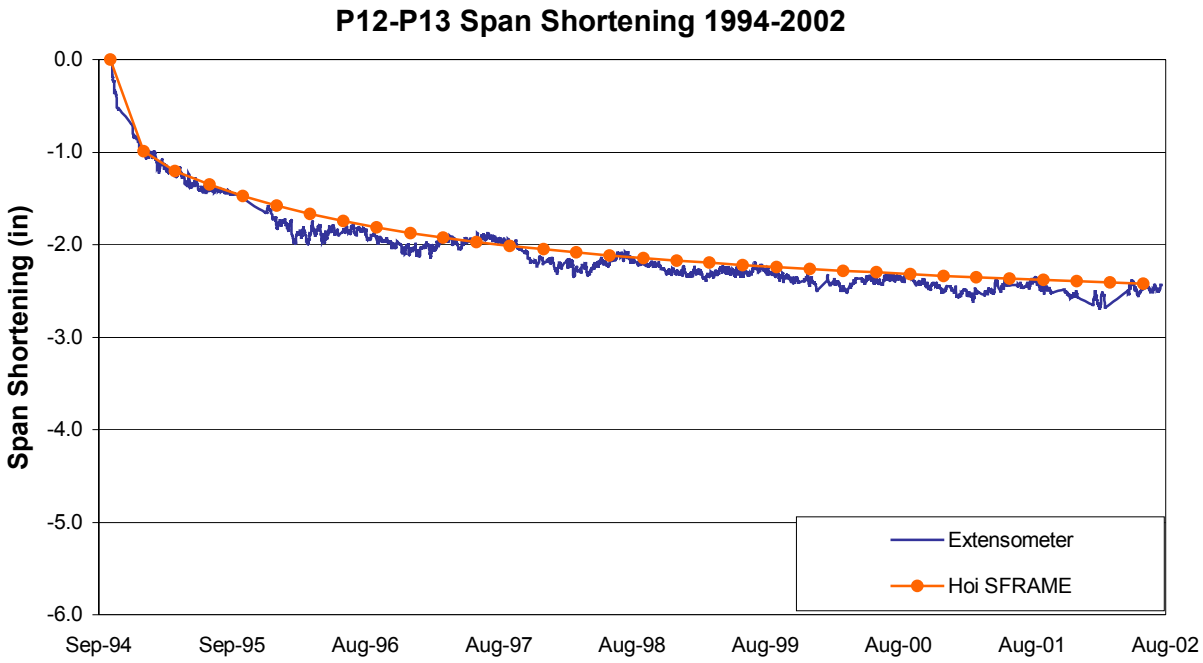

Figure 4.19: P12-P13 Span Shortening 1994-2002

For any given date after construction, the SFRAME output file gives the X-direction (longitudinal) position of each node. The relative X-position was then calculated by taking the difference between the two supporting nodes at the ends of each span. Therefore, the predicted axial shortening for a given date was determined by taking the difference between the initial and final relative X-displacements. The T. Y. Lin as-built SFRAME model did not provide good span shortening predictions, as discussed by Dong and Robertson (1999). The Hoi Final model predictions, shown in Figures 4.16 to 4.19, provide a reasonable estimate of span shortening for these spans in Unit 2IB. Since this model was adjusted to fit the measured vertical deflections for Unit 2IB, this agreement is to be expected. However, variability between the behavior of the other five units of the NHVV lead to the development of upper and lower bound predictions as discussed in Chapter 6. Applying these predictions and averaging the upper and lower bound values produces the curves shown in Figures 4.20 to 4.23. It can be concluded that the upper

bound and lower bound models provide very good bound prediction of the span shortening. Though the upper and lower bound is large, the average of the upper bound and lower bound is very close to the extensometer measured values. The material parameters selected for SFRAME based on vertical deflection predictions work well to predict the span shortening. It is feasible to extend those bounds to the other five units to provide span shortening prediction.

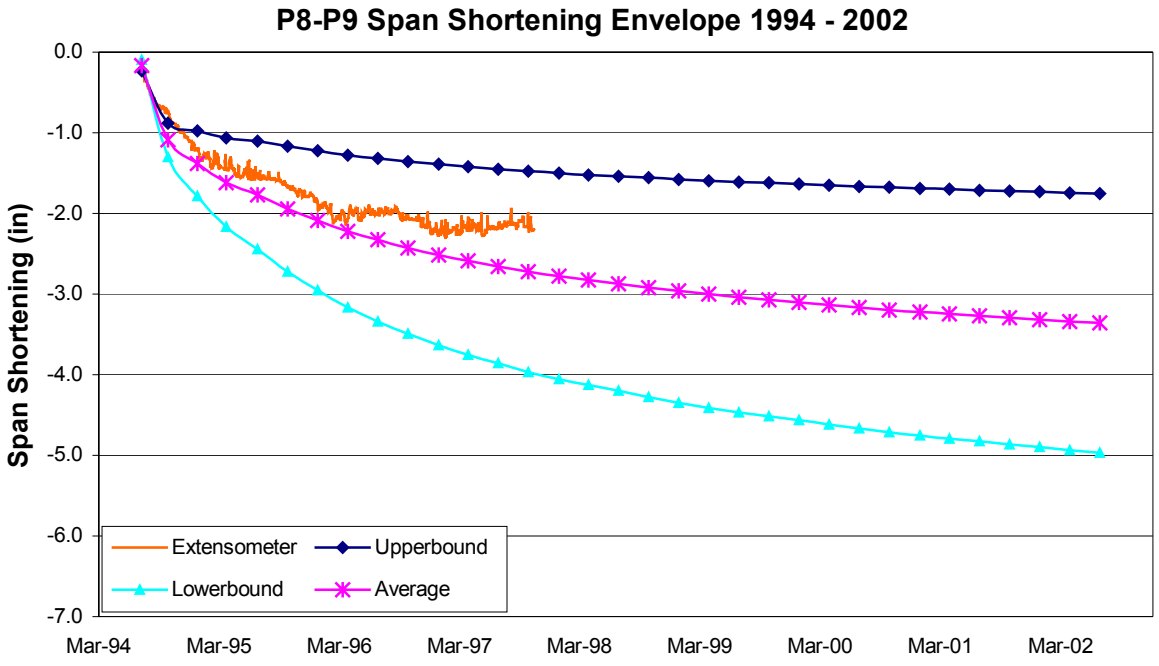

Figure 4.20: P8-P9 Span Shortening Envelope 1994-2002

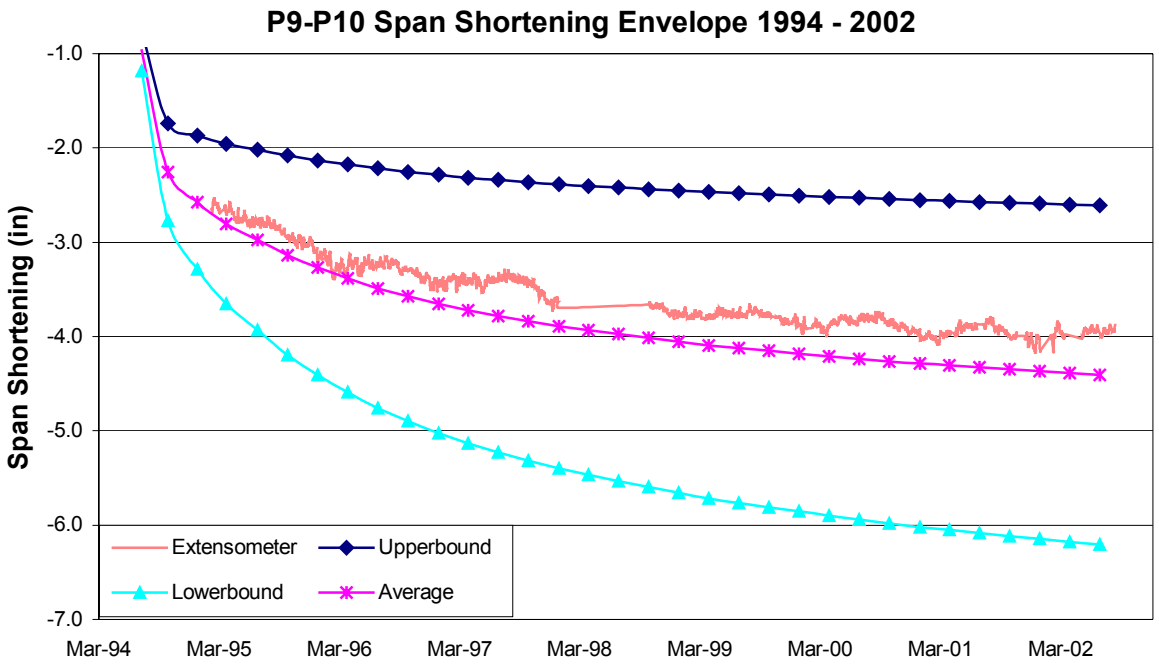

Figure 4.21: P9-P10 Span Shortening Envelope 1994-2002

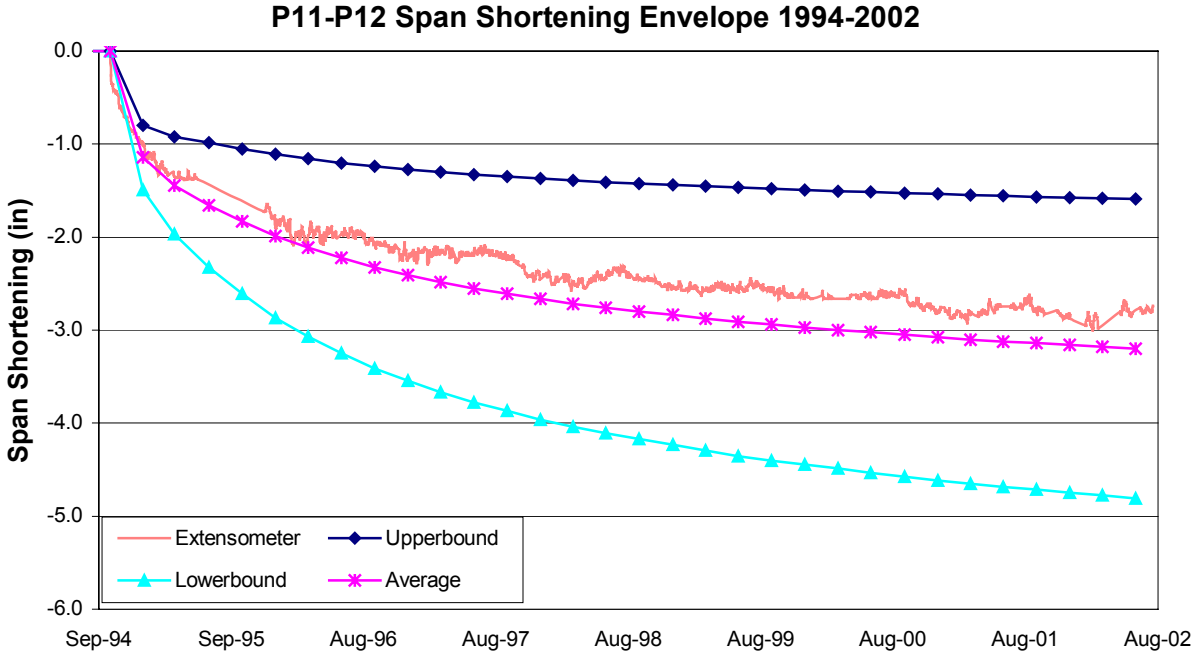

Figure 4.22: P11-P12 Span Shortening Envelope 1994-2002

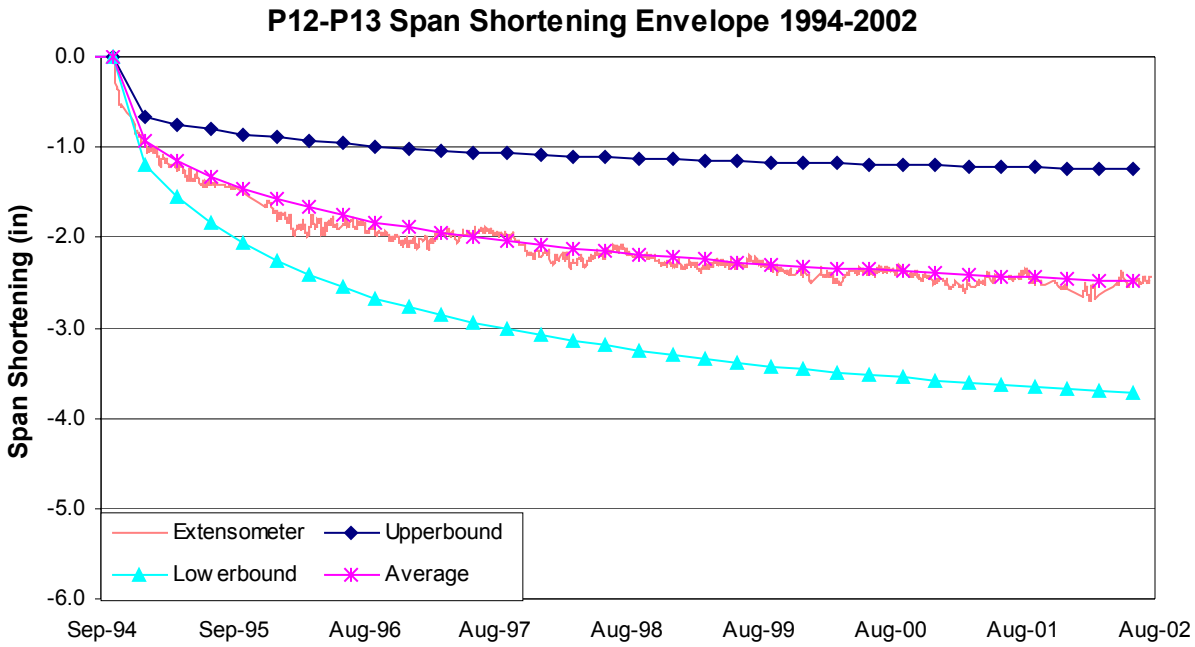

Figure 4.23: P12-P13 Span Shortening Envelope 1994-2002

4.4 Tendon Force Measurements

As with all prestressed concrete structures, segmentally erected box girder bridges are subjected to prestress losses. The load cells installed in the NHVV are used to measure changes in the tendon forces so as to determine the total tendon prestress loss. The load cells selected in this project were cylindrical load cells with 700 kip compressive capacity designed and manufactured by Construction Technology Laboratories. The load cells were installed directly below the stressing anchor blocks prior to stressing of the tendons. Six span tendons were fitted with load cells. At each of the long span conditions from piers P8 to P9 and P9 to P10, two span tendons were fitted with load cells, one in each stem. One of these tendons was a long tendon while the other was a short tendon. The remaining two load cells were installed on span tendons in the spans from pier P11 to P12 and P12 to P13. Table 4.2 shows details of the six tendons

instrumented with load cells. The installation of the load cells used in this project was recorded by Lee and Robertson (1995).

Load cell LC1, installed at the fixed end of tendon SP7 in span P8-P9, was placed between two anchorage blocks as shown in Figure 4.24. Only the outer anchorage block contains wedges to lock the individual prestress strands. During prestressing it was noted that friction between the strands and the inner anchorage block caused the load cell readings to change in a series of

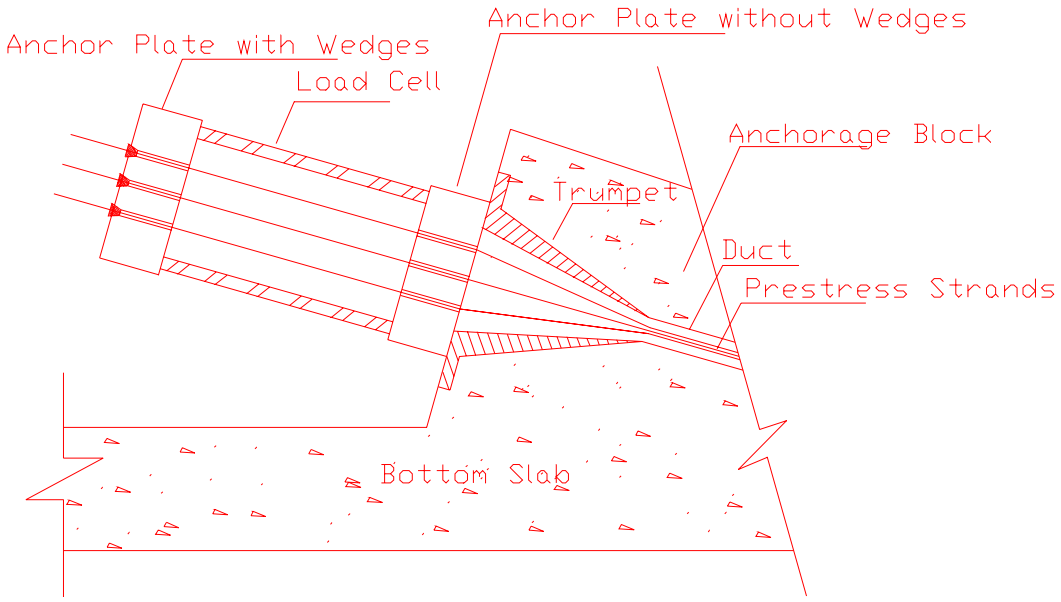

Figure 4.24: Load Cells 1 &2

steps as the increase in prestress exceeded this friction. Figure 4.26 shows a similar series of step during prestress loss. It was concluded that the load cell reading would only change when the tendon prestress differential across the inner anchorage block exceeded the friction between the tendon and the anchorage block. This would explain why the steps each represent approximate the same drop in prestress. However, results from this load cell are considered unreliable. Load cell 2 on span tendon SP1 in span P8-P9 was also placed between two anchorage blocks and so has the same disadvantages as load cell 1. In addition, load cell 2 could only be read manually

using a strain gage read out box. Results from load cell 2 are therefore also considered unreliable.

All other load cells were installed without the inner anchorage block (Figure 4.25) so as to measure the tendon prestress directly. Those load cells produced smooth prestress profiles as shown in Figures 4.28 to 4.31.

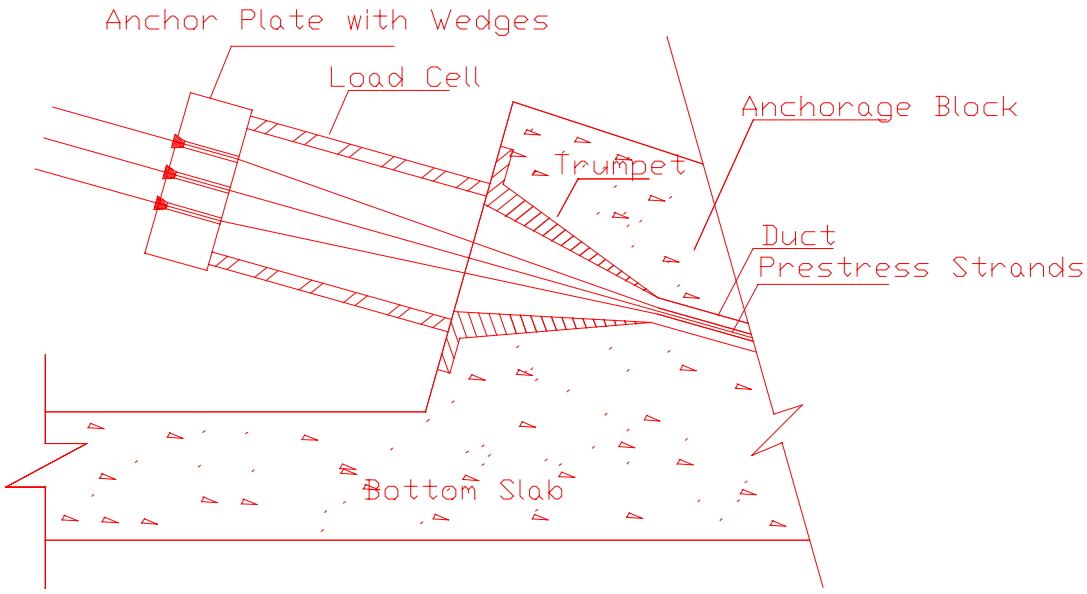

Figure 4.25: Load Cells 3, 4, 5, & 6

Each load cell was calibrated at CTL laboratory prior to shipping to the site. The resulting gage factors are used to convert the bridge reading to a load. During tendon stressing, the load cell readings were recorded using a manual readout box. Subsequently, the load cell lead wires were connected to the nearest data logger for automatic recording. Figures 4.26 to 4.31 show the variation in measured tendon forces with time. They are compared with Hoi SFRAME upper bound, lower bound, and average predictions. Load cell 4 SFRAME average predictions are close to the load cell measured values. For load cell 3, 5, and 6, the measured values are

consistently lower that the average SFRAME prediction, but still within the SFRAME bounds. This is in part attributed to the initial measured prestress forces (Table 4.3) being significantly lower than those assumed in the SFRAME analysis (Table 4.2).

These tendon force figures show that the tendon forces are continuous dropping with time. Initial losses were more rapid while the losses become more gradual in recent years. Table 4.3 summaries the tendon force changes from the initial stressing till December 2001. For the four load cells providing reliable results, the prestress losses over this period varies from 13.8% to 16.2%. These losses are similar to the AASHTO suggested lump sum loss for post-tensioning strands of 33000psi or 16.5% for the tendons in the NHVV (Nawy, 2003). Table 4.4 shows the prestress loss predicted by SFRAME for the same time period using the average of upper and lower bound predictions. The predicted losses vary form 10.4% to 27.7%. This variability in loss estimate is considerably greater than for observed losses, however the observed values fall within the predicted bounds shown in Figures 4.26 to 4.31.

Table 4.2: Load Cell Tendon Details

Load Cell	Span	Tendon	End	Length ft	Strands	Duct	Design Forces (kip)	
							As-built	Fixed end
LC1	P8-P9	9IB SP7	Fixed	196	17-½"ϕ	3– ½" OD	530	
LC2	P8-P9	9IB SP2	Fixed	52	17-½"ϕ	3– ½" OD	520	
LC3	P9-P10	10IB SP7	Fixed	188	17-½"ϕ	3– ½" OD	520	
LC4	P9-P10	10IB SP1	Fixed	44	17-½"ϕ	3– ½" OD	520	
LC5	P11-P12	12IB SP3	Stressing	96	19-½"ϕ	3– ½" OD	575	
LC6	P12-P13	13IB SP4	Stressing	110	19-½"ϕ	3– ½" OD	563	

Table 4.3 Measured Changes in Tendon Force

Load Cell	Stressing Date	Prestress forces (kips)				Remarks
		Initial	Dec 2001	Change	Percent Loss (%)	
LC1	5/25/94	369	289	80	21.7	Unreliable L.C.
LC2	6/14/94	436	389	47	10.8	Manual reading
LC3	7/2/94	367	321	56	15.3	
LC4	8/2/94	412	355	57	13.8	
LC5	9/23/94	470	394	76	16.2	
LC6	10/3/94	503	429	74	14.7	

Table 4.4 Average SFRAME Predicted Changes in Tendon Force

Load Cell	Stressing Day	Prestress forces (kips)			
		Initial	Dec 2001	Change	Percent Loss (%)
LC1	93	477	345	132	27.7
LC2	113	439	350	89	20.3
LC3	131	465	365	100	21.5
LC4	161	417	354	63	15.1
LC5	214	496	425	71	14.3
LC6	224	512	459	53	10.4

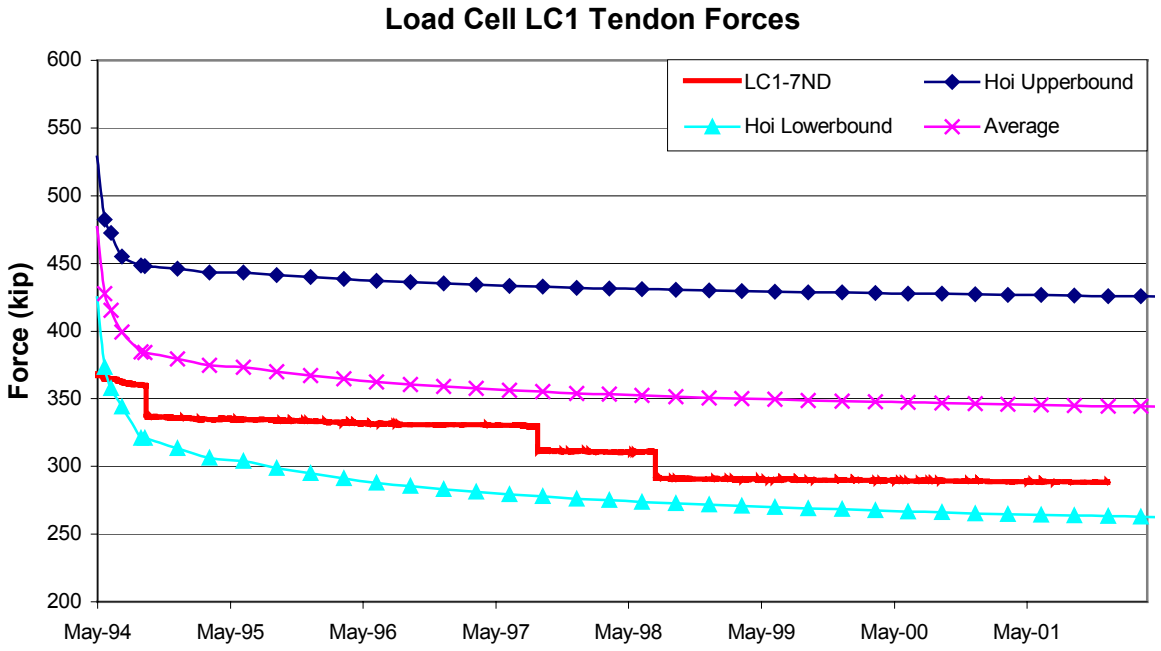

Figure 4.26: Load Cell LC1 Tendon Forces 1994-2001

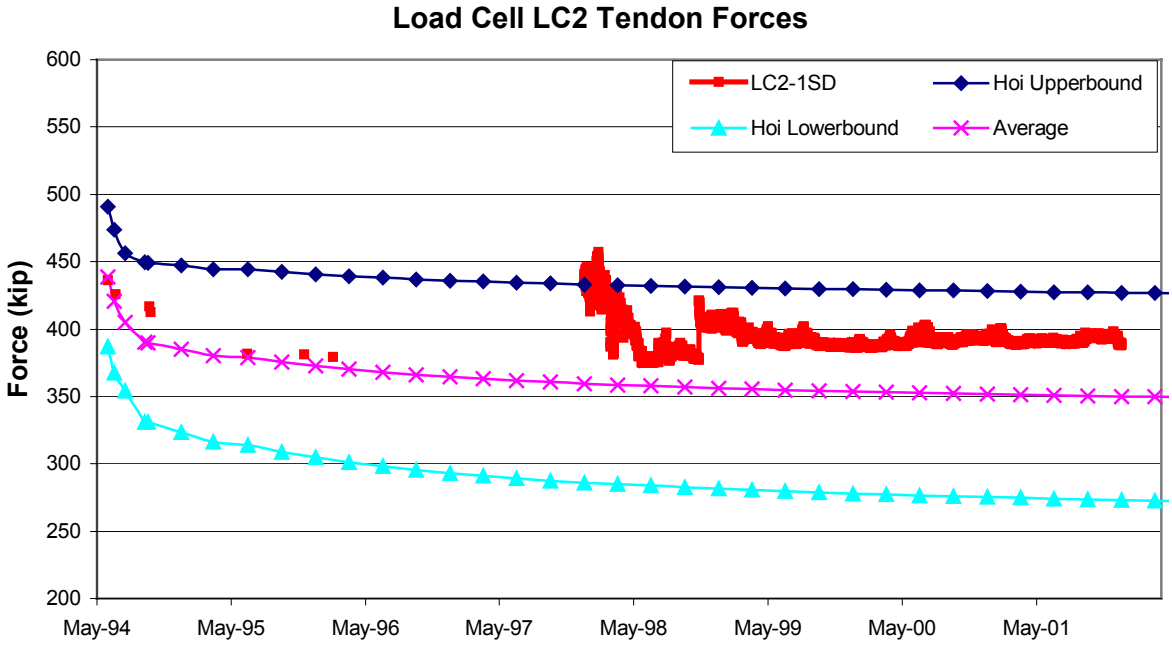

Figure 4.27: Load Cell LC2 Tendon Forces 1994-2001

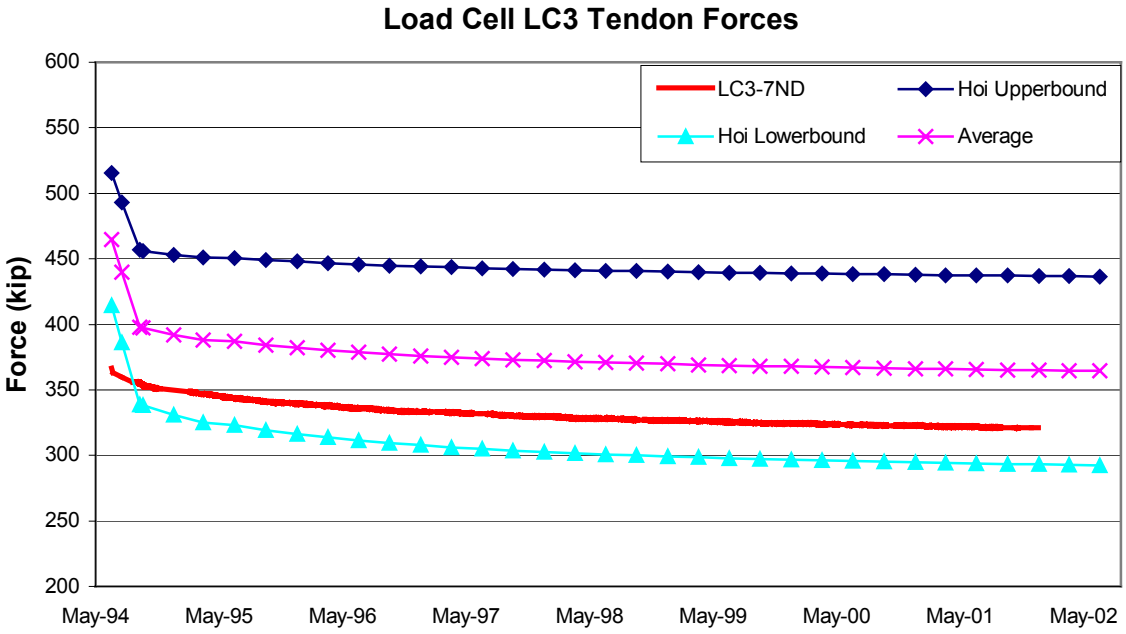

Figure 4.28: Load Cell LC3 Tendon Forces1994-2001

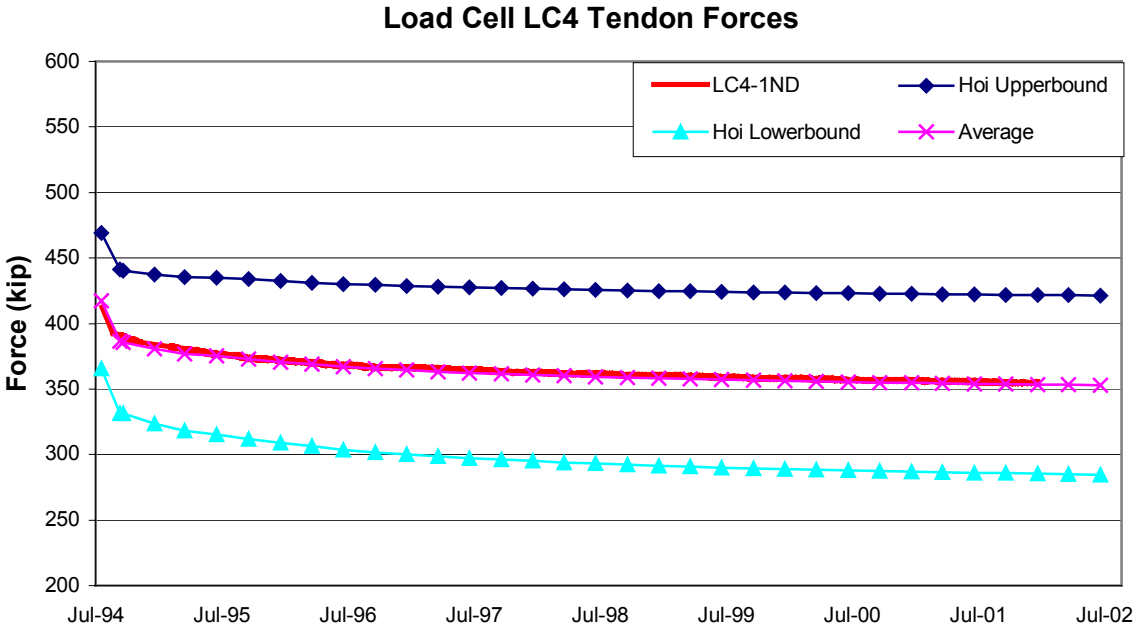

Figure 4.29: Load Cell LC4 Tendon Forces 1994-2001

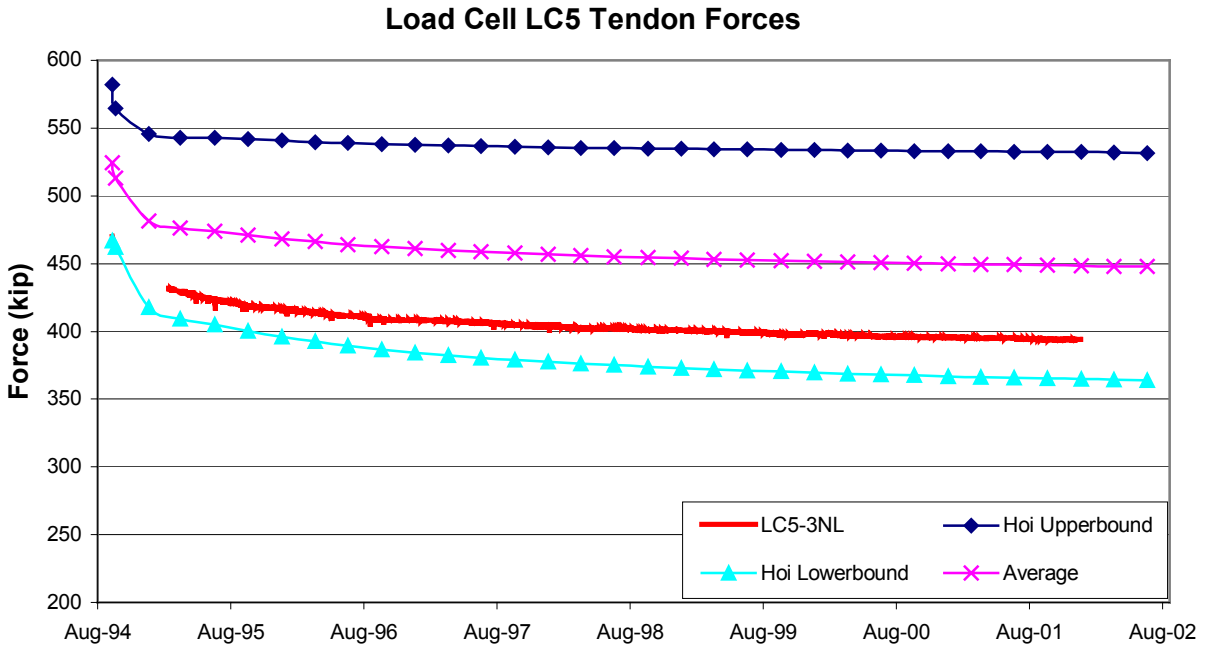

Figure 4.30: Load Cell LC5 Tendon Forces 1994-2001

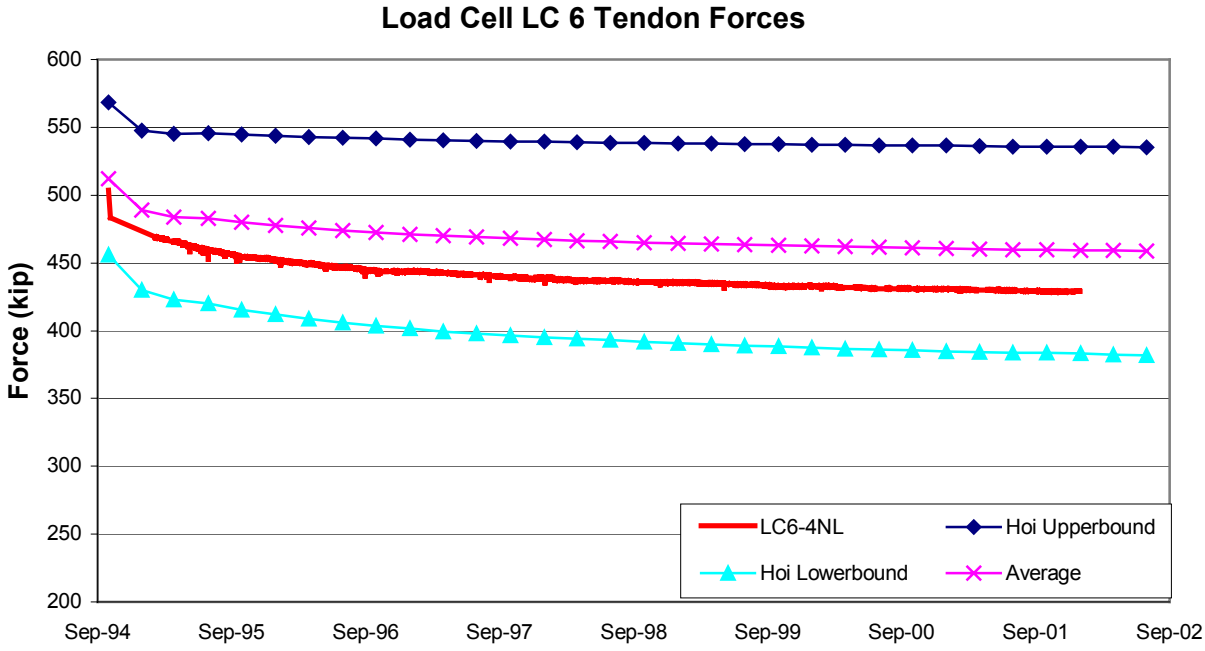

Figure 4.31: Load Cell LC6 Tendon Forces 1994-2001

CHAPTER 5

VERTICAL DEFLECTION—OPTICAL SURVEY

5.1 Introduction

Predicting the complete time dependent response of a segmentally erected box girder bridge is very complex. The response depends on time dependent material properties such as the uncertainty of concrete properties, the tendon prestress losses, the variability of environment, and the construction sequence. Accurate prediction of time dependent deflections of a concrete bridge structure due to creep and shrinkage is complicated by the wide range of physical properties of concrete. The creep and shrinkage characteristics of concrete are highly variable and are never exactly known. Creep and shrinkage vary with aggregate type, ambient temperature, relative humidity, applied stress, volume to surface ratio, and other factors. They also vary with time, location, and from concrete batch to batch even when the same raw materials and mix design are used.

In this chapter, the optical survey results, which represent the actual vertical deflection of the NHVV, are presented along with base-line deflection measurements for the instrumented spans of Unit 2IB. The T. Y. Lin as-built models, which represent the original SFRAME deflection predictions, are also presented for comparison with the optical survey and base-line measurements.

5.2 Long-Term Deflection—Optical Survey

The initial base-line system readings were taken on March 29th, 1995 along with an optical survey of the NHVV roadway. The base-line system installed in Unit 2IB is described by Dong

and Robertson (1999). Subsequent readings were recorded at various dates. Follow up optical surveys of the entire NHVVwere made on June 19, 1997, and May 1, 1999. The differences between the initial and subsequent readings represent the span deflection during each time period. For corresponding vertical deflection predictions, the dates of the field readings were converted to an equivalent number of days after start of construction in the time domain of SFRAME for the specified unit. Table 5.1 lists the equivalent days of each unit on March 29 1995, which is treated as the base line measurement date, when the first optical survey was conducted for both inbound and outbound viaducts. Equivalent days are also given for each of the subsequent optical surveys.

Table 5.1 SFRAME Equivalent Days for Optical Survey on Each Unit

Date of Optical survey	3/29/1995	6/19/1997	5/1/1999
Unit IB1	712	1525	2206
Unit IB2	401	1214	1895
Unit IB3	391	1204	1885
Unit OB1	842	1656	2337
Unit OB2	421	1234	1914
Unit OB3	891	1704	2384

For any input date, the SFRAME output file gives the vertical position of each node. To isolate pure span deflections, the pier settlement must be eliminated from the total vertical movement. The vertical position of the nodes in a span must first be normalized relative to a straight line joining the two ends of the span. To do this, the deflection of each pier center is set to zero. Normalization along this straight line eliminates the effect of pier shortening and settlement. In this way, the pure span deflection can be isolated and compared with the base-line field measurements. The difference between the normalized vertical position at the initial and

subsequent dates represents the predicted deflection during each time period. Comparisons between the normalized base-line reading and predicted deflection up to 1997 are presented by Dong and Robertson (1999). In their study, they compared the Unit 2IB base-line and optical survey deflections with the SFRAME prediction so as to evaluate the SFRAME as-built model predictions. They concluded that the T. Y. Lin as-built model substantially underestimates long-term deflection for the longest span P8-9. Discrepancies also occur in all other spans to different degrees. This report repeats the 1995-1997 vertical deflection comparison for Unit 2IB, and extends the comparison to the other five units of the NHVV. Vertical deflections between 1995 and 1999 are also presented in this study and compared with the T. Y. Lin as-built model predictions. Figures 5.1 to 5.12 present the 1995-1997 and 1995-1999 vertical deflections versus the T.Y. Lin as-built model prediction for all six units. The figures show that the T.Y. Lin as-built model significantly underestimates the bridge vertical deflection for some of the longer spans, while over-predicting deflections for other spans. Figures 5.3 and 5.4 also include the base-line system measurement of vertical deflections for 1995-1997 and 1995-1999, which confirm the optical survey results.

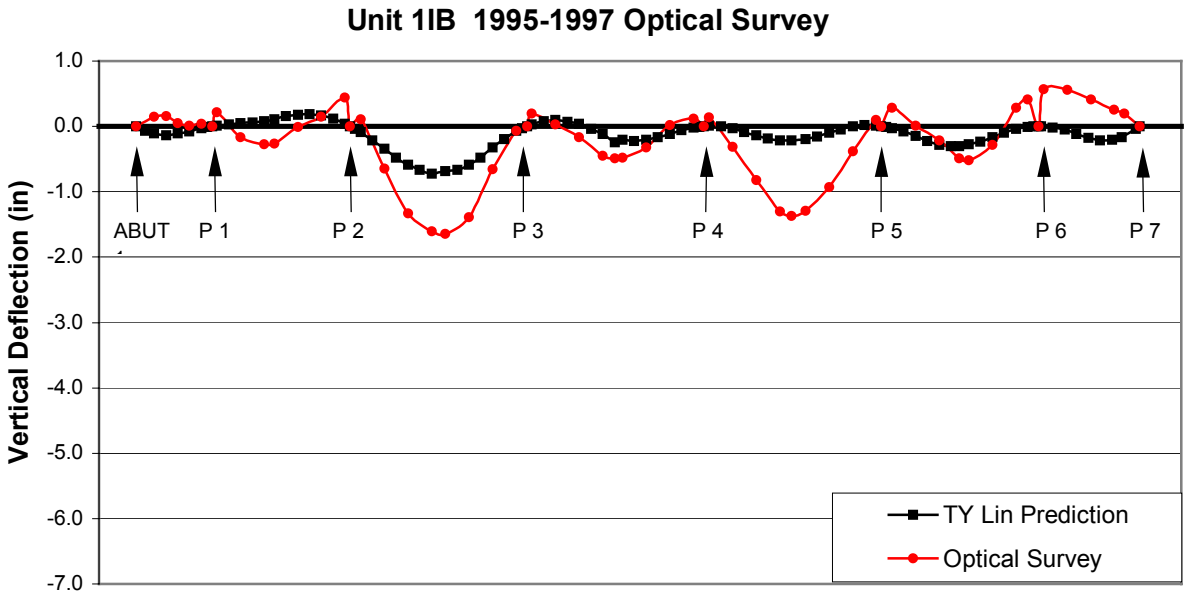

Figure 5.1: Unit 1IB Vertical Deflection -- Optical Survey (1995-1997)

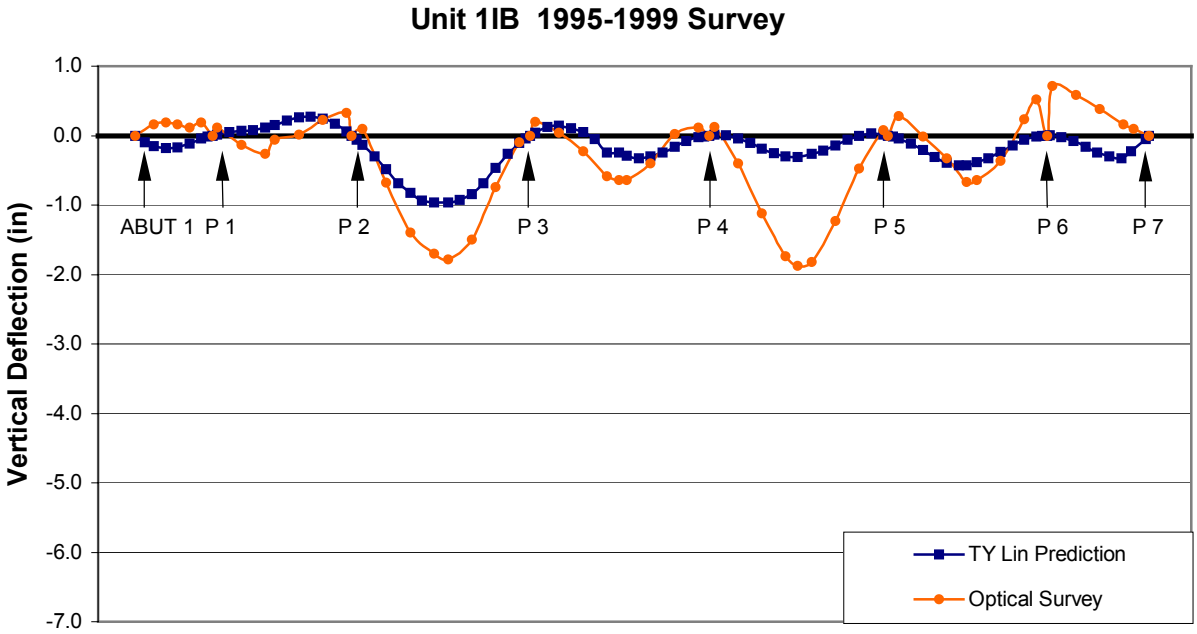

Figure 5.2: Unit 1IB Vertical Deflection -- Optical Survey (1995-1999)

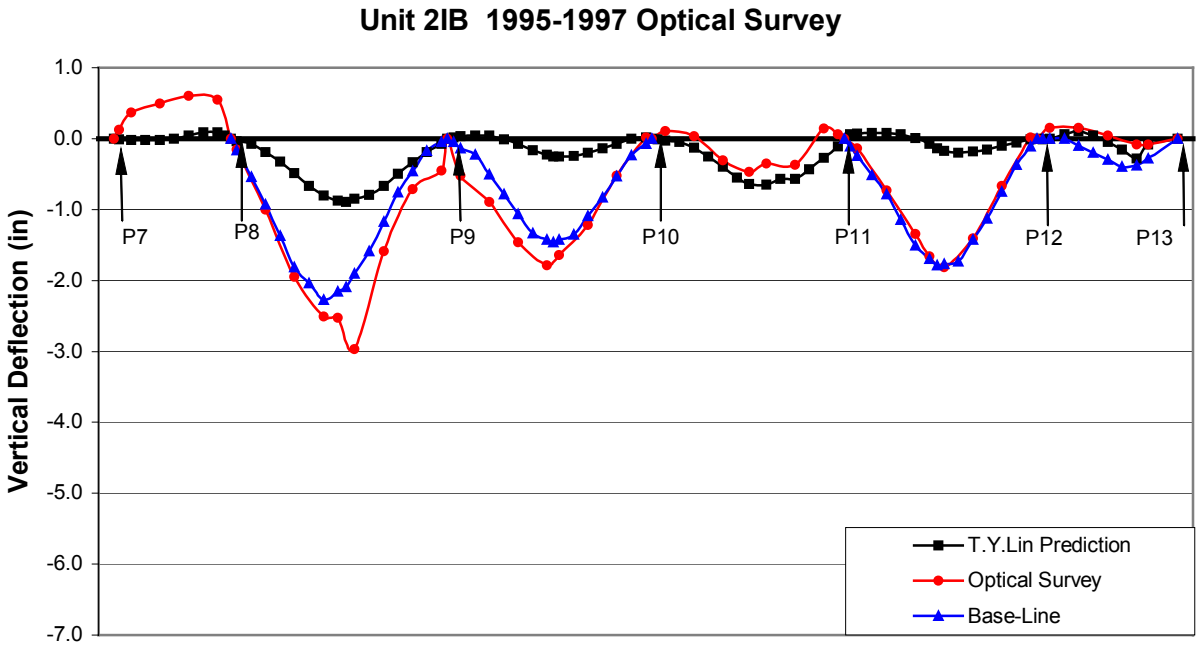

Figure 5.3: Unit 2IB Vertical Deflection -- Optical Survey (1995-1997)

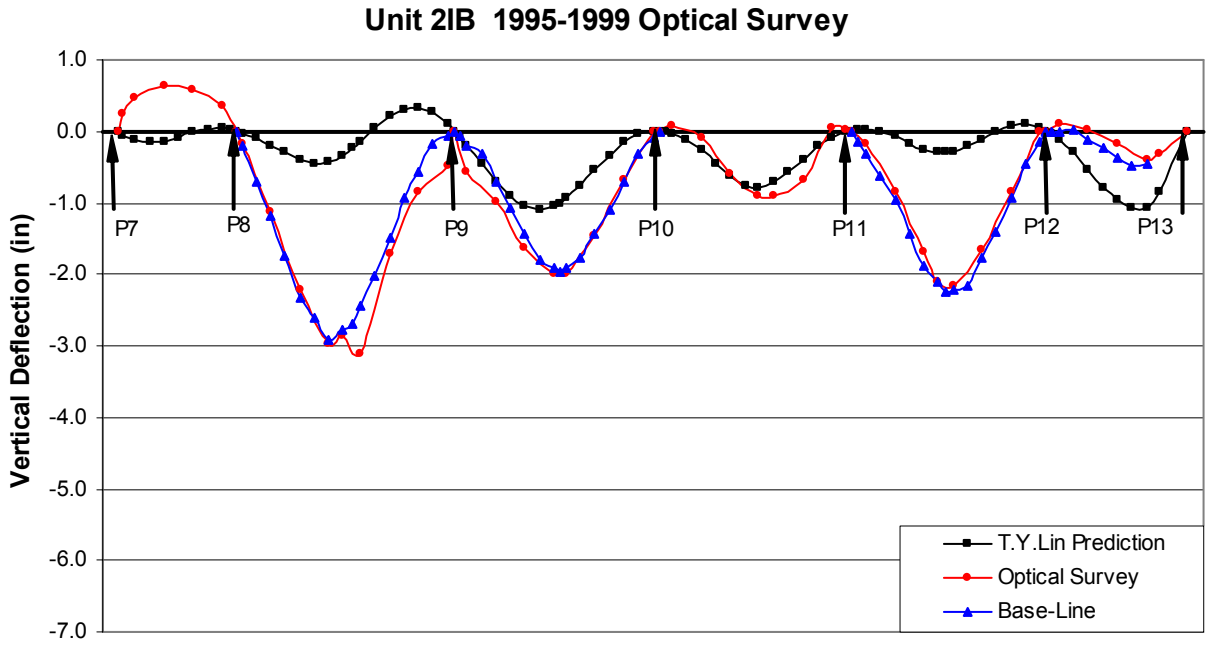

Figure 5.4: Unit 2IB Vertical Deflection -- Optical Survey (1995-1999)

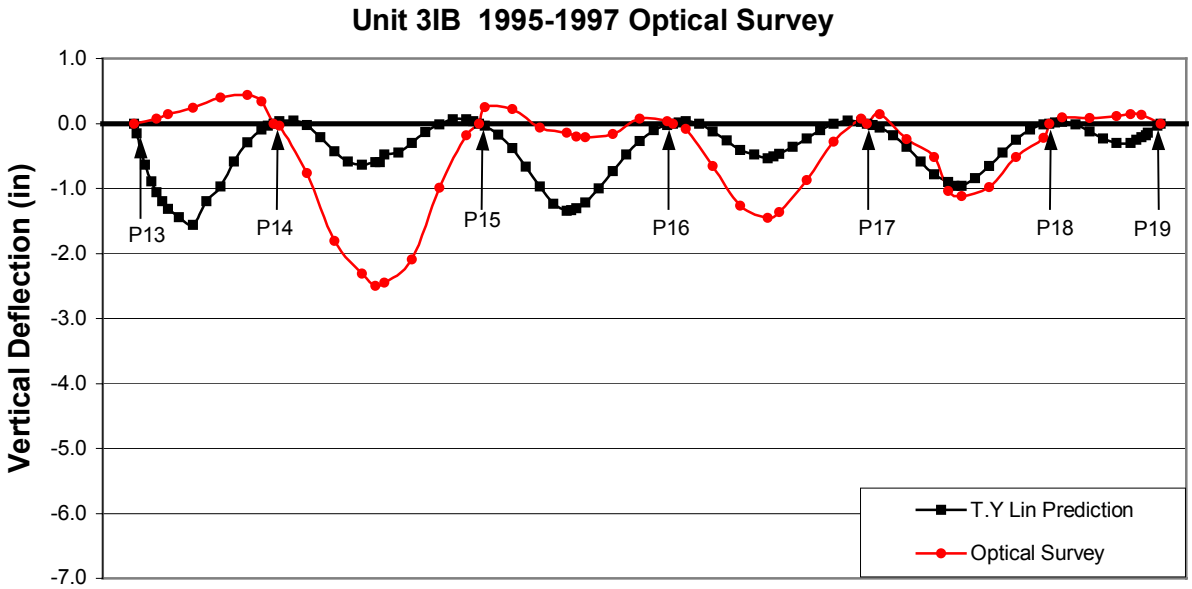

Figure 5.5: Unit 3IB Vertical Deflection -- Optical Survey (1995-1997)

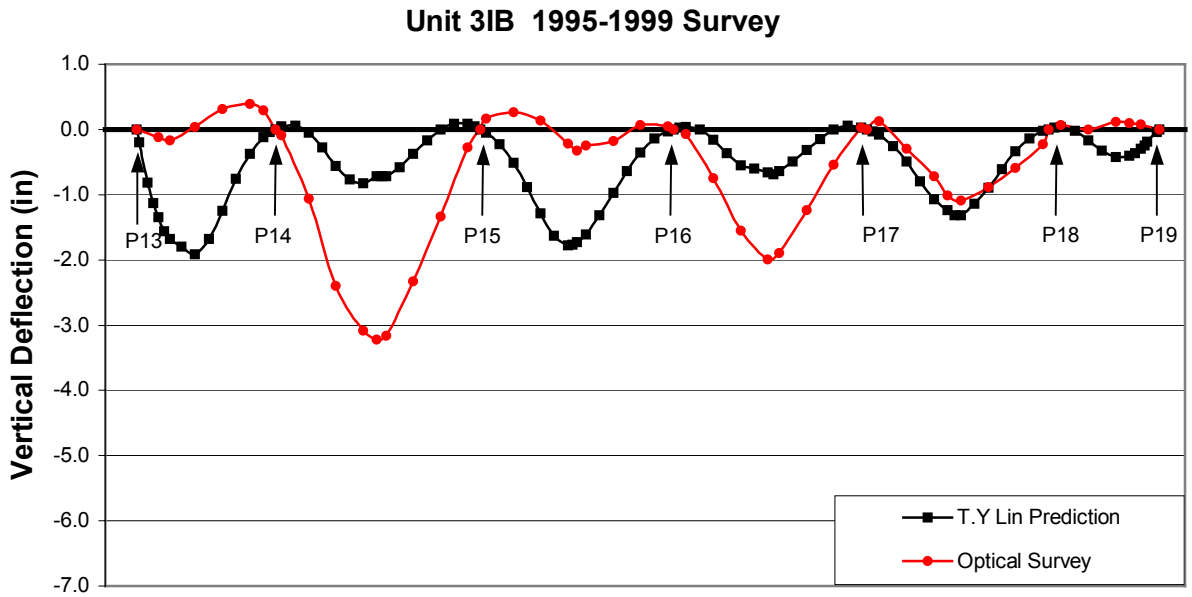

Figure 5.6: Unit 3IB Vertical Deflection -- Optical Survey (1995-1999)

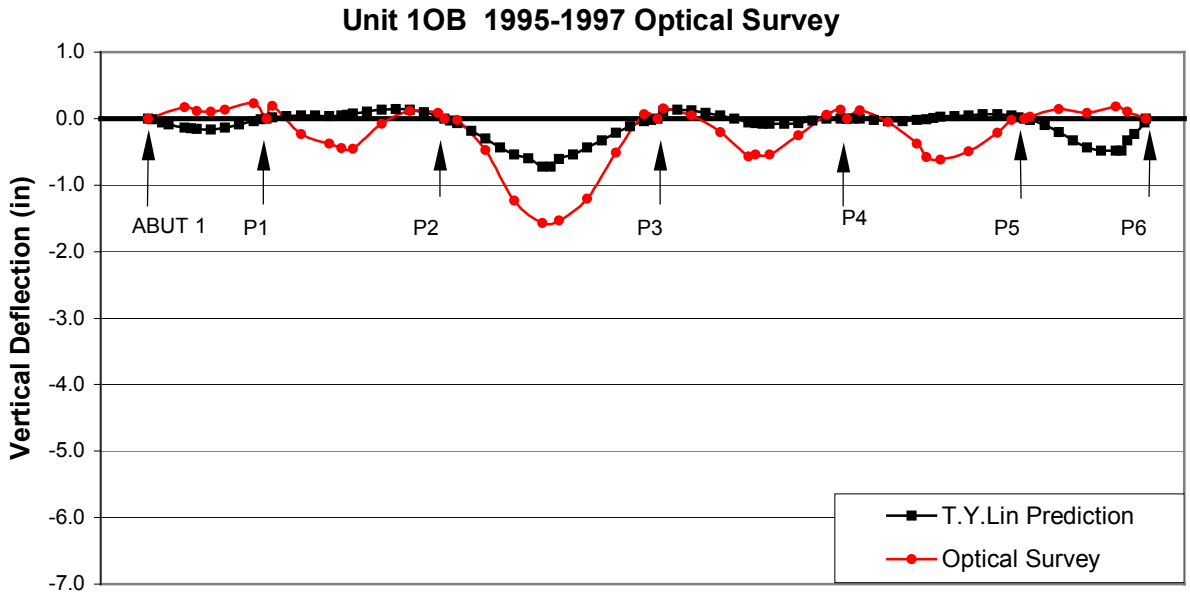

Figure 5.7: Unit 1OB Vertical Deflection -- Optical Survey (1995-1997)

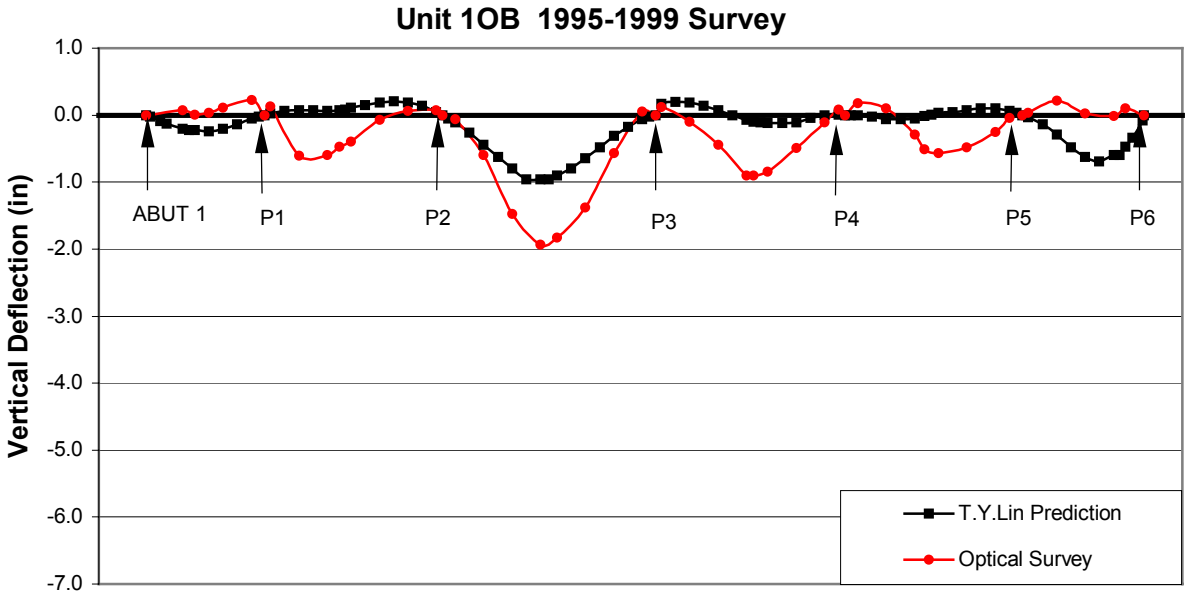

Figure 5.8: Unit 1OB Vertical Deflection -- Optical Survey (1995-1999)

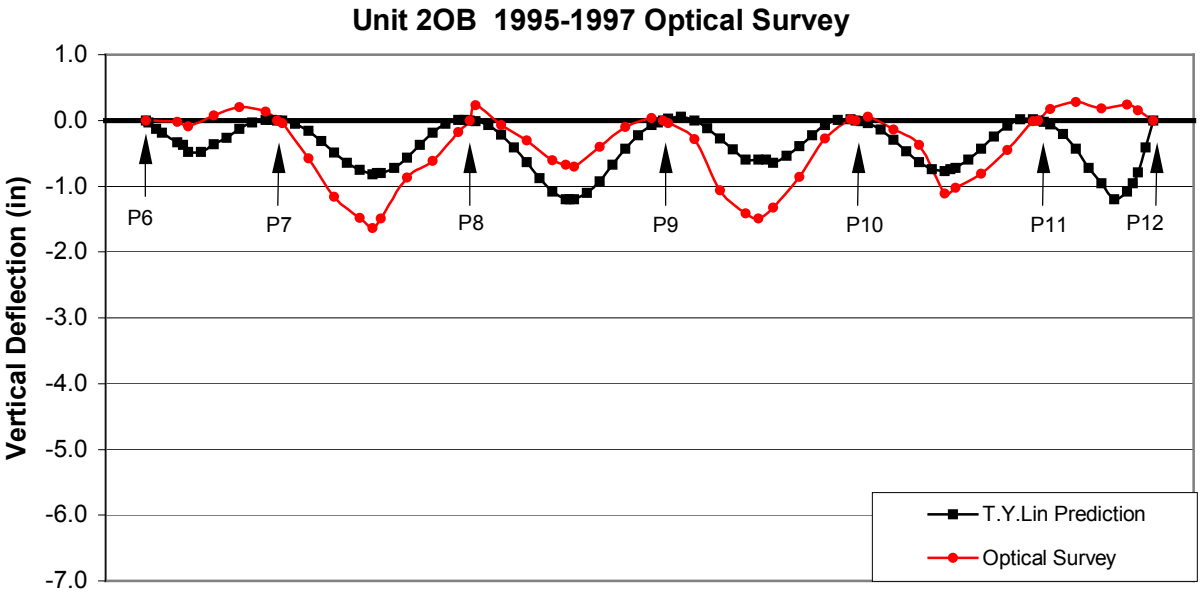

Figure 5.9: Unit 2OB Vertical Deflection -- Optical Survey (1995-1997)

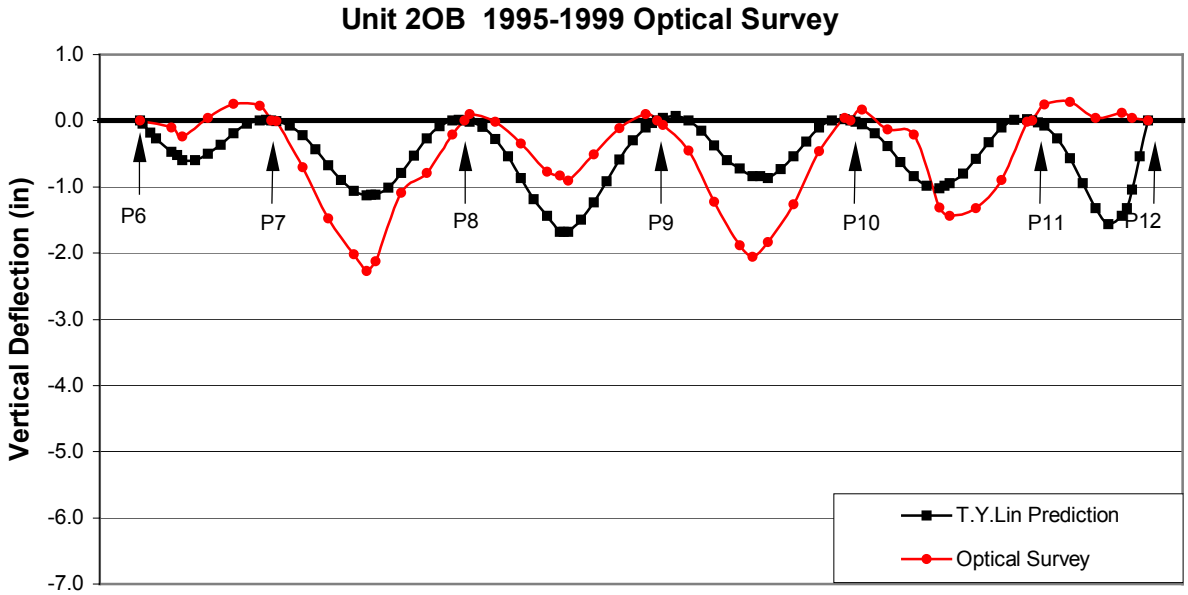

Figure 5.10: Unit 2OB Vertical Deflection -- Optical Survey (1995-1999)

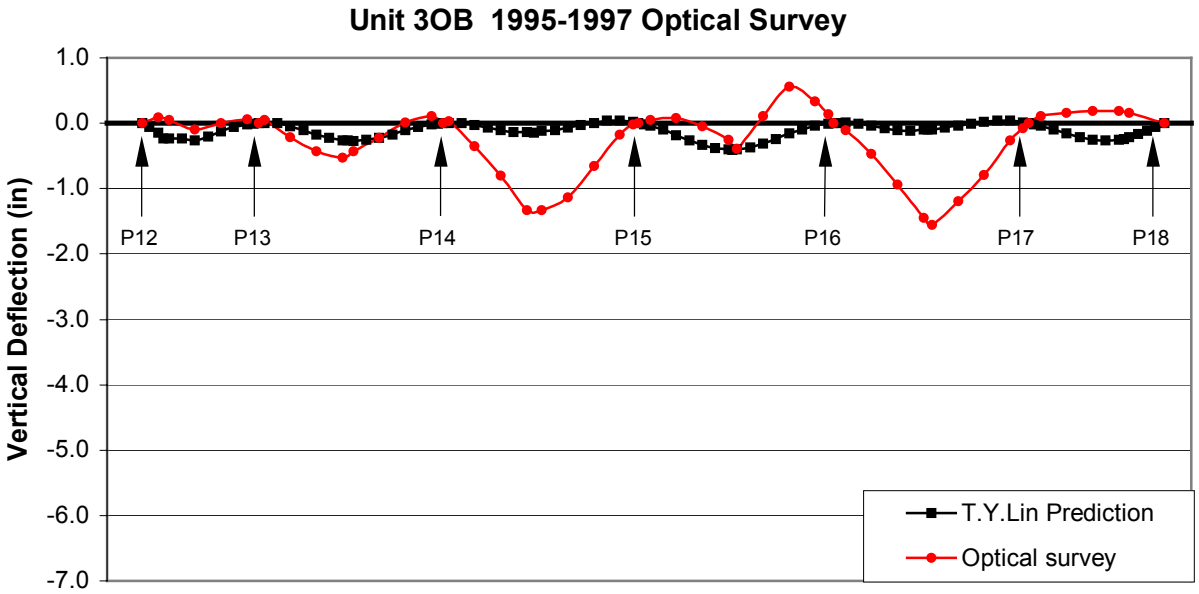

Figure 5.11: Unit 3OB Vertical Deflection -- Optical Survey (1995-1997)

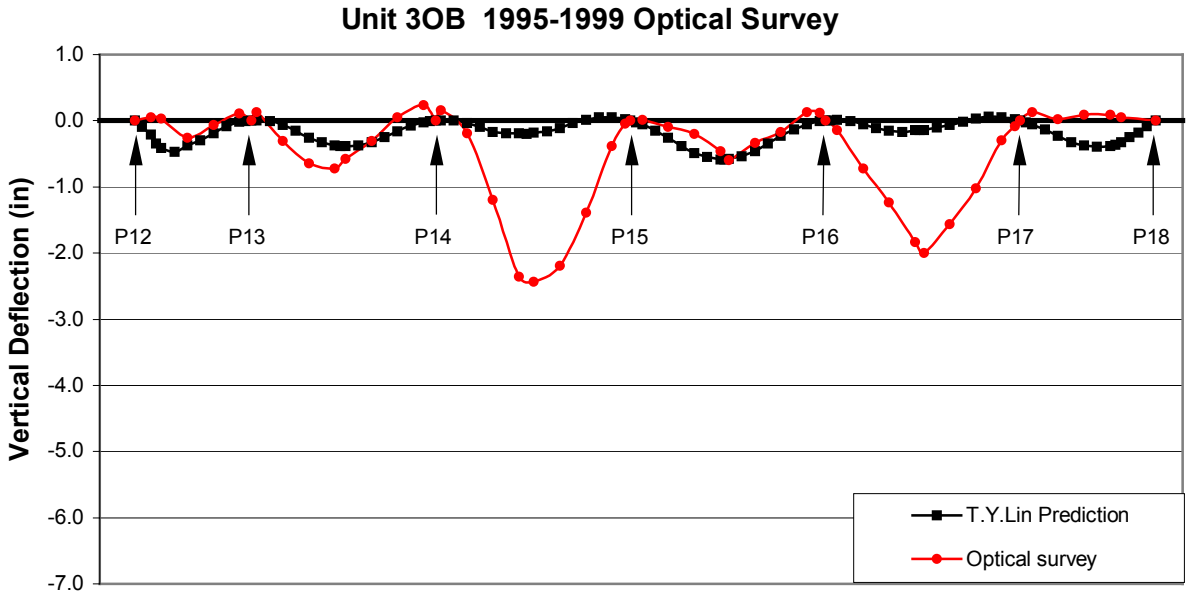

Figure 5.12: Unit 3OB Vertical Deflection -- Optical Survey (1995-1999)

CHAPTER 6

DEVELOPMENT OF VERTICAL DEFLECTION ENVELOPE

6.1 Introduction

In this chapter, SFRAME is used to provide analytical prediction of the long-term vertical deflection. These analytical predictions are compared with the optical survey results, which represent the actual deflection. As shown in Chapter 5, the T. Y. Lin as-built models, which represent the original design modified for as-built conditions, do not provide satisfactory prediction of the measured deflection. This disagreement between the analytical and observed deflections is mainly attributed to the assumptions made regarding the anticipated concrete material properties, such as creep and shrinkage coefficients. Based on short-term creep and shrinkage data from the Unit 2IB concrete, Dong and Robertson (1999) considered various adjustments to the material property models for Unit 2IB. These results were turned to match the field measurements for the Unit 2IB. This model was subsequently adjusted by Hoi and Robertson (2003) based on feedback from T.Y. Lin International to produce the Hoi finalmodel. The SFRAME predictions of Hoi finalmodels for all six units of the NHVV are presented in Section 6.2.

A single set of assumed input parameters cannot be expected to provide accurate deflection predictions for all spans of a multi-span viaduct. It is therefore necessary for the designer to create a reasonable bound for these parameters and develop upper and lower bounds so as to provide more realistic deflection envelopes. Although these parameter combinations do not provide the actual prediction, they provide a reasonable upper and lower bound of the bridge's

long-term deflection. There is no instrumentation installed in the other five units, and no lab data available for those five units. Therefore, the upper and lower bounds for the other five units are based on the same parameters as those used in Unit 2IB.

The parameters which affect the deflection predictions are discussed in Section 6.3. The parameter combinations used to create upper and lower bound of vertical deflection predictions are presented in Section 6.4. The vertical deflection prediction envelopes are presented in Section 6.5.

6.2 Hoi Finalmodel Predictions

Based on the optical survey and base-line system measurements of vertical deflections, Dong and Robertson (1999) create a SFRAME finalmodel input file, Hoi and Robertson (2003) refined this model, which provides accurate prediction for most spans of Unit 2IB. To investigate whether this model is suitable for the other five units, the same parameter combinations are used in SFRAME analysis of the other five units to create finalmodel output for each unit.

The finalmodel parameters are as follows:

- Relative humidity: 85%
- Creep scaling factor: 1.3
- Shrinkage scaling factor: 0.7
- Prestressing force scaling factor for span tendon, cantilever tendon, and continuity tendons: 0.9.

Figures 6.1 to 6.12 show SFRAME finalmodel vertical deflection predictions of all six units for 1995-1997 and 1995-1999, compared with the optical survey. It can be concluded that the

finalmodels vertical deflection predictions close to the optical survey results in some spans, while under-predicted or over-predicted in other spans. It also can be concluded that a single set of input parameters combination cannot provide accurate deflection prediction for all spans of a multi-spans viaduct.

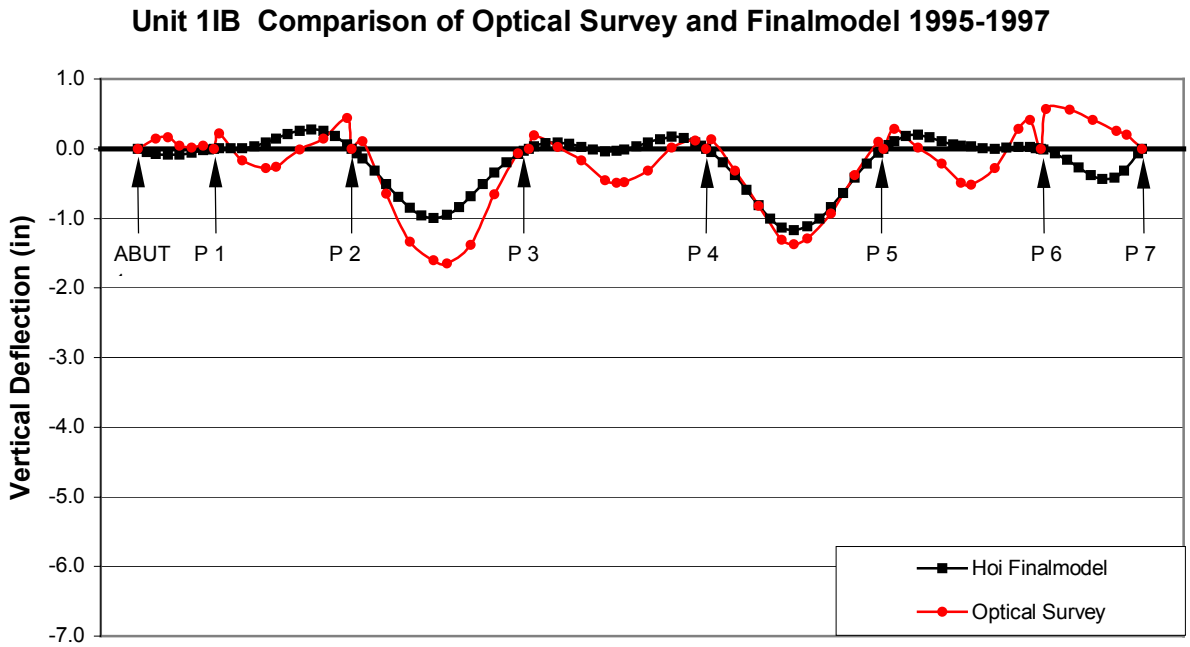

Figure 6.1: Unit 1IB Finalmodel Vertical Deflection 1995-1997

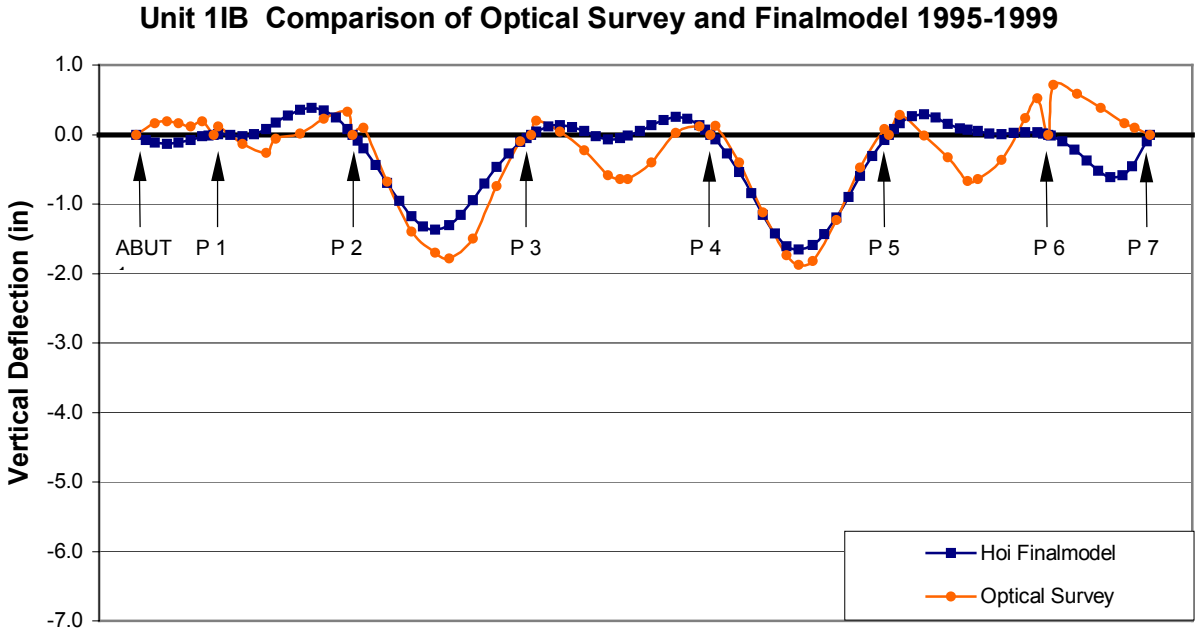

Figure 6.2: Unit 1IB Finalmodel Vertical Deflection 1995-1999

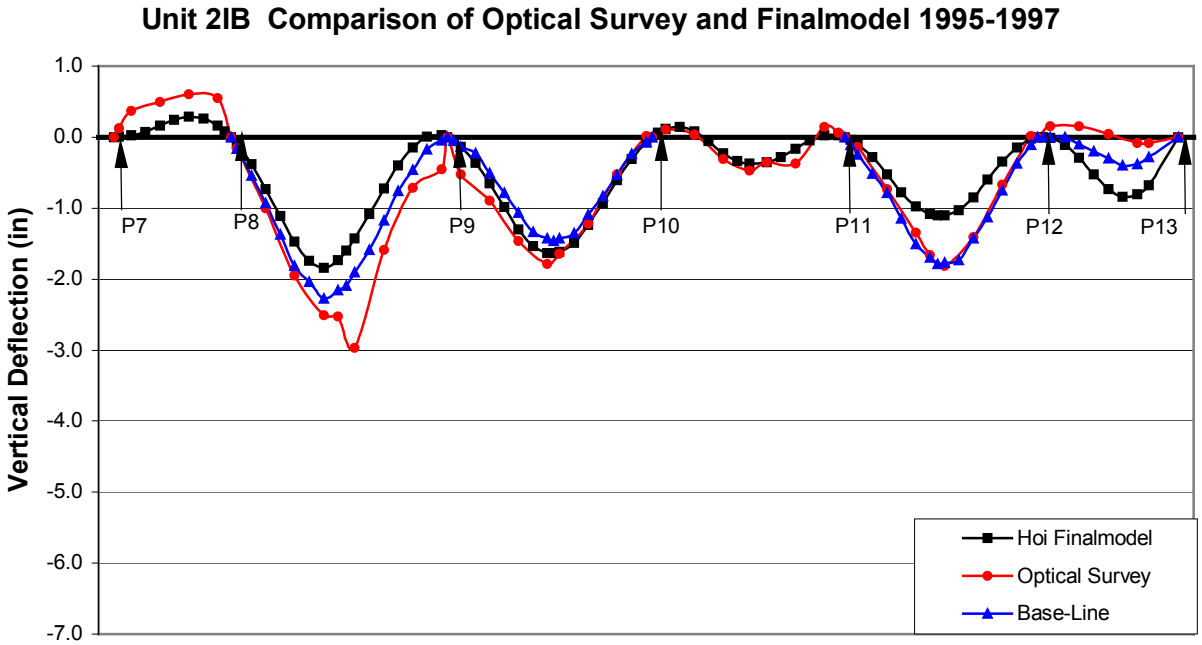

Figure 6.3: Unit 2IB Finalmodel Vertical Deflection 1995-1997

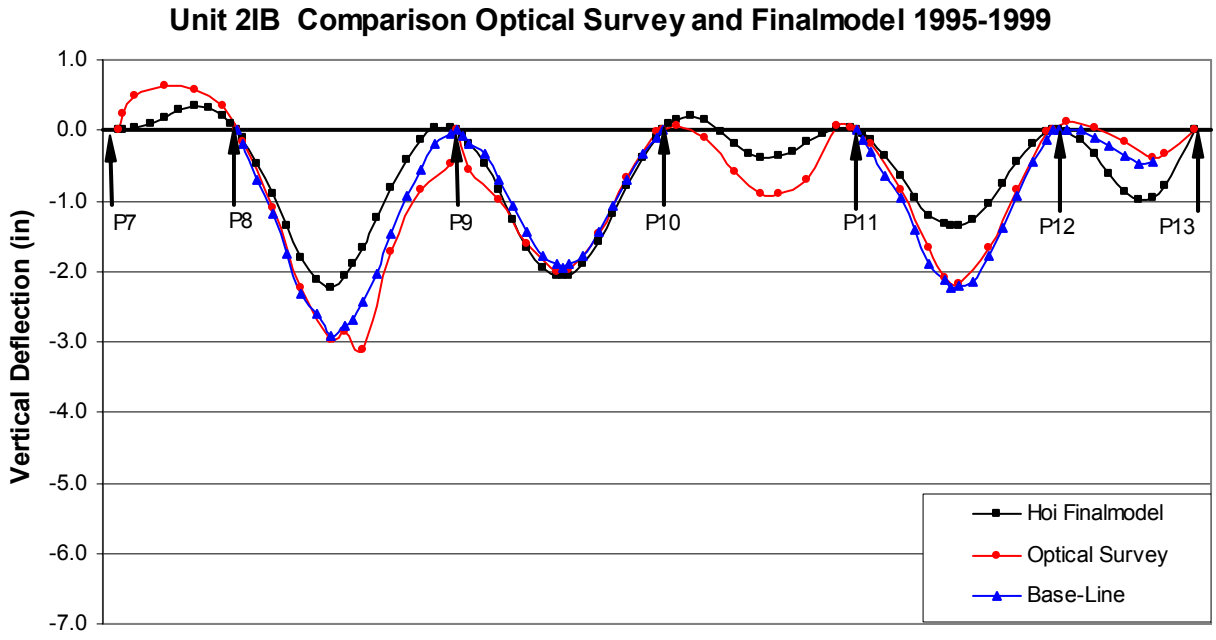

Figure 6.4: Unit 2IB Finalmodel Vertical Deflection 1995-1999

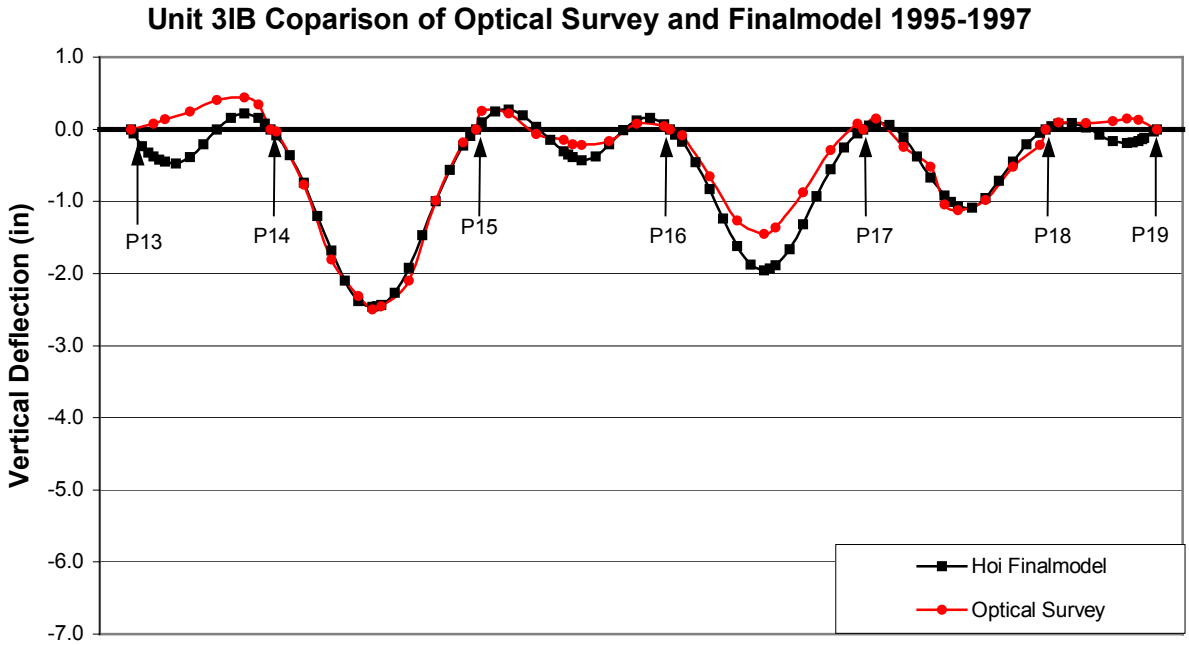

Figure 6.5: Unit 3IB Finalmodel Vertical Deflection 1995-1997

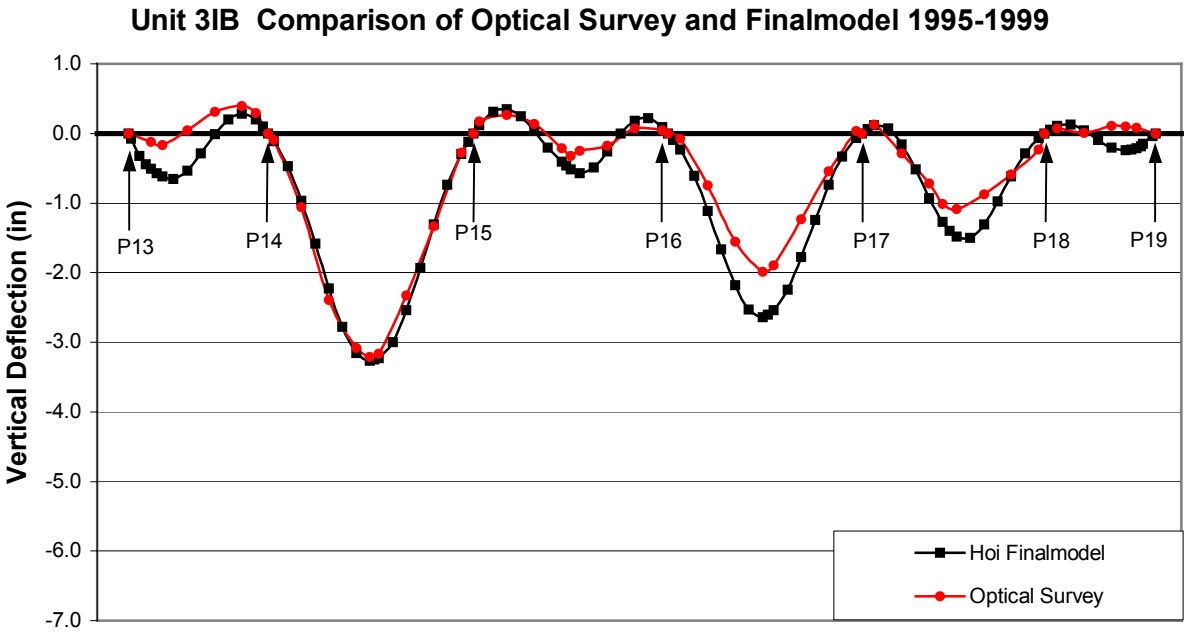

Figure 6.6: Unit 3IB Finalmodel Vertical Deflection 1995-1999

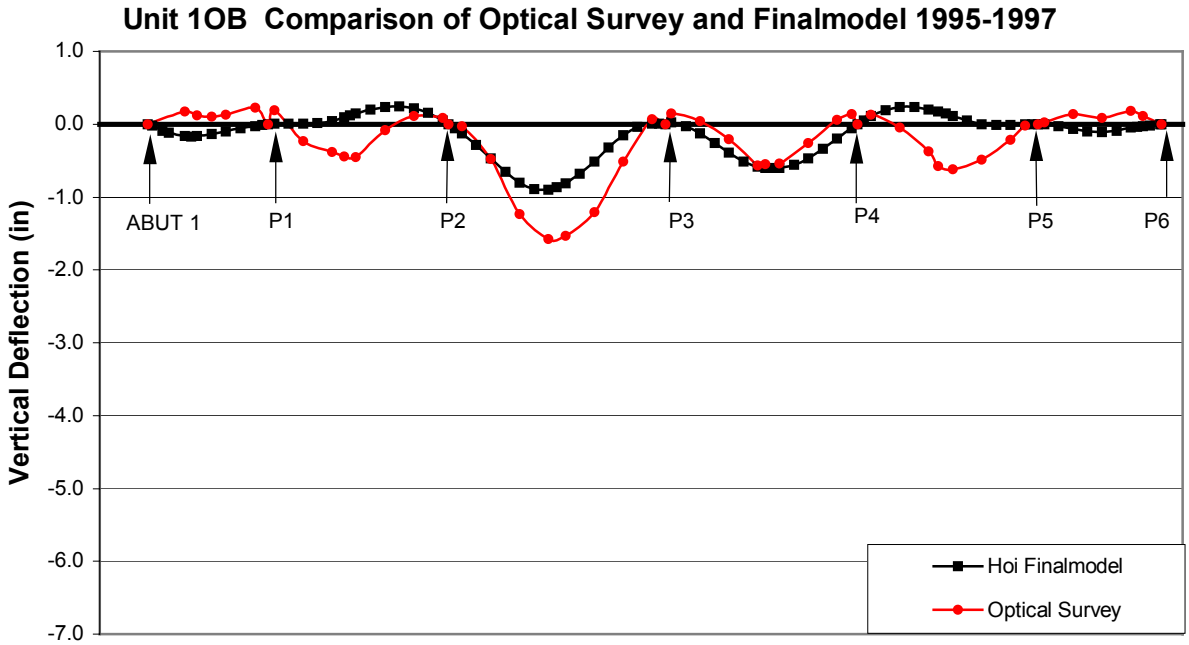

Figure 6.7: Unit 1OB Finalmodel Vertical Deflection 1995-1997

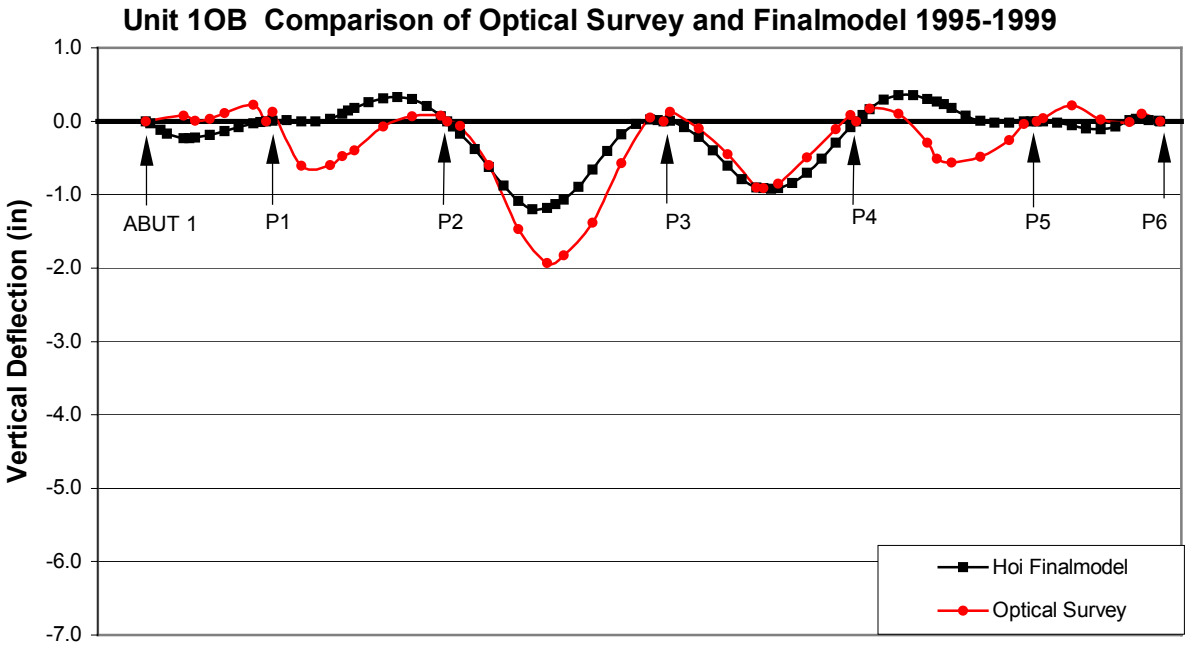

Figure 6.8: Unit 1OB Finalmodel Vertical Deflection 1995-1999

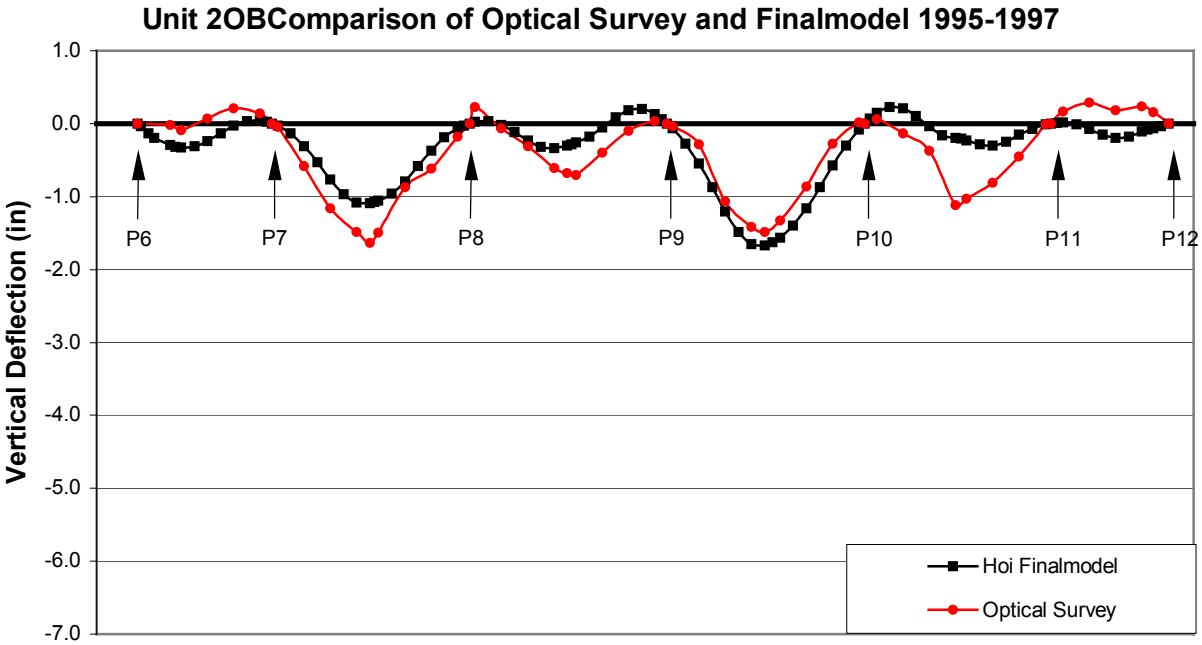

Figure 6.9: Unit 2OB Finalmodel Vertical Deflection 1995-1997

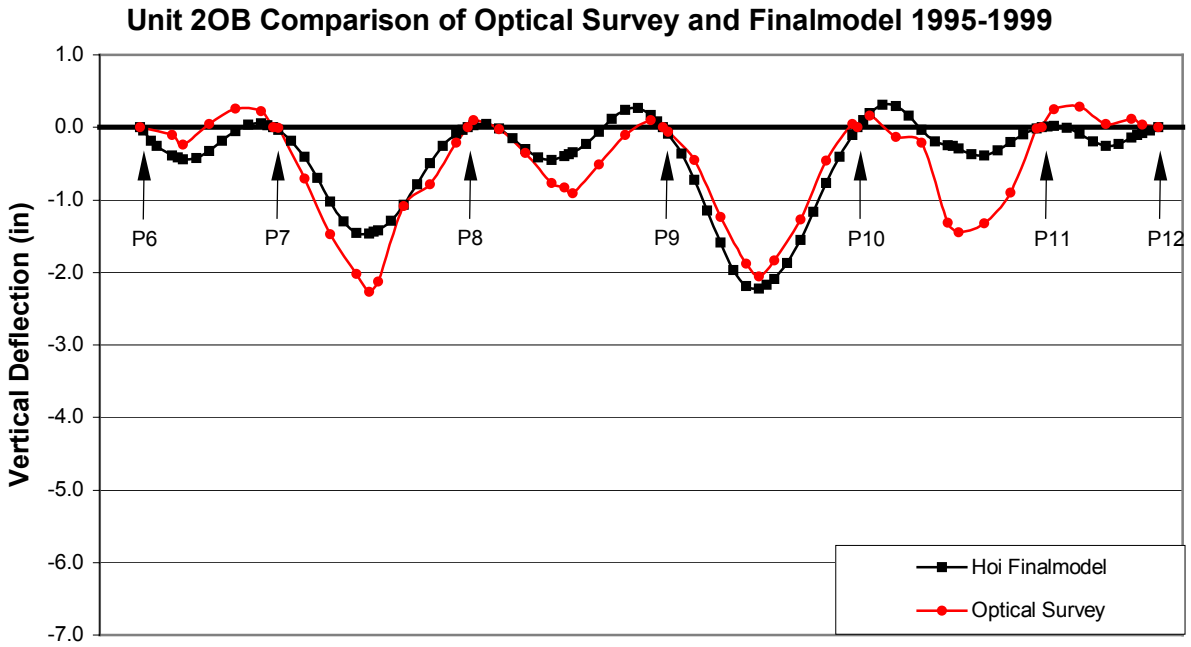

Figure 6.10: Unit 2OB Finalmodel Vertical Deflection 1995-1999

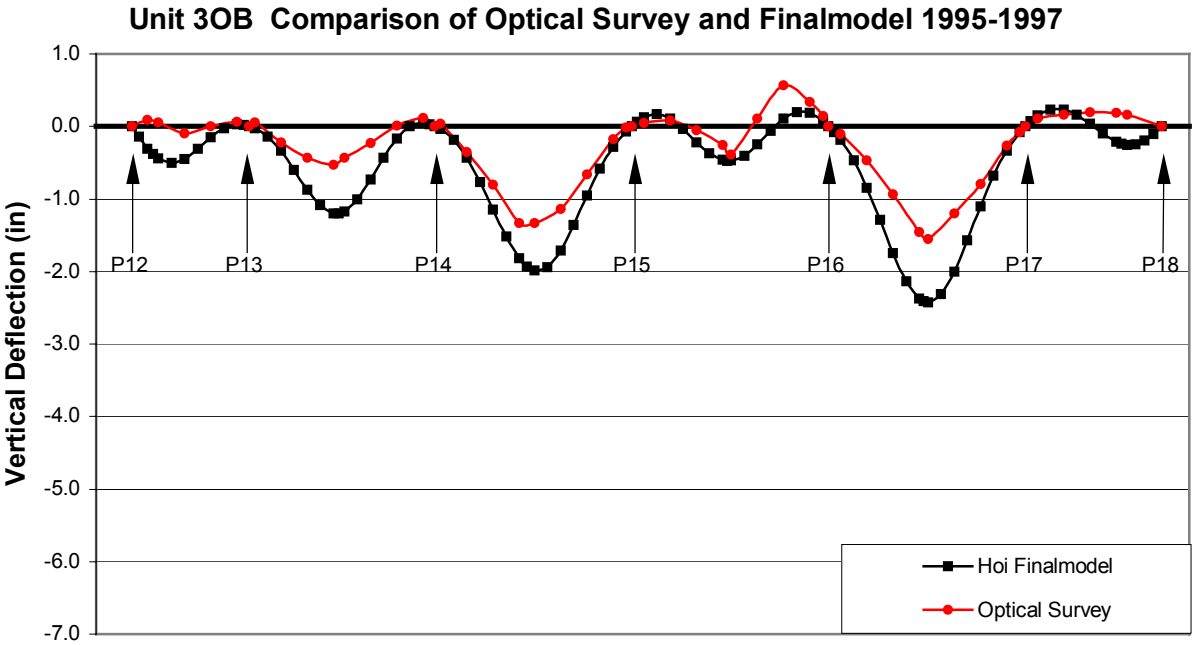

Figure 6.11: Unit 3OB Finalmodel Vertical Deflection 1995-1997

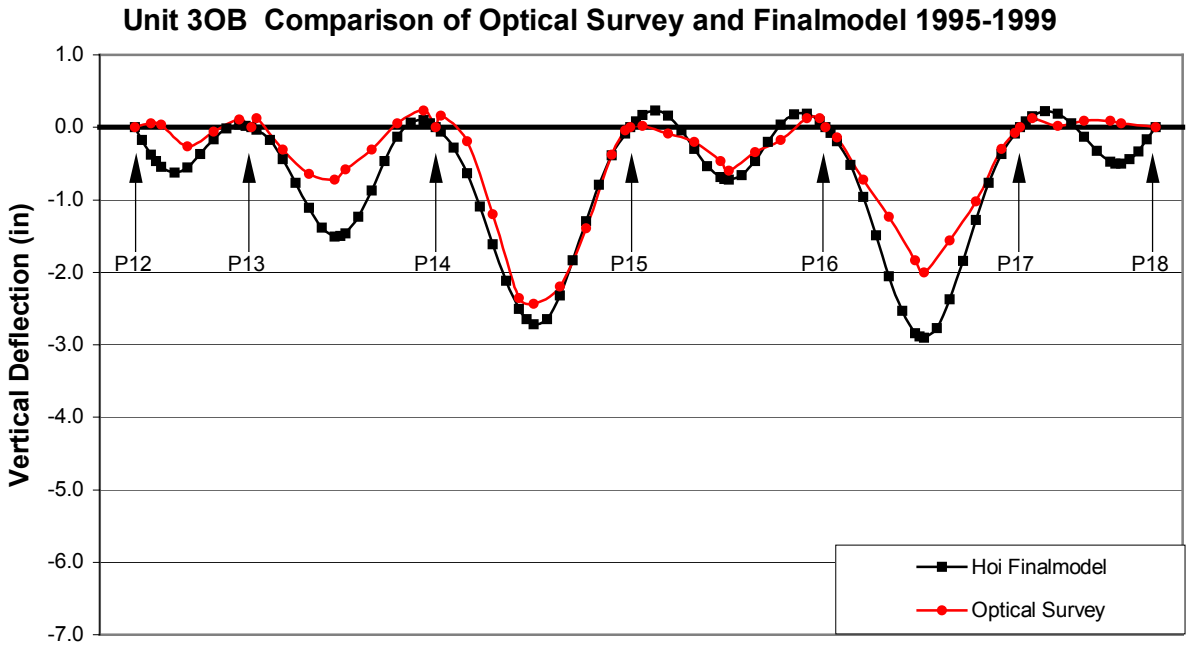

Figure 6.12: Unit 3OB Finalmodel Vertical Deflection 1995-1999

6.3 Range of Parameters

The CEB creep and shrinkage models used in the T.Y. Lin as-built analysis underestimated both the creep and shrinkage strain for the concrete used in the NHVV (Dong & Robertson, 1999). To create the upper and lower bound of the envelope, all parameters are chosen to reflect the anticipated variation under NHVV conditions. Dong and Robertson (1999) addressed the parameter ranges; Hoi and Robertson (2003) refined these ranges based on feedback from T. Y. Lin regarding tendon prestress levels.

Creep and shrinkage of concrete are known to have variability of ± 30% (Gilbert, 1988). The NHVV concrete creep and shrinkage measured under constant temperature and humidity conditions in the laboratory show variations of ± 25% (Durbin and Robertson, 1998). Therefore, it is likely that creep and shrinkage predictions in the field could vary by ± 30%. The upper and lower bounds for creep and shrinkage scaling factors are therefore set at 0.7 and 1.3 respectively.

The daily average relative humidity measured in the field varied from about 80% to 90% (Dong & Robertson 1999). Hence, the upper and lower bounds of the relative humidity are selected as 90% and 80% respectively. The creep and shrinkage components of the concrete constitutive model were modified accordingly.

As observed in the span tendon stressing described in Chapter 4, prestressing forces in tendons will deviate from the design values. Based on the load cell measurements addressed in section 4.4, 85% of the design prestressing force is a reasonable lower bound for the span tendons. Based on feedback from engineers at T.Y. Lin international, the lower bound for prestressing

forces in the cantilever and continuity tendons are set at 90% of the design values. Since both prestress force and extension measurements are used to measure the initial jacking forces, the prestress force is not likely to exceed the design values by more than about 5%. Hence 105% is set as the upper bound prestress limit.

6.4 Parameter Combinations

Based on the parameter ranges discussed above, the most favorable conditions are combined to create the upper bound, which represents the minimum vertical deflection. All the least favorable conditions are combined to create the lower bound, which represents the maximum vertical deflection. Dong and Robertson (1999) considered concrete self-weight as a variable to develop these envelopes. However, measurement of concrete self-weight by CTL shows little variation among different batches using the same raw materials and mix design. This parameter was therefore not considered as variable in developing the bounds presented in this report.

The parameters providing the lower bound (maximum) deflections for all spans are as follow:

- relative humidity: 80%,
- creep scaling factor: 1.3,
- shrinkage scaling factor: 1.3,
- prestressing force scaling factor for span tendons 0.85, cantilever and continuity tendons: 0.9.

The parameters providing upper bound (minimum) deflections for all spans are:

- relative humidity: 90%,

- creep scaling factor: 0.7,
- shrinkage scaling factor: 0.7,
- prestressing force scaling factor for all tendons: 1.05.

6.5 Vertical Deflection Envelope

Figures 6.13 to 6.24 display the resulting span vertical deflection envelopes for the periods from March 1995 to June 1997, and March 1995 to May 1999, for all six units. The corresponding optical survey and base-line measurements are plotted for comparison.

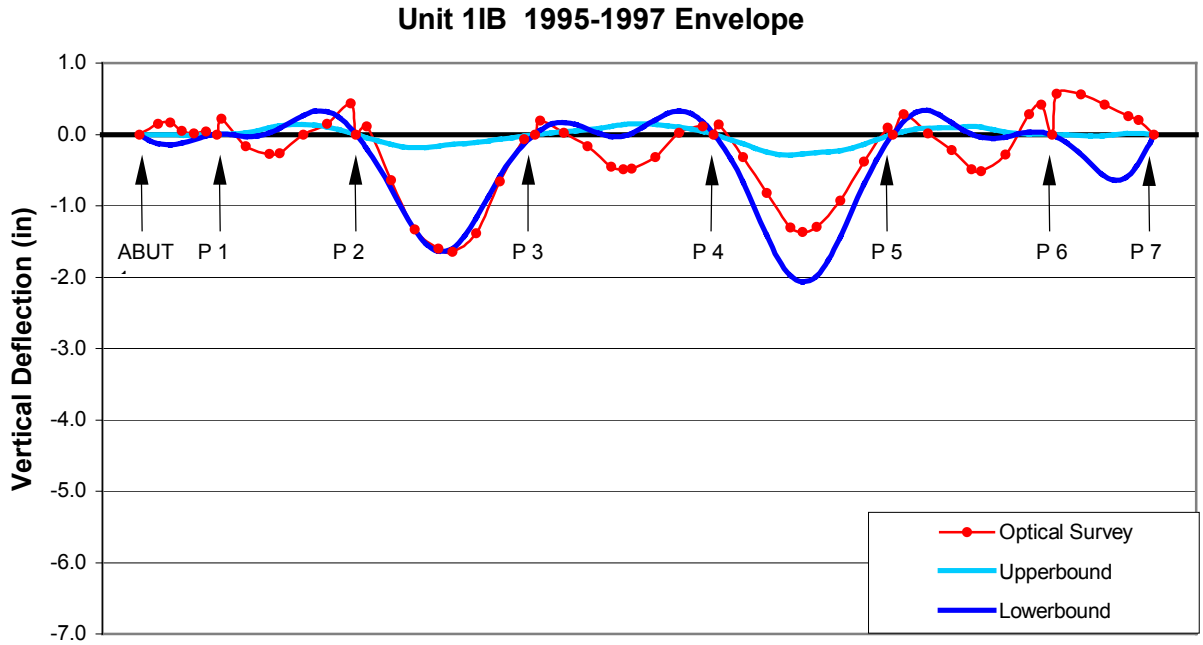

Figure 6.13: Unit 1IB Deflection Envelope 1995-1997

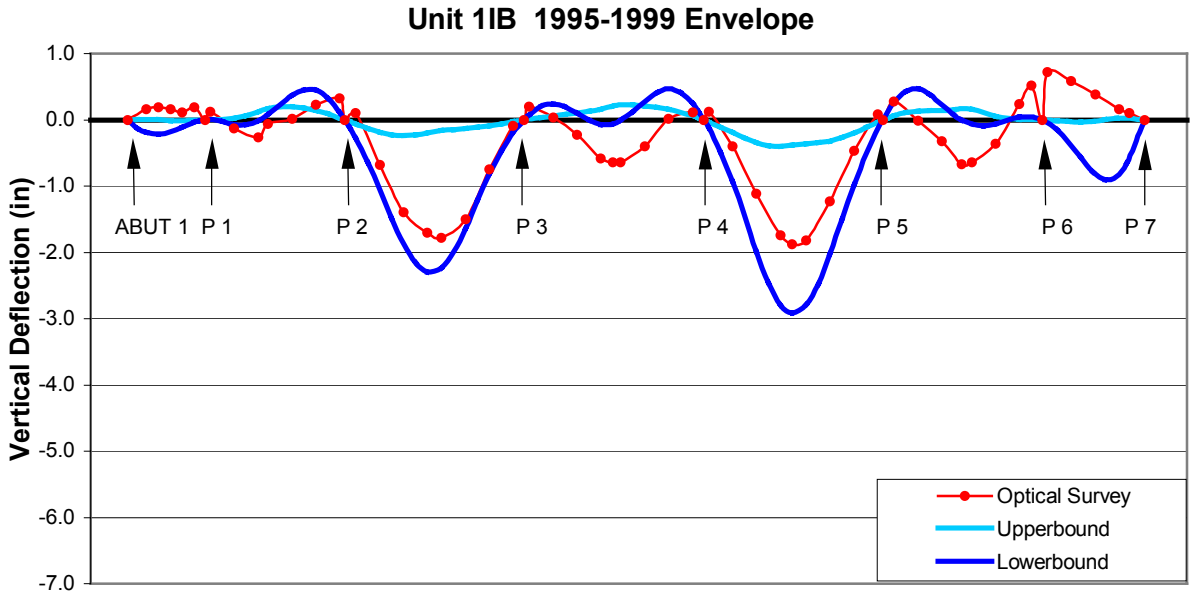

Figure 6.14: Unit 1IB Deflection Envelope 1995-1999

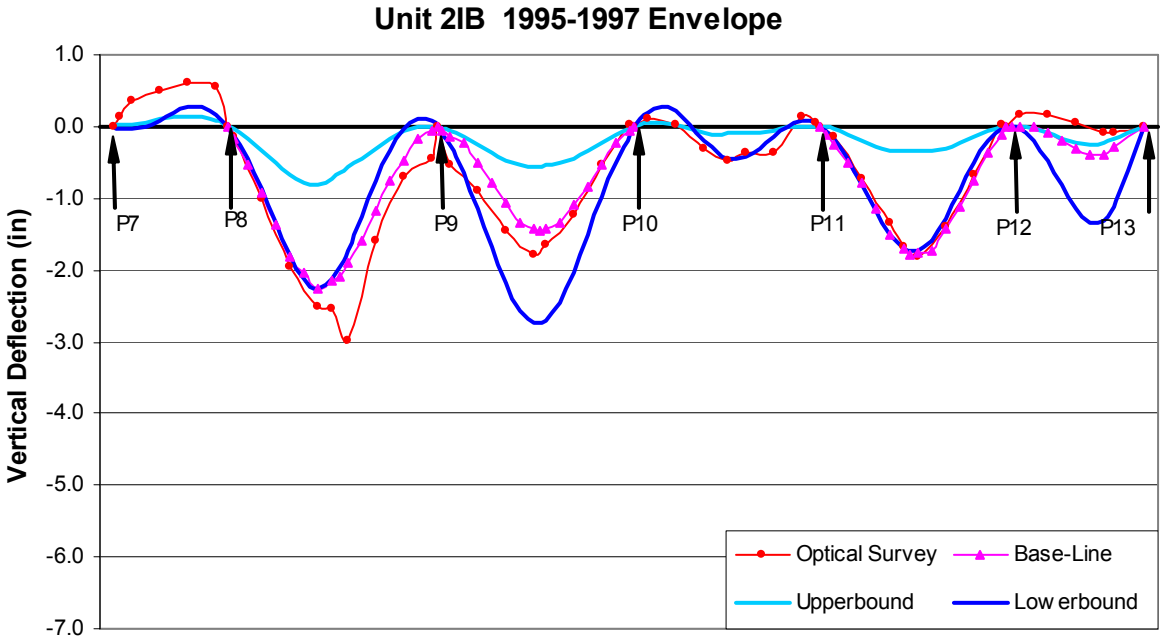

Figure 6.15: Unit 2IB Deflection Envelope 1995-1997

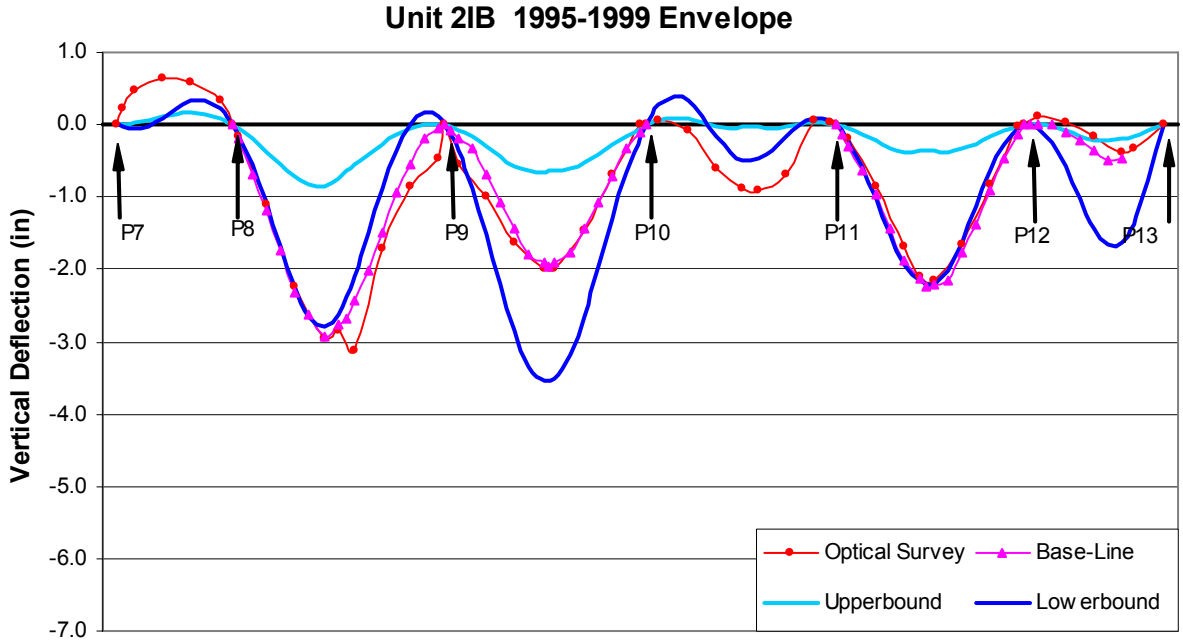

Figure 6.16: Unit 2IB Deflection Envelope 1995-1999

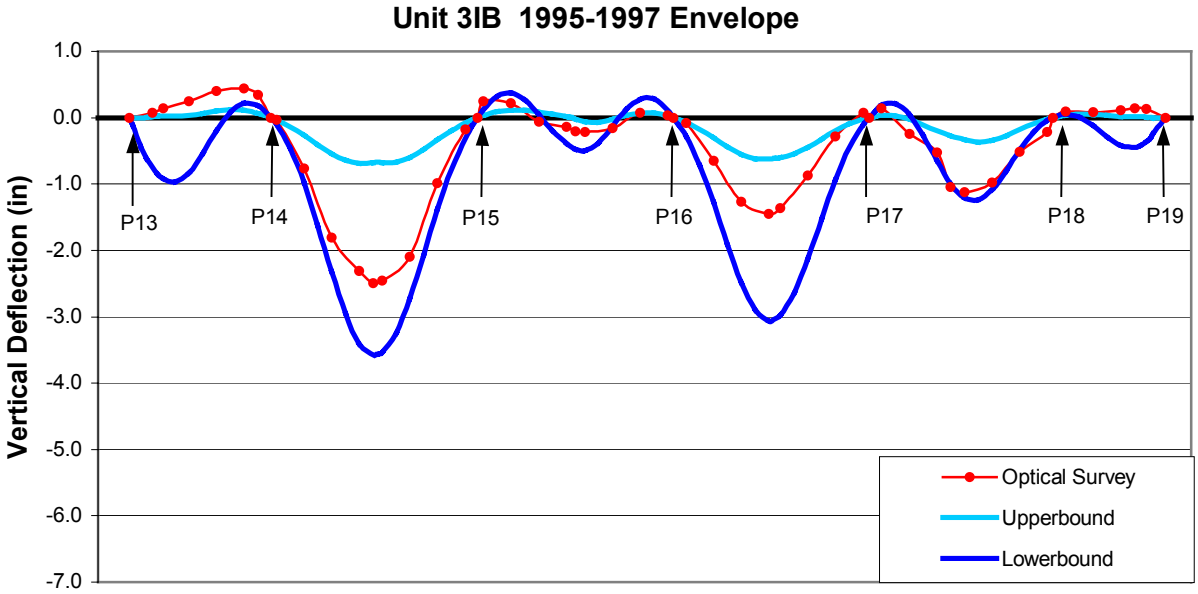

Figure 6.17: Unit 3IB Deflection Envelope 1995-1997

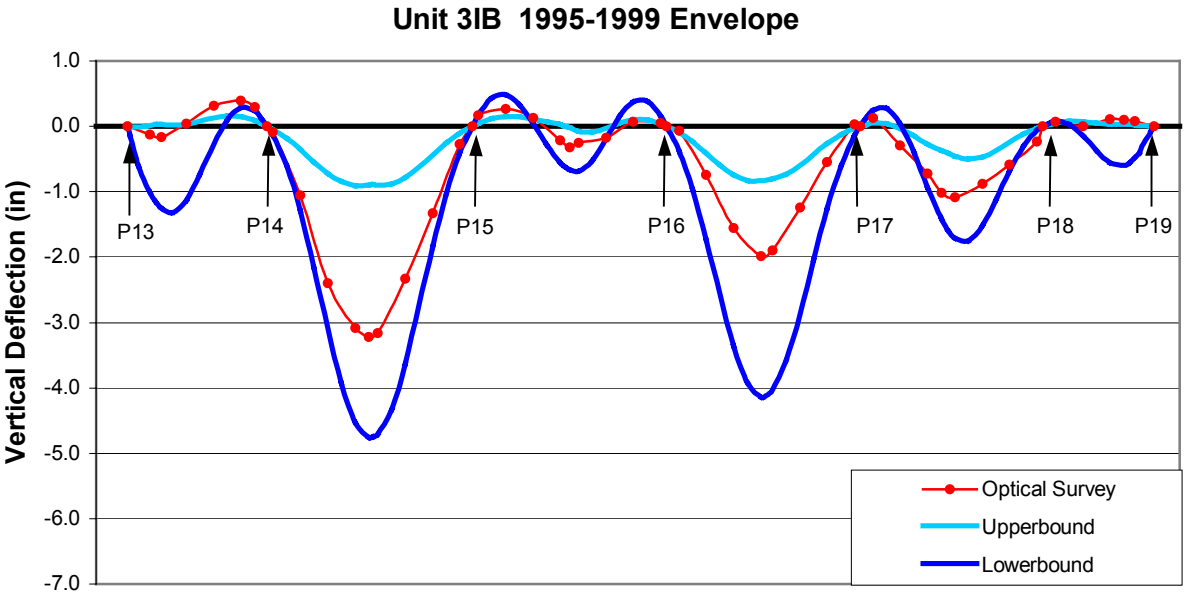

Figure 6.18: Unit 3IB Deflection Envelope 1995-1999

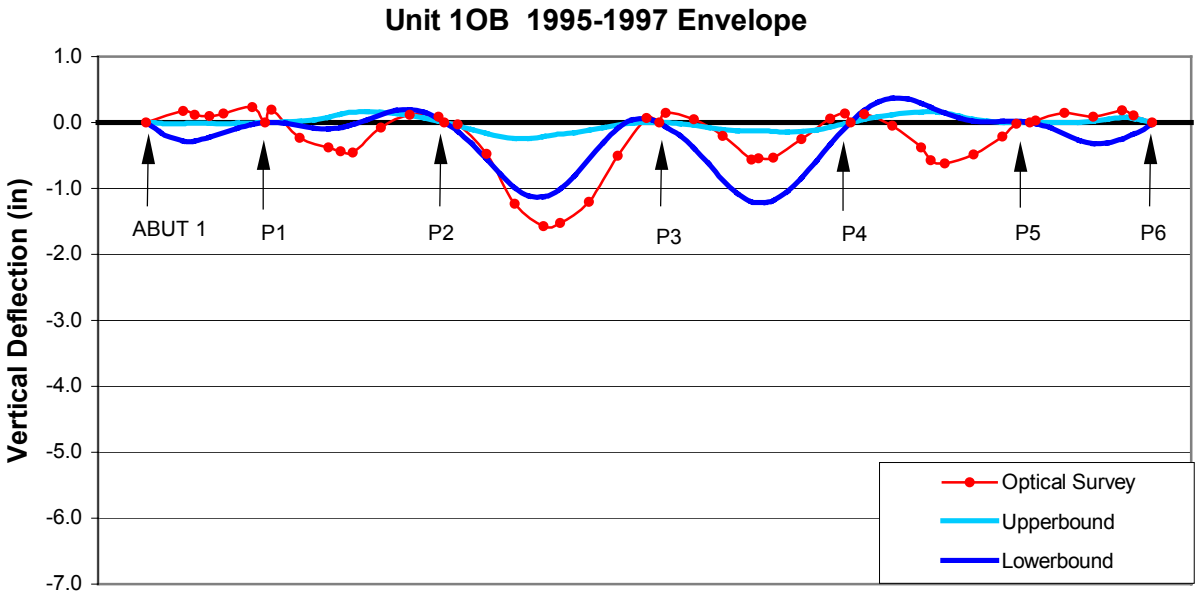

Figure 6.19: Unit 1OB Deflection Envelope 1995-1997

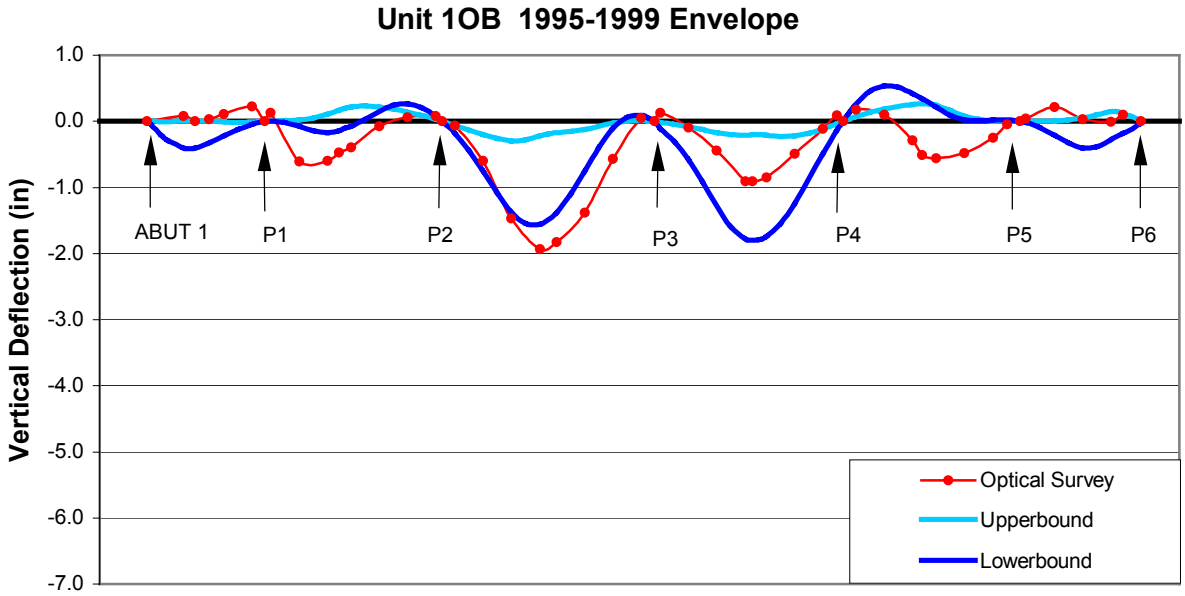

Figure 6.20: Unit 1OB Deflection Envelope 1995-1999

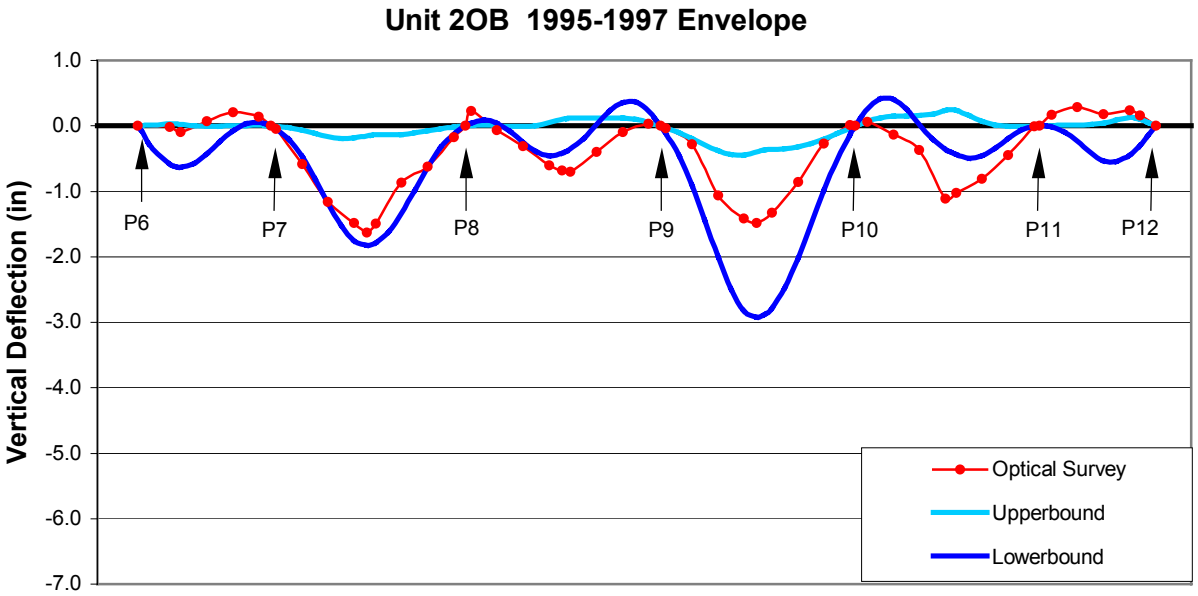

Figure 6.21: Unit 2OB Deflection Envelope 1995-1997

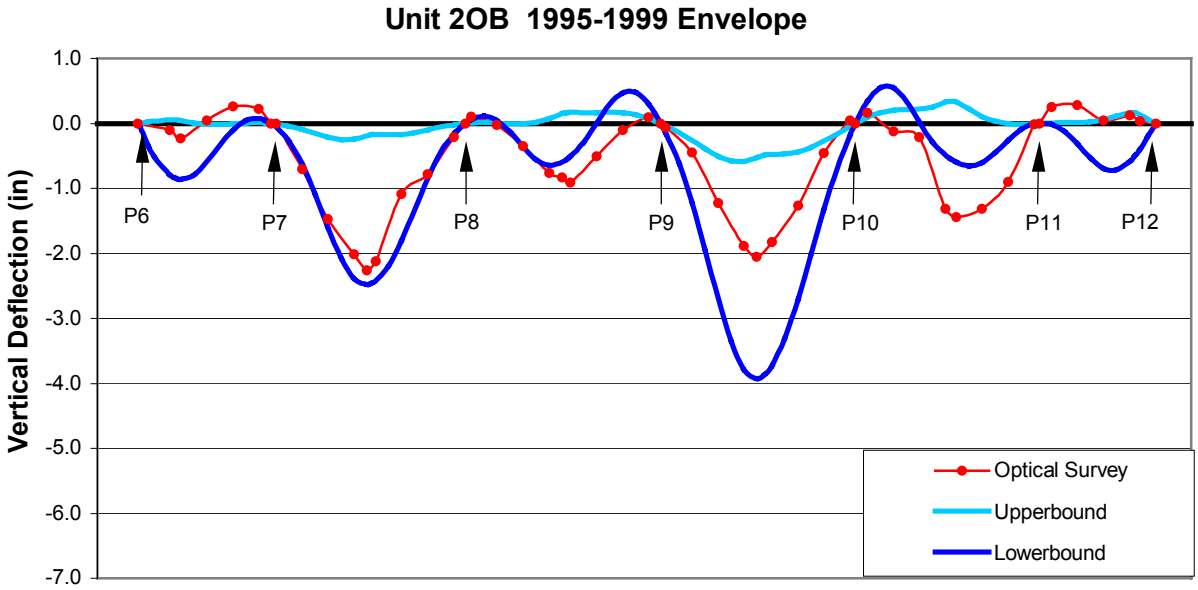

Figure 6.22: Unit 2OB Deflection Envelope 1995-1999

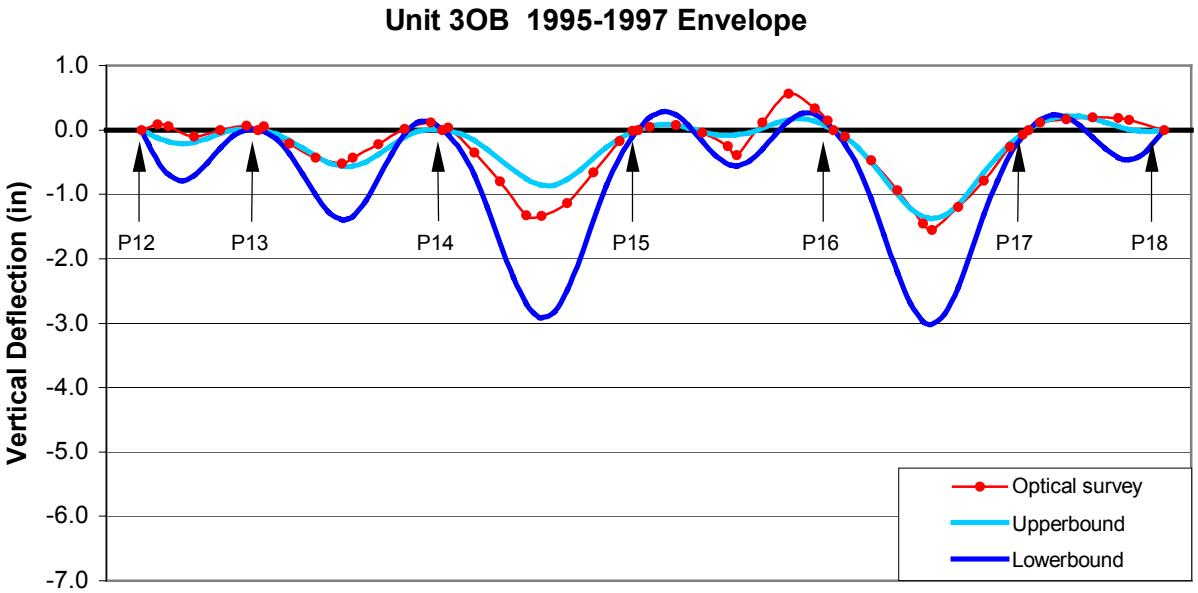

Figure 6.23: Unit 3OB Deflection Envelope 1995-1997

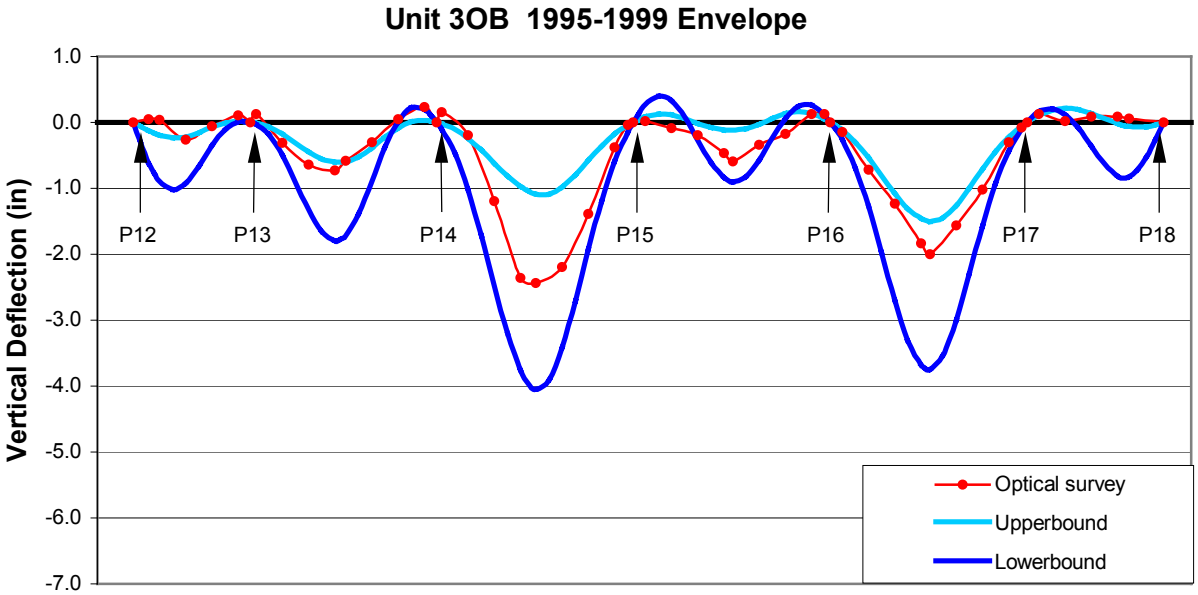

Figure 6.24: Unit 3OB Deflection Envelope 1995-1999

The majority of optical survey deflections fall within the predicted deflection envelopes. In particular, the observed deflections for Units 3IB and 3OB consistently fall within the predicted envelopes. The other four units typically have one or two spans where the measured deflection falls outside the predicted envelope. It appears that SFRAME often underestimates the deflection for short spans adjacent to longer spans.

Even though the parameter ranges considered in this report are reasonable, it can be seen that the most favorable and least favorable parameter combinations produce widely varying deflection bounds. These bounds may appear excessively wide, however, in some spans the actual deflection approaches the maximum bound, while elsewhere it approaches the minimum bound, and even exceeds the predicted bounds in few instances. Although the likelihood that all the best or worst parametric conditions will occur simultaneously is small, this model will enable the designer to provide a reasonable bound of deflection predictions to the client.

Having developed the upper and lower deflection envelopes, it is now possible to predict the viaduct deflection in the future with some confidence. The envelopes have been shown to fit the deflected shape after two years (March 95 to June 97) and four years (March1995 to May 1999). They will therefore provide the best estimate of future deflected shapes. Continued monitoring of the bridge deflections will allow for future confirmation of these analytical model predictions.

CHAPTER 7

CONCLUSION

7.1 Summary

This report was conducted using field instrumentations to measure the actual bridge long-term behaviors, and using a time dependent finite element analysis program SFRAME to study the long-term structural performance of the North Halawa Valley Viaduct (NHVV). The long-term structural responses considered in this study are the concrete longitudinal strain, span shortening, prestress losses, and vertical deflection. Field measurements were compared to the original SFRAME predictions performed by T.Y. Lin International during design of the viaduct. Updated material properties were used by prior researchers to develop improved SFRAME prediction model for Unit 2IB of the NHVV. This study applied these improved prediction models to all six units of the NHVV and developed prediction bounds based on parameter variability to provide more reliable long-term predictions.

7.2 Instrumentation Conclusions

Based on this study, the following conclusions are drawn regarding the instrumentation systems installed in the NHVV:

1. The vibrating wire strain gages used in this instrumentation program proved very reliable for both short-term and long-term monitoring.
2. The span extensometers confirmed the overall span shortening indicated by the average strain measurements at midspan and endspan sections.

3. In order for the load cells to provide accurate tendon force measurements, they must be installed so as to avoid introducing additional friction to the tendon.
4. optical survey measurements of the box girder vertical deflections confirmed the long-term stability of the internal base-line deflection system.

7.3 SFRAME Prediction Conclusions

1. Original SFRAME predictions of long-term deflection performed as part of the viaduct design were based on assumed material properties and creep shrinkage predictions from the CEB model code. These predictions significantly underestimated the measured deflection for all units of the NHVV.
2. After adjustment of the material properties based on short-term measurements of the concrete creep and shrinkage, and based on observed deflections of Unit 2IB, the SFRAME predictions improved significantly.
3. To improve the long-term predictions made during the design phase, the engineer must estimate likely ranges for each of the critical parameters affecting the long-term structural response rather than using single set of assumed values. These parametric ranges can then be combined to provide deflection envelopes in order to provide a reliable estimate of potential structural response.
4. Using the bounds developed for the NHVV, SFRAME was used to predict vertical deflection envelopes for all six units. With only a few exceptions, all long-term deflections fell within these envelopes.
5. The SFRAME bounds were also used to predict span shortening and tendon prestress losses. The span shortening measurements agree well with the average of the upper and lower

SFRAME bounds. The prestress force profiles measured by the load cells generally fell below the average of the upper and lower SFRAME bounds, but were still within these bounds.

REFERENCES

1 Dong and Robertson (1999), *Long-Term Structural Modeling of the North Halawa Valley Viaduct*. Research Report UHM/CE/99-04, University of Hawaii.

2 Gilbert, R.I (1988), *Time Effects in Concrete Structures*, Elsevier Science Publishers B.V., 1988.

3 Hoi & Robertson (2003), *Improved Creep and Shrinkage Prediction Models for the North Halawa Valley Viaduct*, Draft Research Report, University of Hawaii.

4 Ketchum, M.A. (1986), *Redistribution of Stress in Segmentally Erected Prestressed Concrete Bridges*, (SFRAME), UCB/SESM Report No. 86-07, University of California at Berkeley, Department of Civil Engineering.

5 Lee and Robertson (1995), *Instrumentation and Long-term Monitoring of the North Halawa Valley Viaduct*, Research Report UHM/CE/95-08, University of Hawaii.

6 Nawy E.G (2003), *Prestressed Concrete—A Fundamental Approach* (4^{th} edition), Prentice Hall, p74.

7 Shushkewich K.W., Vo N.T., Robertson I.N. (1998), *Instrumentation of the North Halawa Valley Viaduct Oahu*, Hawaii Progress Report, Sep. 1998.